A STUDY OF THE GIANT DIPOLE RESONANCE REGION OF ^{89}Y VIA POLARIZED AND UNPOLARIZED PROTON CAPTURE

by

Randall Delane Ledford

Department of Physics
Duke University

Date: _____

Approved:

_____
N. Russell Roberson, Supervisor

_____

_____

_____

_____

A dissertation submitted in partial fulfillment of the requirements for the degree of Doctor of Philosophy in the Department of Physics in the Graduate School of Arts and Sciences of Duke University

1976

ABSTRACT

(Physics)

A STUDY OF THE GIANT DIPOLE RESONANCE REGION

OF ^{89}Y

VIA POLARIZED AND UNPOLARIZED PROTON CAPTURE

by

Randall Delane Ledford

Department of Physics
Duke University

Date: _____

Approved:

_____
N. Russell Roberson, Supervisor

_____

_____

_____

_____

An abstract of a dissertation submitted in partial fulfillment of the requirements for the degree of Doctor of Philosophy in the Department of Physics in the Graduate School of Arts and Sciences of Duke University

1976

A STUDY OF THE GIANT DIPOLE RESONANCE REGION

OF ^{89}Y

VIA POLARIZED AND UNPOLARIZED PROTON CAPTURE

by

Randall Delane Ledford

Fourteen angular distributions of cross section and analyzing power have been measured in the giant dipole resonance (GDR) region of ^{89}Y with the $^{88}Sr(\vec{p},\gamma_0)^{89}Y$ reaction. These were analyzed to extract transition matrix elements and the relative phases for electric dipole (E1) and electric quadrupole (E2) radiation. A similar analysis was performed for eight angular distributions measured with the $^{88}Sr(\vec{p},\gamma_1)^{89}Y$ reaction, but for this latter case only E1 matrix elements and phases were obtained.

In addition, the 90^{o} yield curves for $^{88}Sr(p,\gamma_0)^{89}Y$ and $^{88}Sr(p,\gamma_1)^{89}Y$ reactions were measured for proton energies from 5.5 to 27.0 MeV and 7.5 to 27.0 MeV, respectively. The total integrated strength for each transition exhausted approximately 1% of the classical dipole sum rule.

The cross sections and analyzing powers of two isobaric analogue states (IAS) at E_p=6.06 and 7.50 MeV were measured at θ_{lab}=70°. These data, taken with energy steps of 25 keV, were analyzed to determine the effects of the interference of the IAS with the GDR. The resonance parameters of these IAS were extracted from an S-matrix fit to $^{88}Sr(\vec{p},p_o)^{88}Sr$ data.

Evidence for a strong resonance in ^{89}Y has recently been observed in inelastic electron scattering experiments near the predicted excitation energy of $135/A^{1/3}\simeq 30$ MeV for a collective isovector E2 resonance. Only unpolarized protons were available at the energies necessary to excite this region. Measurements of the cross sections for the $^{88}Sr(p,\gamma_1)^{89}Y$ reaction were made at 55°, 90°, and 125°. The fore-aft asymmetry obtained from these measurements was used in determining the resonance parameters of this resonance. The parameters obtained are compared with the electron scattering data.

ACKNOWLEDGEMENTS

I wish to express my appreciation to my advisor, Dr. N. R. Roberson, for his encouragement, interest, and support during my graduate career. I extend a special thanks to Dr. H. R. Weller for numerous helpful conversations. I also wish to thank Dr. D. R. Tilley, Dr. D. G. Rickel, and Dr. R. A. Blue for their assistance in data collection.

I extend my gratitude to Mr. C. P. Cameron for many helpful discussions, data collection, and various computer codes. I also wish to thank Mr. J. D. Turner and Mr. R. C. McBroom for their assistance in data collection. I extend my gratitude to the entire technical staff for assistance with the accelerator and electronic systems. Special thanks are extended to Mrs. M. Bailey for her assistance in preparing the illustrations. I am grateful to Dr. H. W. Newson and Dr. E. G. Bilpuch for providing me with the research assistantship.

A very special thanks is extended to my wife, Wanda, for her continued encouragement and assistance in typing. I

am also indebted to my parents for their continued encouragement.

This work was supported in part by the U. S. Energy Research and Development Administration.

R. D. L.

CONTENTS

LIST OF FIGURES

LIST OF TABLES

A STUDY OF THE GIANT DIPOLE RESONANCE REGION OF ^{89}Y VIA POLARIZED AND UNPOLARIZED PROTON CAPTURE

Chapter I

INTRODUCTION

The theoretical limit of the energy integrated cross section for the electric dipole (E1) absorption of photons by atoms is given by the Thomas-Reiche-Kuhn (TRK) sum rule (Thomas, 1925; Reiche and Thomas, 1925; Kuhn, 1925). This dipole sum rule has also been extended to apply to nuclei (see Appendix C). Photon absorption in nuclei is characterized by a large maximum in the cross section with a width of 3-10 MeV and located at an excitation energy of approximately $80/A^{1/3}$ MeV for medium and heavy nuclei (Hayward, 1970). Because the experimental integrated cross section of this photoabsorption resonance is often of the order of the dipole sum rule, it is commonly referred to as the giant dipole resonance (GDR) of the nucleus. In fact, a compilation by Hayward (1970) shows that for nuclei of mass heavier than Z=50, the GDR contains almost one dipole sum.

The GDR has been investigated by numerous experiments involving reactions other than photon absorption. These methods

include inelastic electron scattering, elastic and inelastic proton scattering, inelastic ^{3}He scattering, and inelastic alpha particle scattering. The GDR has also been studied by exciting this resonance by particle capture and measuring the gamma radiation resulting from its subsequent decay; i.e., the inverse reaction to photon absorption. Some of the most common of these radiative capture reactions are proton capture, alpha capture, and neutron capture.

The capture of polarized protons has proven to be a method of significant utility in investigating the GDR in several nuclei (H. F. Glavish, et al., 1972; S. S. Hanna, et al., 1972; Weller, et al., 1974). Cross section measurements from unpolarized proton capture are generally insufficient to unambiguously determine the magnitudes and relative phases of the amplitudes contributing to the GDR. However, polarized proton capture experiments which measure the analyzing power as well as the gamma-ray angular distribution can provide supplementary data to remove these ambiguities (Weller, et al., 1976). Of particular significance is the fact that such measurements may also be used to determine the electric quadrupole (E2) cross section in the region of the GDR (S. S. Hanna, et al., 1974; Kuhlmann, et al., 1975). This is of particular importance with respect to establishing the existence and properties of a giant quadrupole resonance (GQR).

In the present investigation polarized protons were captured by ^{88}Sr (Q=7.07 MeV) to excite ^{89}Y. This is a particularly interesting case since the gamma-ray decay of the GDR to the ground state of ^{89}Y ($J^{\pi}=1/2^{-}$) is restricted to only two amplitudes (see Chapter III). Angular distributions of cross section and analyzing power were measured throughout the region of the GDR in order to determine these E1 amplitudes of the GDR as well as the E2 amplitudes in the region of the isoscalar GQR.

Unfortunately, an analysis of the angular distributions obtained via the $(\vec{p},\gamma)$ reaction often leads to double solutions with respect to the composition of the GDR (see Chapter III). A method to remove this ambiguity by measuring the interference of the GDR with isobaric analogue states (IAS) was investigated in this work. In ^{89}Y, the IAS (analogues of the ^{89}Sr nucleus) are at an excitation energy which places them in the GDR region and permits an evaluation of this method. Earlier analyses of these IAS have neglected the interference of the IAS with the GDR (S. M. Shafroth and G. T. E. Legge, 1968).

Evidence for a collective isovector GQR has recently been observed by inelastic electron scattering on ^{89}Y (Buskirk, private communication). The region around this proposed GQR was investigated with unpolarized proton capture and by observing the gamma decay to the first excited state (γ_1) of ^{89}Y. Previous experiments using proton capture in ^{209}Bi have indicated

the utility of fore-aft asymmetry measurements (see Chapter IV) in determining the resonance parameters of the GQR (K. A. Snover, et al., 1974). With this technique, resonance parameters for an isovector GQR in ^{89}Y have been obtained which are in reasonable agreement with the inelastic electron scattering data.

Chapter II

EXPERIMENTAL APPARATUS AND PROCEDURE

A. Ion Beams

The polarized protons used to measure the angular distributions of cross section and analyzing power in this study were produced by the Lamb-shift polarized ion source (T. B. Clegg, et al., 1970) at the Triangle Universities Nuclear Laboratory. The negative polarized H^- ions were accelerated with the TUNL FN tandem van de Graaff accelerator up to energies of 16 MeV. After exiting the accelerator, the beam was momentum analyzed by a pair of 90 degree bending magnets and a 30 degree switching magnet. A pair of variable horizontal and vertical slits defined the beam at the exit of the switching magnet. The beam was then directed through a single collimator in front of the target via a quadrupole lense and steering magnets. After passing through the target, the beam was stopped in a tantalum lined Faraday cup 4 m downstream from the target chamber.

The unpolarized protons employed for the measurement of the differential cross section and fore-aft asymmetry at higher energies were obtained from the TUNL Cyclo-Graaff accelerator (F. O. Purser, et al., 1969). Negative 15 MeV H^- ions were produced in a cyclotron and injected into the FN tandem for further acceleration.

B. Target Chamber and Shielding

All data were taken in a brass target chamber which has an internal diameter and a depth of 15.6 cm and 8.9 cm, respectively. The chamber itself was electrically insulated from the rest of the beam line. A single collimator consisting of a tantalum ring with an inside diameter of 3 mm mounted in a teflon inset inside the beam line was positioned approximately 5 cm in front of the target. The current on the collimator was continuously minimized (typically <1% of the total beam current) throughout the experiment in order to reduce background radiation. The slits at the exit of the switching magnet were shielded by 20 cm of concrete, 15 cm of lead, and approximately 30 cm of paraffin; the Faraday cup shielding consisted of 15 cm of lead and 30 cm of paraffin doped with lithium carbonate.

C. Targets

The Strontium-88 targets were obtained from the Isotopes Division of the Oak Ridge National Laboratory. The 99.84% enriched Strontium-88 targets were mounted between two aluminum target rings and stored in evacuated glass ampules for shipment. The targets were removed from their containers and mounted in a vacuum interlock/target mount for transfer between the target chamber and a storage vacuum (see Appendix A). The ORNL specified thickness of these targets was 2.1 mg/cm^2. A comparison of the elastically scattered proton cross section with previous measurements indicates that the error in this value is approximately 5% (Cosman, et al., 1968; Cosman, et al., 1970; Genz, et al., 1975).

D. Detectors

The gamma-rays were detected by a cylindrical 25.4 cm x 25.4 cm NaI crystal. The crystal was housed in a stainless steel casing and viewed by six RCA-8575 photomulitplier tubes. The detector is surrounded by a well-shaped anticoincidence shield (Suffert, et al., 1968) of NE110 plastic whose thickness was 7.6 cm and 12.7 cm in the front and sides, respectively. The shield was viewed by eight XP1031 photomultiplier tubes. In

order to reduce the background counting rate, the crystal-shield assembly was surrounded by 10 cm of lead, cadmium sheet, and 20 cm of paraffin. The paraffin was approximately 50% lithium carbonate (Li_2CO_3) by weight. Data were taken at target-detector distances of 56 cm and 81 cm with total angular acceptances of 18^o and 14^o, respectively. The detector could be rotated through angles of 50^o to 130^o, with respect to the beam direction, in the 56 cm position and through 42^o to 142^o in the 81 cm position. At each position a lead collimator was used which illuminated the back face of the crystal. The entire assembly is shown schematically in fig. 1.

Silicon surface barrier detectors were used for charged particle detection throughout the experiment. They offered excellent resolution and a small size compatible with the size of the target chamber. Two detectors at $+160^o$ and -160^o were used to monitor the beam polarization during most of the angular distribution measurements taken with polarized protons. For the isobaric analogue resonance studies, four such detectors were used at 70^o, 90^o, 125^o, and 160^o to obtain angular distributions of elastically scattered protons. The detectors had thicknesses of 1500 μm to 2000 μm.

The NaI detector efficiency was determined by means of the $^{12}C(p,\gamma_o)^{13}N$ reaction (F. S. Dietrich, et al., 1968) with a ^{12}C target which was about 45 keV thick for 14.2 MeV protons.

Figure 1. Schematic diagram of the NaI detector system.

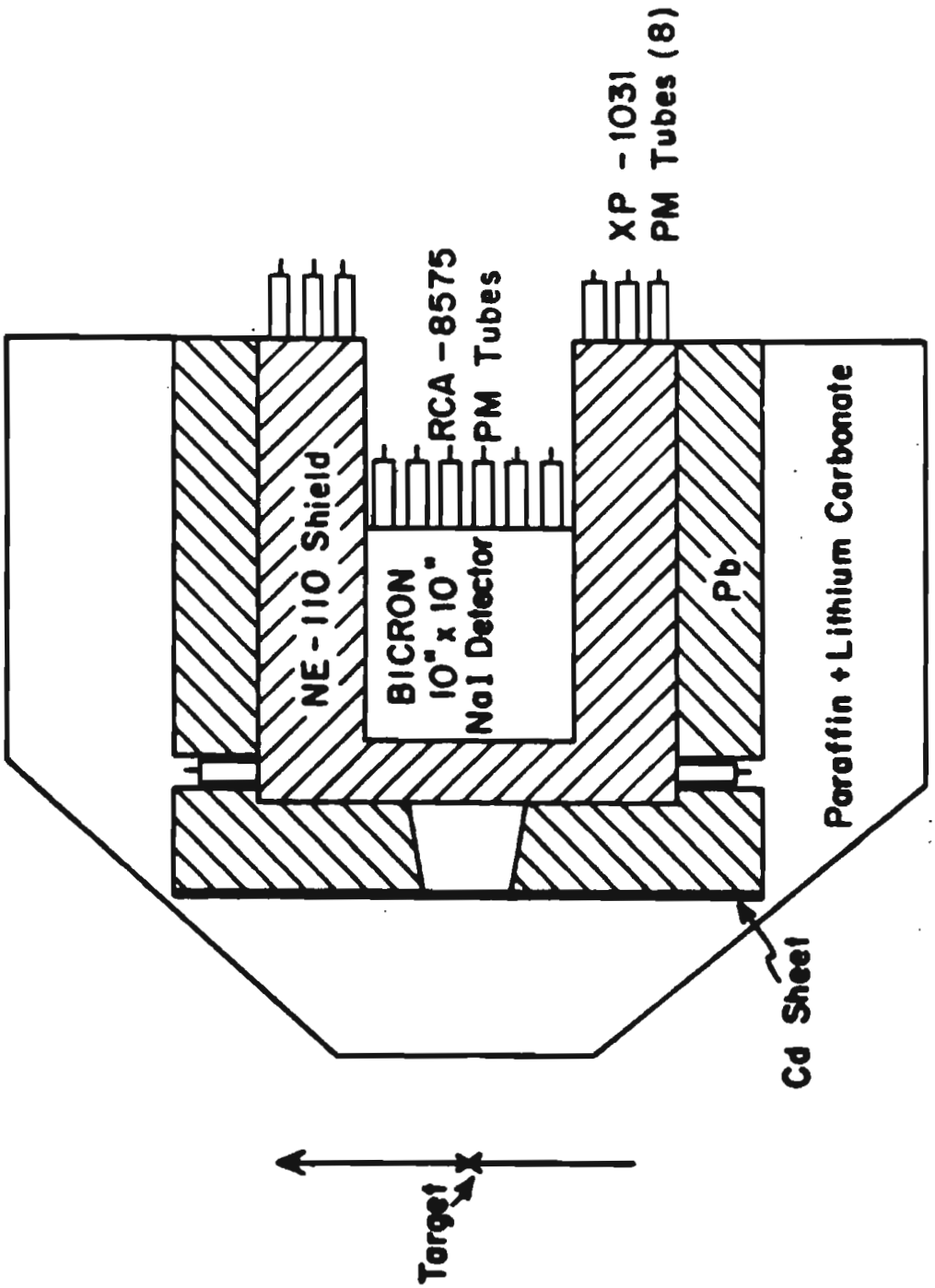
XP - 1031
PM Tubes (8)
RCA - 8575
PM Tubes
NE - 110 Shield
BICRON
10" x 10"
NaI Detector
Pb
Paraffin + Lithium Carbonate
Cd Sheet
Target
X

Measurements were made of the yield curve of the 15.07 MeV resonance in ^{13}N and on and off resonant angular distributions. Combining this data with the known cross section ({6.83 ± 0.22} x 10^{-9} gamma-ray/proton (R. E. Mans, et al., 1975)) determined the efficiency of the NaI detector to be (26 ± 6)%.

E. Electronics

A simplified block diagram of the electronics used in this experiment is shown in fig. 2. Anode signals were taken directly from the NaI photomultiplier tubes and summed with a linear mixer. Prior to a fast linear gate, this signal was clipped with a 50 ohm cable terminated by a 12 ohm resistor which produced a clean unipolar signal approximately 250 nsec long. The linear gate was opened only for 400 nsec which reduced the possibility of pile-up events. The signal was then amplified, shaped and processed by an analog to digital converter (ADC).

The signals from the shield photomultiplier tubes were rather small and were amplified (x4) before mixing. The resulting summed signal was clipped to 10 nsec and applied to a standard fast coincidence circuit. A similar fast signal for the coincidence circuit was obtained from the NaI mixer but with a 60 nsec clipping time.

Figure 2. Block diagram of the electronic configuration. Electronics used to measure the accidental rate and elastically scattered protons are not shown.

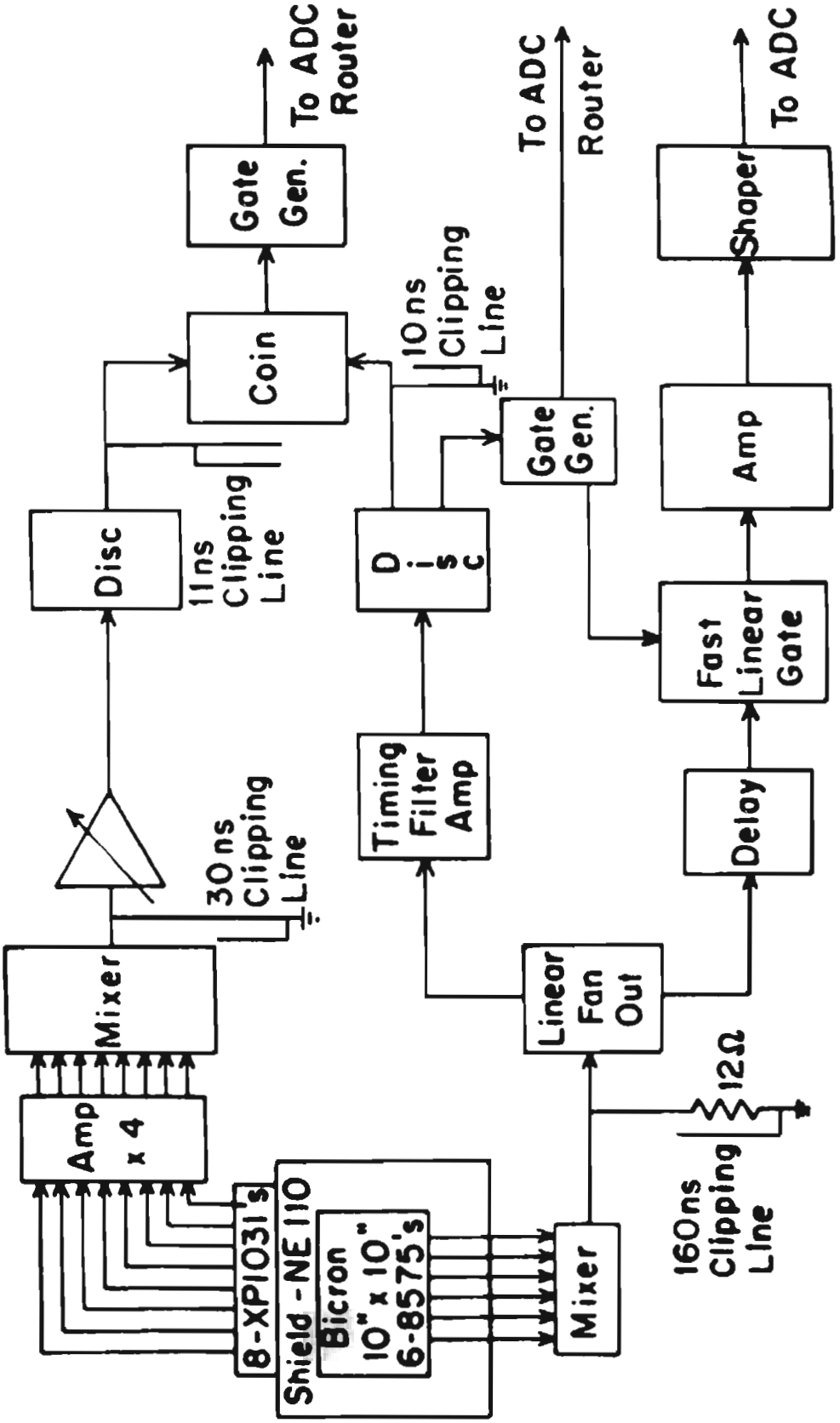
Shield - NE 110
Bicron
10" x 10"
6-8575's
8-XP1031's
Amp
x 4
Mixer
30 ns
Clipping
Line
Disc
11 ns
Clipping
Line
Coin
Gate
Gen.
To ADC
Router
Timing
Filter
Amp
D
i
s
c
10 ns
Clipping
Line
Gate
Gen.
To ADC
Router
Linear
Fan
Out
Mixer
160 ns
Clipping
Line
12Ω
Delay
Fast
Linear
Gate
Amp
Shaper
To ADC

The NaI gamma-ray signals which were not in coincidence with a shield event were stored with an on-line computer (see below) as true events while those in coincidence with a shield event were stored in a separate memory location as rejected events. The rejected NaI signals included cosmic-rays, Compton scattered gamma-rays, and annihilation radiation from pair production. By adjusting the gain of a fast amplifier in the shield electronics, the fraction of the first and second escape peaks rejected from the true events could be fixed. For most of the data discussed in this work, the rejection fraction was set to provide a clean separation between the ground state and first excited state decay gamma-rays.

A light-emitting-diode (LED) was mounted on the back face of the NaI detector. The monoenergetic signals from the LED were employed as a reference by an on-line computer to correct for gain shifts in the spectra.

The resolution of the system was determined to be approximately 2.4% under ideal conditions (H. R. Weller, et al., 1976). In practice, gain shifts related to the background counting rate resulted in more typical resolutions of 3-4%. The 3-4% resolution could be maintained by keeping the total NaI counting rate less than 10^5 counts per second. A spectrum taken with this system is shown in fig. 3.

Figure 3. The $^{88}Sr(p,\gamma)^{89}Y$ spectrum for a proton energy of 4.5 MeV. The gamma transitions to the ground state and excited states are indicated by arrows. The excitation energies and J^{π} values are taken from Johns, et al. (1971).

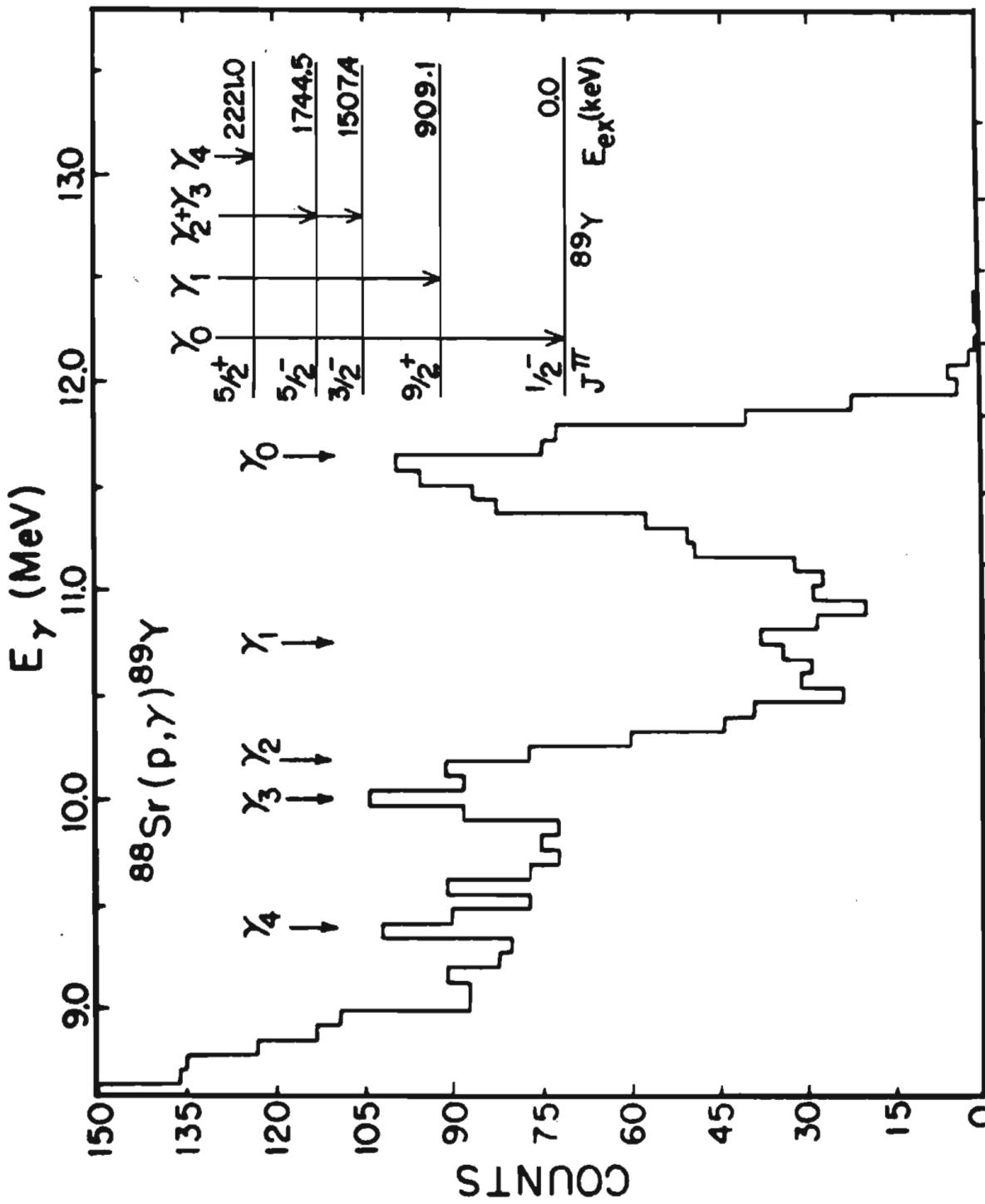
E_γ (MeV)
$^{88}Sr(p,\gamma)^{89}Y$
γ_0
γ_1
γ_2
γ_3
γ_4
γ_0 γ_1 $\gamma_2+\gamma_3$ γ_4
5/2+ 5/2- 3/2- 9/2+ 1/2-
J^π
0.0
909.1
1507.4
1744.5
2221.0
E_{ex}(keV)
^{89}Y
COUNTS
CHANNEL NUMBER

The signals from the charged particle detectors were processed by standard preamplifiers. The amplified signals were shaped, summed, and processed by a second ADC. Logic pulses used for routing were generated for each detector by sending a bipolar output from each amplifier through a timing single channel analyzer.

An on-line computer, a DDP-224, was programmed to store spectra in 512 channel arrays. These spectra for true gamma-rays, rejected gamma-rays, and charged particles for each of the two proton spin states were recorded on magnetic tape for later off-line analysis.

While the data was accumulating, the beam which was collected in the Faraday cup was integrated by an electronic current meter and integrator. For every unit of charge accumulated, the integrator generated a pulse which went to three scalars. The first scalar was gated off when the computer was busy with a gamma-ray event or the pile-up gate was on, and thus measured the live charge for the gamma-ray detection system. The second scalar was gated off when the computer was busy with a charged particle event and recorded the live charge for the solid state detectors. The third scalar was ungated and hence measured total charge accumulated. Additional scalars monitored the accidental and true coincidence rates, as well as the single counting rates in the NaI and shield. A final scalar stored the

real time associated with the collection of each data point. These scalars were read into the computer and written onto magnetic tape along with the spectra after the completion of each run.

When using the Cyclo-Graaff, the above electronic system was modified by including a time to amplitude converter (TAC) which was employed to reduce the background radiation associated with the neutrons produced by the high energy proton beam. The time dependence of the pulsed cyclotron beam was determined by a pick-up coil located near the cyclotron RF oscillator. A signal corresponding to the zero crossing of the cyclotron dee voltage was used as the stop signal for the TAC, while the start signal was generated by an event in the NaI crystal. A time window was set on the TAC spectra corresponding to the gamma-flash and this was used to gate events from the NaI detector and the resulting gamma-ray spectra were stored in the computer. Events occurring above and below the time window were collected as well in order to monitor the neutron background and to check that the TAC window was set properly.

F. Procedure

1. General. The ^{88}Sr target was transferred from the storage vacuum to the target chamber as described in Appendix A

and the target chamber evacuated. With beam on target, the timing of shield and detector pulses was adjusted to produce coincidence signals to be used for rejection. The shield discriminators were adjusted to produce the desired rejection fraction while the NaI discriminator was set so that only high energy gamma-ray events were processed by the computer. This latter adjustment controlled both the computer dead time and the accidental rate. The LED pulser was set to produce 200 pulses per second, and its corresponding peak in the gamma-ray spectrum was initialized as the reference channel in the computer gain stabilization program.

2. $^{88}Sr(p,\gamma_o)^{89}Y$ and $^{88}Sr(p,\gamma_1)^{89}Y$ Cross Sections.

Unpolarized protons were used to measure the gamma-ray 90^o yield curve for incident proton energies of 5.2 MeV to 16.1 MeV. Proton energy steps of 50 keV and 100 keV were taken for the intervals of 5.2 MeV to 8.0 MeV and 8.0 MeV to 16.1 MeV, respectively. The NaI detector was positioned at a laboratory angle of 90^o and at a distance of 56 cm from the target where it subtended a solid angle of 7.55×10^{-2} steradians. The differential cross sections at 90^o was determined for γ_o and γ_1 from the incident proton flux, the target thickness, the solid angle, and the detector efficiency. The efficiency for the detector was assumed constant for all gamma ray energies of 12-35 MeV. The method for summing γ_o and γ_1 is discussed in the next chapter.

3. Angular Distributions of Cross Section and Analyzing Power Measurements. Polarized protons were used to measure angular distributions of cross section and analyzing power at 14 energies throughout the giant resonance region of ^{89}Y. In 9 of these, the NaI detector was positioned at 56 cm from the target and data were taken at 50°, 70°, 90°, 110°, and 130°. In the other 5 cases, the detector was moved to 81 cm which allowed more extreme angles to be taken. Seven angles were measured in these instances: 42°, 55°, 70°, 90°, 110°, 125°, and 142°. At each angle, data were accumulated by running the beam alternately in the spin up and the spin down modes.

The analyzing power $A(\theta)$ was obtained at a given angle and energy from the expression

$$A(\Theta) = \frac{1}{P}\left(\frac{N_+ - N_-}{N_+ + N_-}\right) \qquad (1)$$

where N_+ and N_- are the number of counts obtained for the spin up and spin down modes. The quantity P (see below) denotes the beam polarization. The cross sections were determined from the sum, $N_+ + N_-$.

The polarization of the proton was determined at the completion of each run by the quench-ration technique (T. A. Trainor, et al., 1974). The polarization was essentially

constant for this experiment with a typical value of 0.82 ± 0.03. In part of these measurements, solid state detectors were located at ±160° with respect to the incident beam. The asymmetry in the $^{88}Sr(\vec{p},p_0)^{88}Sr$ reaction provided an additional check on the proton polarization.

4. Cyclo-Graaff Measurements. The cross section data were extended to the proton energy region 17.0 to 28.0 MeV using unpolarized protons from the TUNL Cyclo-Graaff. Energy increments of 500 keV were taken in this range. In addition to the 90° cross section data, measurements were made at laboratory angles of 55° and 125° in order to determine the fore-aft asymmetry in this region, where the asymmetry is defined as

$$a = \sqrt{3}\left(\frac{N(55) - N(125)}{N(55) + N(125)}\right) \qquad (2)$$

and N(55) and N(125) are the number of counts obtained for θ_γ=55° and 125°, respectively.

5. Measurements at Isobaric Analogue States. Two isobaric analogue states (IAS) (Cosman, et al., 1968) at proton energies of 6.06 and 7.55 MeV were studied by with polarized protons. The energy intervals, 5.6 - 6.4 MeV and 7.2 - 7.8, respectively, were studied with proton energy increments of 25

keV. The NaI detector was positioned at 56 cm from the target and at a laboratory angle of 70^{o} and data were taken to determine the cross section and analyzing power. Four solid state detectors were positioned at 70^{o}, 90^{o}, 125^{o}, and 160^{o} inside the target chamber and at a distance of 6.6 cm from the target. A 1.59 mm diameter tantalum collimator placed directly in front of each detector defined a subtended angle of 4.54×10^{-4} steradians. A second tantalum collimator with a diameter of 3.18 mm was positioned 2.5 cm in front of the first collimator which insured that each detector was only illuminated by the target and not its mount or surrounding material.

Chapter III

EXPERIMENTAL RESULTS AND DATA ANALYSIS

A. Determination of Gamma-Ray Line Shapes and Sums

A standard gamma-ray line shape was determined by fitting the ground state transition obtained with the $^{3}H(p,\gamma)^{4}He$ reaction. Since the first excited state of ^{4}He is at 20.2 MeV (Meyerhof and Tombrello, 1968), the γ_0 decay provides a well separated gamma-ray peak for establishing line shape parameters. It was determined that the shape could be represented by two cubic exponentials smoothly joined at the low energy side of the peak. One of the exponentials determines the shape of the peak and the other describes the shape of the low energy tail. The details of this procedure and the line shape parameters are given by McBroom (1977).

In each gamma-ray spectra, the highest energy gamma-ray would be fitted and subtracted from the spectrum. The next

gamma-ray was then fitted from the residual spectrum. This process was continued until all the gamma-rays of interest were fitted. For each gamma-ray, the region summed to obtain the number of events in the peak was chosen to be consistent with the summation region used in determining the efficiency of the NaI detector. In practice only γ_0 and γ_1 could be reliably extracted. Figure 4 shows the result of fitting the sample spectrum of fig. 3.

B. Differential Cross Section Measurements for the $^{88}Sr(p,\gamma_0)^{89}Y$ and $^{88}Sr(p,\gamma_1)^{89}Y$ Reactions

At a laboratory angle of 90^{o}, spectra were taken from 5.2 - 27.0 MeV. Sums of the γ_0 and γ_1 peaks were obtained using the fitting procedure described in the previous section. These sums were used to obtain the differential cross sections for these two transitions as described in Chapter II and the results are shown in fig. 5 and fig. 6. The maxima of the γ_0 excitation curve is located near the expected centroid of the giant dipole resonance; $80/A^{1/3}$=17.9 MeV. The centroid for the γ_1 excitation curve is shifted upward by the energy of the first excited state of ^{89}Y (909.1 keV) and is therefore expected to be near 18.8 MeV in excitation.

Figure 4. Calculated line shapes to the individual gamma rays of fig. 3 are shown as dotted lines. The solid curve represents the sum of the individual fits.

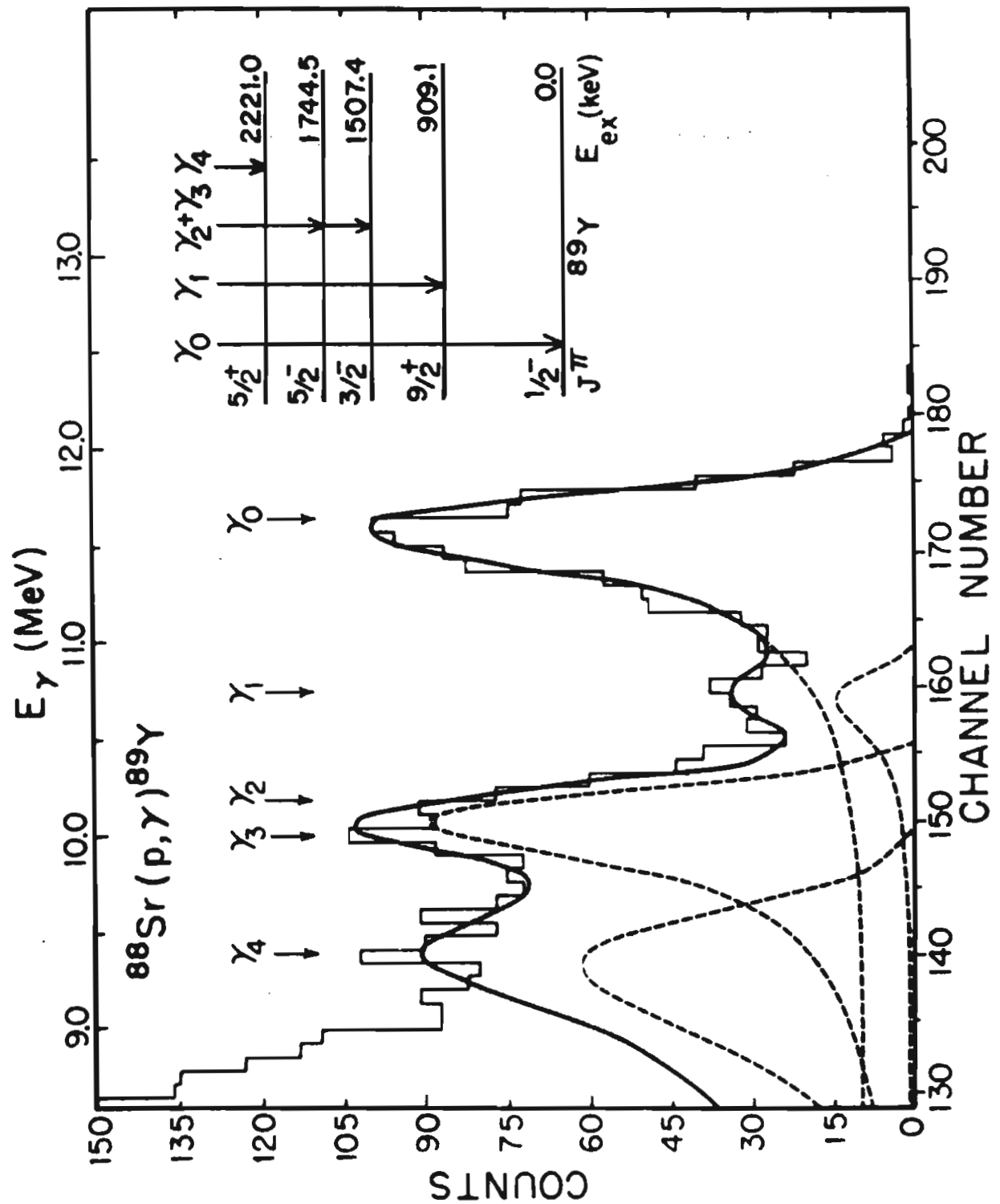
$^{88}Sr(p,\gamma)^{89}Y$
E_γ (MeV)
9.0
10.0
11.0
12.0
13.0
γ_0
γ_1
γ_2
γ_3
γ_4
γ_0 γ_1 $\gamma_2+\gamma_3$ γ_4
2221.0
1744.5
1507.4
909.1
0.0
E_{ex}(keV)
^{89}Y
J^π
$5/2^+$
$5/2^-$
$3/2^-$
$9/2^+$
$1/2^-$
COUNTS
0
15
30
45
60
75
90
105
120
135
150
CHANNEL NUMBER
130
140
150
160
170
180
190
200

Figure 5. The differential cross section for the $^{88}Sr(p,\gamma_0)^{89}Y$ reaction taken at a laboratory angle of 90^{o}. The energy is center of target energy. The error bars represent the statistical error associated with the data points. The solid curve is a smooth line through the data points.

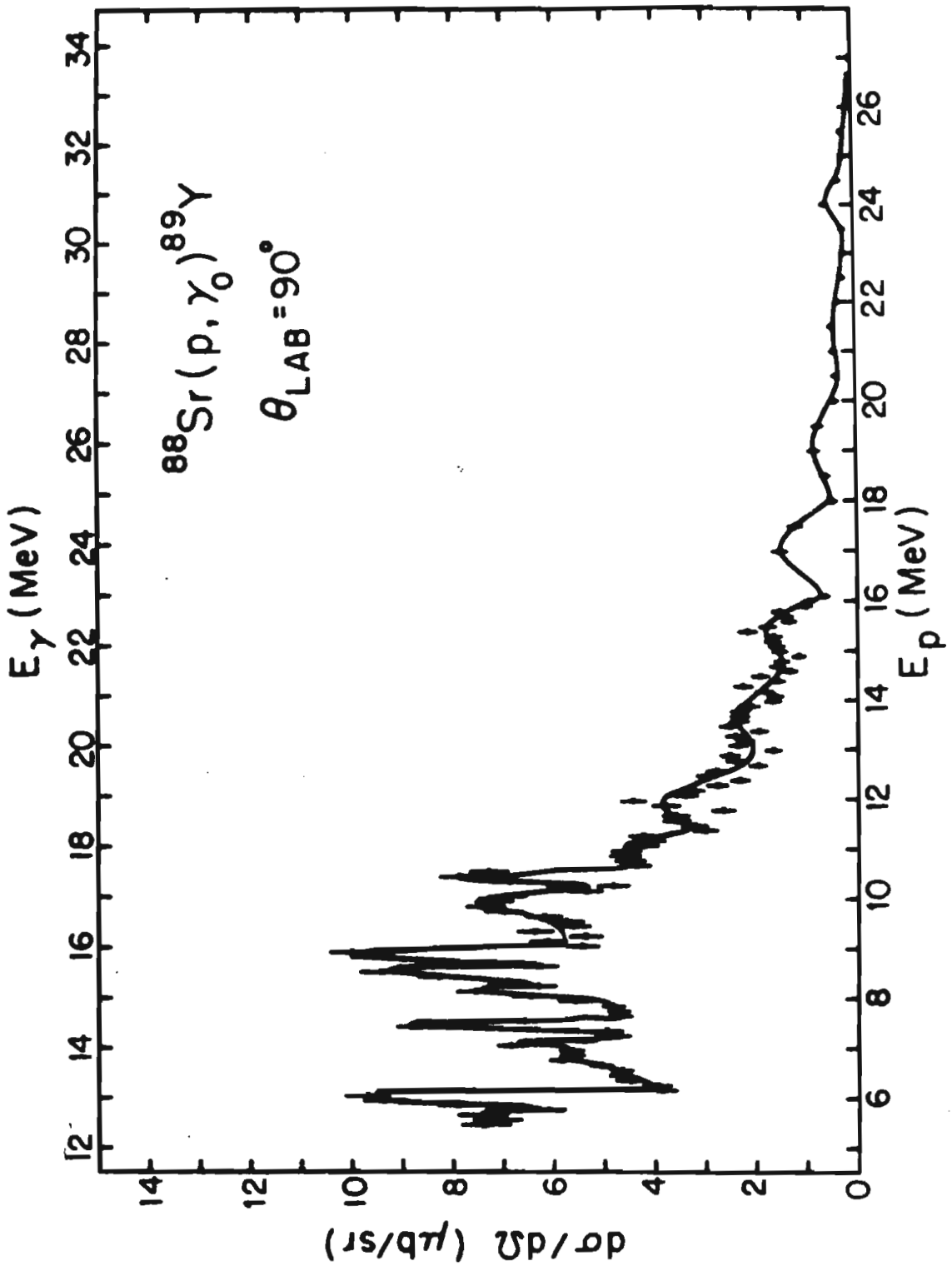
$^{88}Sr(p,\gamma_0)^{89}Y$
$\theta_{LAB}=90°$
E_γ (MeV)
E_p (MeV)
$d\sigma/d\Omega$ (μb/sr)

Figure 6. The differential cross section for the $^{88}Sr(p,\gamma_1)^{89}Y$ reaction taken at a laboratory angle of 90^{o}. The energy is center of target energy. The error bars represent the statistical error associated with the data points. The solid curve is a smooth line through the data points.

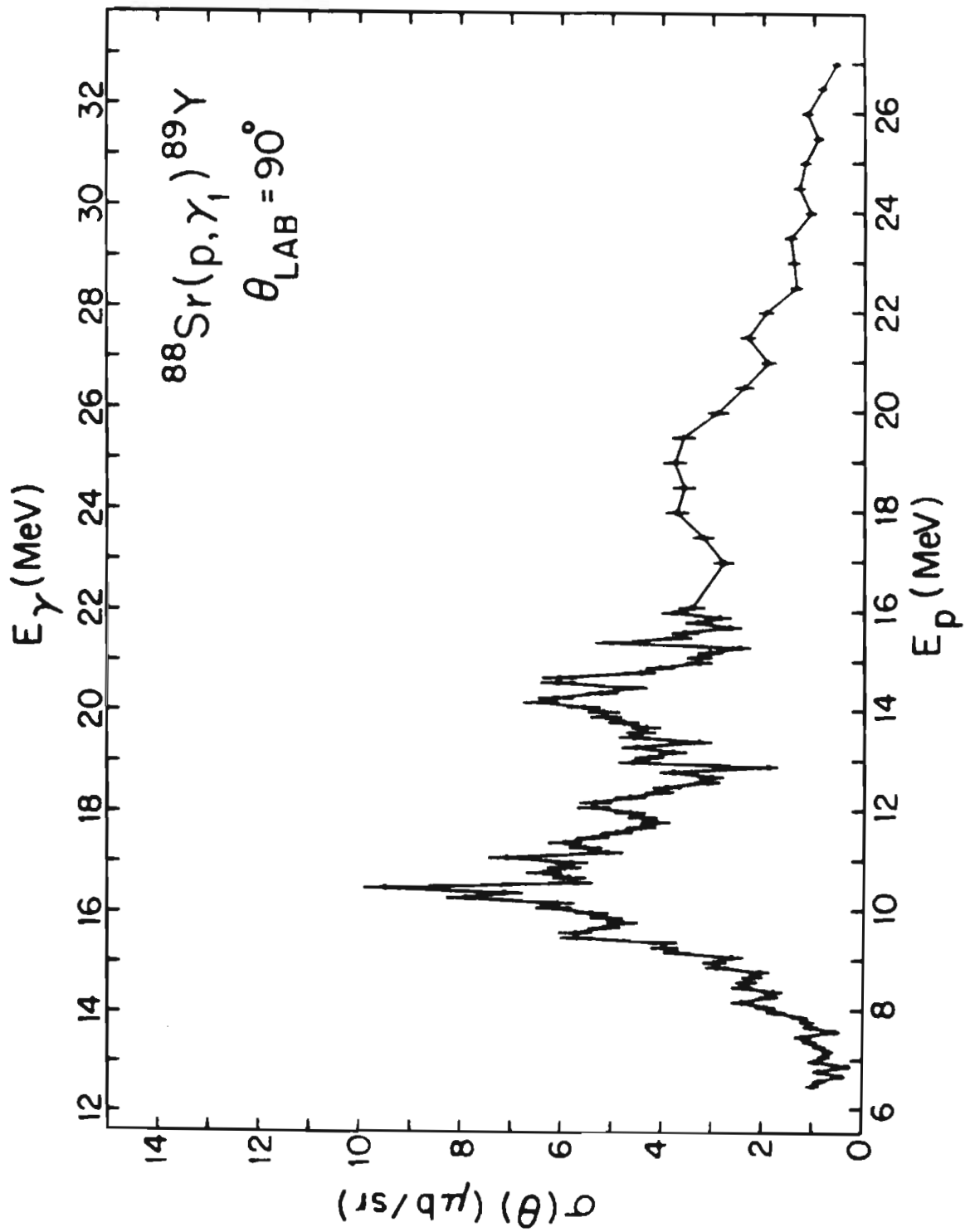
$^{88}Sr(p,\gamma_1)^{89}Y$
$\theta_{LAB} = 90°$
E_γ (MeV)
E_p (MeV)
$\sigma(\theta)$ (μb/sr)

Since the spins and parities of the ground state of ^{89}Y ($J^{\pi}=1/2^{-}$) and the first excited state ($J^{\pi}=9/2^{+}$) are different, the El radiation which decays to each must originate from different excited states. Excitation of these different states requires different reaction amplitudes in the formation channel, which in this experiment, is the entrance channel of the captured proton. Because of this difference of origin, the γ_0 and γ_1 excitation curves actually represent two distinct giant dipole resonances. It is common to distinguish between them by referring to the GDR's "built upon" the ground state or the first excited state.

It has been suggested {see summaries by (Hayward, 1970) and (P. Paul, 1973)} that the GDR might be split into two isospin components ($T_<=T_0$ and $T_>=T_0+1$, where in this case, T_0 is the isospin of the ground state of ^{89}Y). An estimate of the magnitude of this splitting (R. O. Akyuz and S. Fallieros, 1971) has been given as

$$\Delta E = \frac{60\,(T_0+1)}{A} \quad MeV \qquad (3)$$

which for ^{89}Y suggests a splitting of 4.3 MeV.

Evidence for isospin splitting in this nucleus has been discussed on the basis of some unpublished work (see J. D.

Vergados and T. T. S. Kuo, 1971) which extended only to E_p=16.0 MeV. It was proposed that the three peaks around E_p≃12.0, 13.5, and 15.5 MeV contained the $T_>$ strength of the γ_o GDR. It is interesting to note that the $^{89}Y(\gamma,n)^{88}Y$ reaction also indicates the presence of these three peaks (A. Lepretre, et al., 1971). In the present work the cross section has been extended to E_p=27 MeV. This data indicates two additional peaks at E_p≃17 and 19 MeV which suggests that the $T_>$ strength in the γ_o GDR may be located in five peaks instead of three and is spread more than previously suggested.

The two lowest peaks in the γ_1 cross section at E_p≃17 and 20 MeV were also proposed as the $T_<$ and $T_>$ parts of the γ_1 GDR. Extending the γ_1 cross section revealed a third peak at E_p≃19 MeV. This peak makes the separation of the γ_1 GDR into $T_<$ and $T_>$ parts much more complicated.

The (p,γ) cross section can be converted to a photon absorption cross section by the method of detailed balancing (E. G. Fuller and E. Hayward, 1962) via the expression

$$\sigma(\gamma,p) = \frac{2J_{A-1}+1}{2J_A+1} \quad \frac{A-1}{A} \quad \frac{2Mc^2\,(E_{ex}-T)^2}{E_{ex}^2}\,\sigma(p,\gamma) \qquad (4)$$

where J_{A-1} and J_A are the spins of the initial and final nuclei in the proton capture reaction. T, E_{ex}, and M are the proton binding energy, the excitation energy of the nucleus of mass A, and a nucleon mass, respectively. The cross section for the $^{89}Y(\gamma,p_o)^{88}Sr$ reaction is shown in fig. 7. The energy integrated strength for this curve is 15.5 mb· MeV which represents only about 1.2% of the dipole sum rule (see Appendix C). Similar evaluation of the γ_1 excitation curve represents about 1.4% of the dipole sum rule. A comparison of this data with the (γ,n) data of Lepretre et al. (1971) which exhausts almost 100% of the dipole sum rule indicates that most of the strength for nuclear gamma-ray absorption is in the neutron decay channel.

C. Angular Distributions of the Cross Section and Analyzing Power for the $^{88}Sr(\vec{p},\gamma_o)^{89}Y$ Reaction

The capture of a particle with total angular momentum $\vec{L}_1=\vec{\ell}_1+\vec{x}_1$ by a nucleus with spin $\vec{I}_i$ leads to an excited state with angular momentum $\vec{J}$. The quantities $\vec{\ell}_1$ and $\vec{x}_1$ are the orbital angular momentum and the spin of the captured particle, respectively. The excited level may decay by gamma radiation of multipolarity L_2 to the ground state (or excited state) with spin $\vec{I}_F$. This process may be depicted as

Figure 7. The differential cross section for the $^{89}Y(\gamma,p_o)^{88}Sr$ reaction obtained from the proton capture cross section by the method of detailed balancing. The energy is center of target energy.

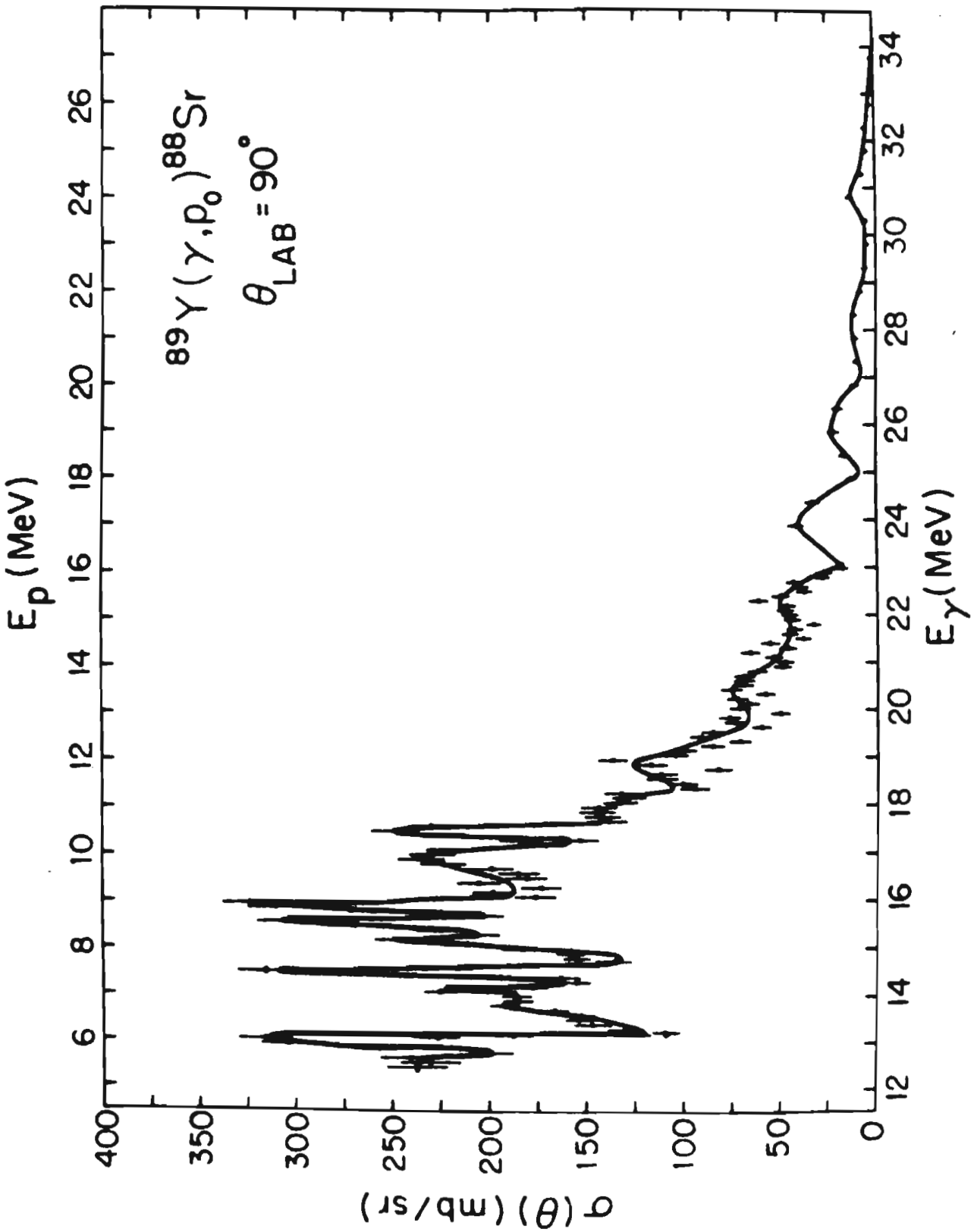
$^{89}Y(\gamma,p_0)^{88}Sr$
$\theta_{LAB} = 90°$
E_p (MeV)
E_γ (MeV)
$\sigma(\theta)$ (mb/sr)

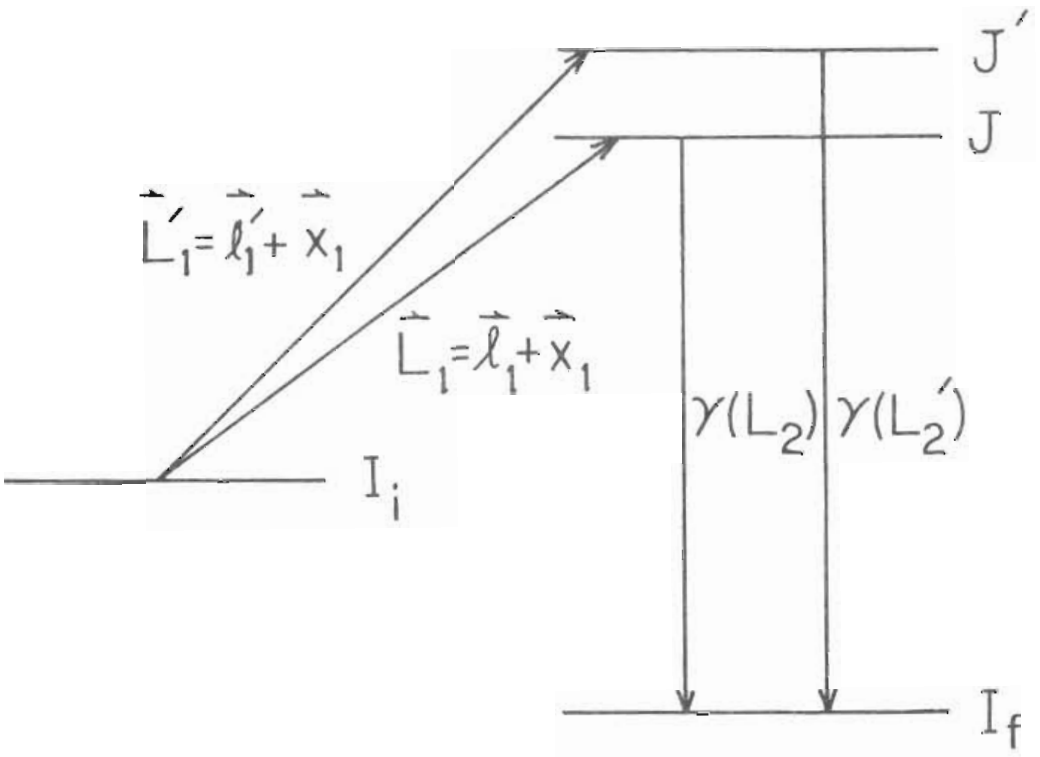

The primed quantities represent the possibility different levels which may be excited and whose subsequent gamma decay may interfere with the unprimed decay. The general expression for the differential cross section has been derived by Blatt and Biedenharn (1952) and corrected by Huby (1954) to be given by

$$\frac{d\sigma}{d\Omega} = \frac{\lambda^2}{4(2I_i+1)(2X_1+1)} \sum_{\substack{k\,\ell\,\ell' \\ L_2 L_2' S_1}} (-)^{S_1 - I_f} \bar{Z}(\ell_1 J \ell_1' J'; S_1 k)\, \bar{Z}_1(L_2 J L_2' J'; I_f k) \times Re\{R R'^*\}\, P_k(\cos\theta) \qquad (5)$$

where $R = \langle L_2 J \| T \| \ell_1 L_1 J \rangle$ and $R' = \langle L_2' J' \| T \| \ell_1' L_1' J' \rangle$

where T is the transition matrix for the system and the entrance channel spin $\vec{s}_1$ is defined by $\vec{s}_1=\vec{I}_i+\vec{x}_1$. The quantities $\lambda\!\!\!^{-2}$ and θ are reduced proton wavelength and center of mass reaction angle, respectively. The $\bar{z}$ and $\bar{z}_1$ coefficients are defined by Devons and Goldfarb (1957).

The analyzing power defined by eq. (1), presented as $\sigma(\theta)A(\theta)$, may be written as (Glavish, 1974)

$$\sigma(\theta)A(\theta)=\sum_{\beta}\frac{(-)^{q}f}{2I_i+1}\hat{J}^2\hat{J}'^2\hat{L}_2\hat{L}_2'\hat{L}_1\hat{L}_1'\hat{l}_1\hat{l}_1'\left\{\frac{3(2k+1)}{k(k+1)}\right\}^{\frac{1}{2}}\langle k1|k1o1\rangle$$

$$\times\langle ko|l_1l_1'oo\rangle\langle ko|L_2L_2'1\text{-}1\rangle W(L_2JL_2'J';I_fk)W(L_1JL_1'J';I_ik)$$

$$\times\begin{Bmatrix} l_1 & x_1 & L_1 \\ l_1' & x_1 & L_1' \\ k & 1 & k \end{Bmatrix}\quad Im\{RR'^{*}\}\,P_k^1(\cos\theta) \qquad (6)$$

WHERE :

$$\beta = l_1\,l_1'\,L_1\,L_1'\,J\,J'\,L_2\,L_2'\,k$$

$$f=\frac{1}{2}\left(1\pm(-)^{L_2+L_2'+k}\right)\begin{cases} + & \text{PURE } E(\lambda) \text{ OR } M(\lambda) \\ - & \text{MIXED } E(\lambda) \text{ AND } M(\lambda)\end{cases}$$

$$q=l_1'+L_1'+I_i-I_f-2x_1+1$$

$$\hat{x}_1^2=2x_1+1\quad,\ \text{etc.}$$

where the W's are Racah coefficients.

The experimental cross sections measured in this experiment were fitted with a least squares criterion to eq. (5) rewritten as

$$\sigma(\theta) = \sum_k Q_k a_k P_k(\cos\theta) \tag{7}$$

where Q_k is a geometrical correction factor resulting from the finite detector size (Ferguson, 1965). Center of mass corrections and statistical errors were taken into account as well.

Similarly the analyzing power measurements, presented in terms of the quantity $\sigma(\theta)A(\theta)/a_o$, were also fitted to eq. (6) rewritten in the form

$$\frac{\sigma(\theta)A(\theta)}{a_o} = \sum_k Q_k b_k P_k^1(\cos\theta) \tag{8}$$

The normalization is chosen here such that a_o is set equal to 1.0. The geometrical factors Q_k, the depolarization effects due to azimuthal angular range, and center of mass corrections were taken into account. The data along with these fits are shown in figs. 8 - 11.

Figure 8. Angular distributions from the $^{88}Sr(\vec{p},\gamma_o)^{89}Y$ reaction for the quantities $\sigma(\theta)/a_o$ and $\sigma(\theta)A(\theta)/a_o$ for E_p=6.05 and 6.20 MeV. The error bars represent the statistical errors associated with the data points. The solid curves are the result of fitting the data as described in the text.

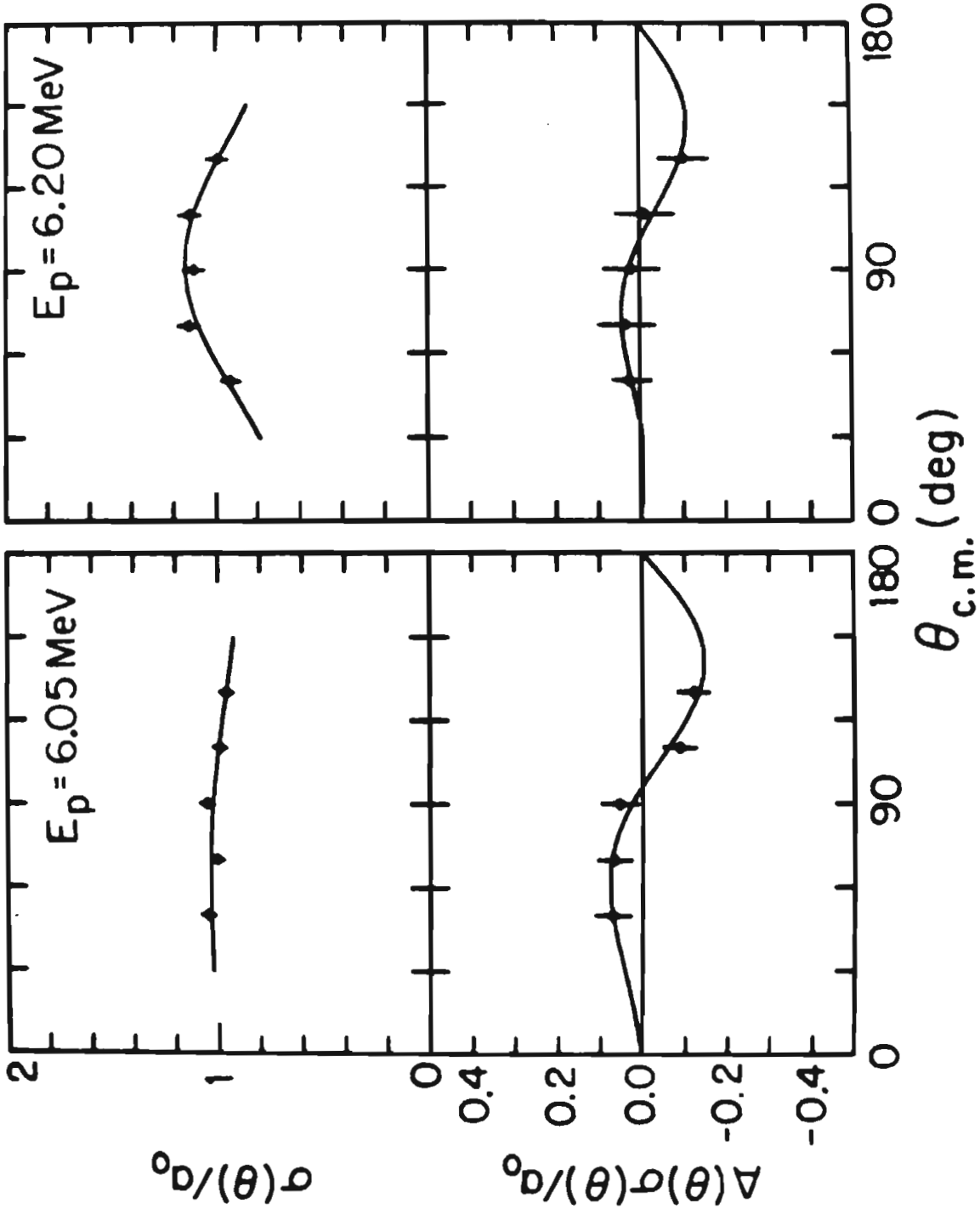
E_p= 6.05 MeV
E_p= 6.20 MeV
$\sigma(\theta)/\sigma_0$
$A(\theta)\sigma(\theta)/\sigma_0$
$\theta_{c.m.}$ (deg)
2
1
0
0.4
0.2
0.0
-0.2
-0.4
0
90
180

Figure 9. Angular distributions from the $^{88}Sr(\vec{p},\gamma_o)^{89}Y$ reaction for the quantities $\sigma(\theta)/a_o$ and $\sigma(\theta)A(\theta)/a_o$ for E_p=7.45, 7.55, 7.75, and 8.30 MeV. The error bars represent the statistical errors associated with the data points. The solid curves are the result of fitting the data as described in the text.

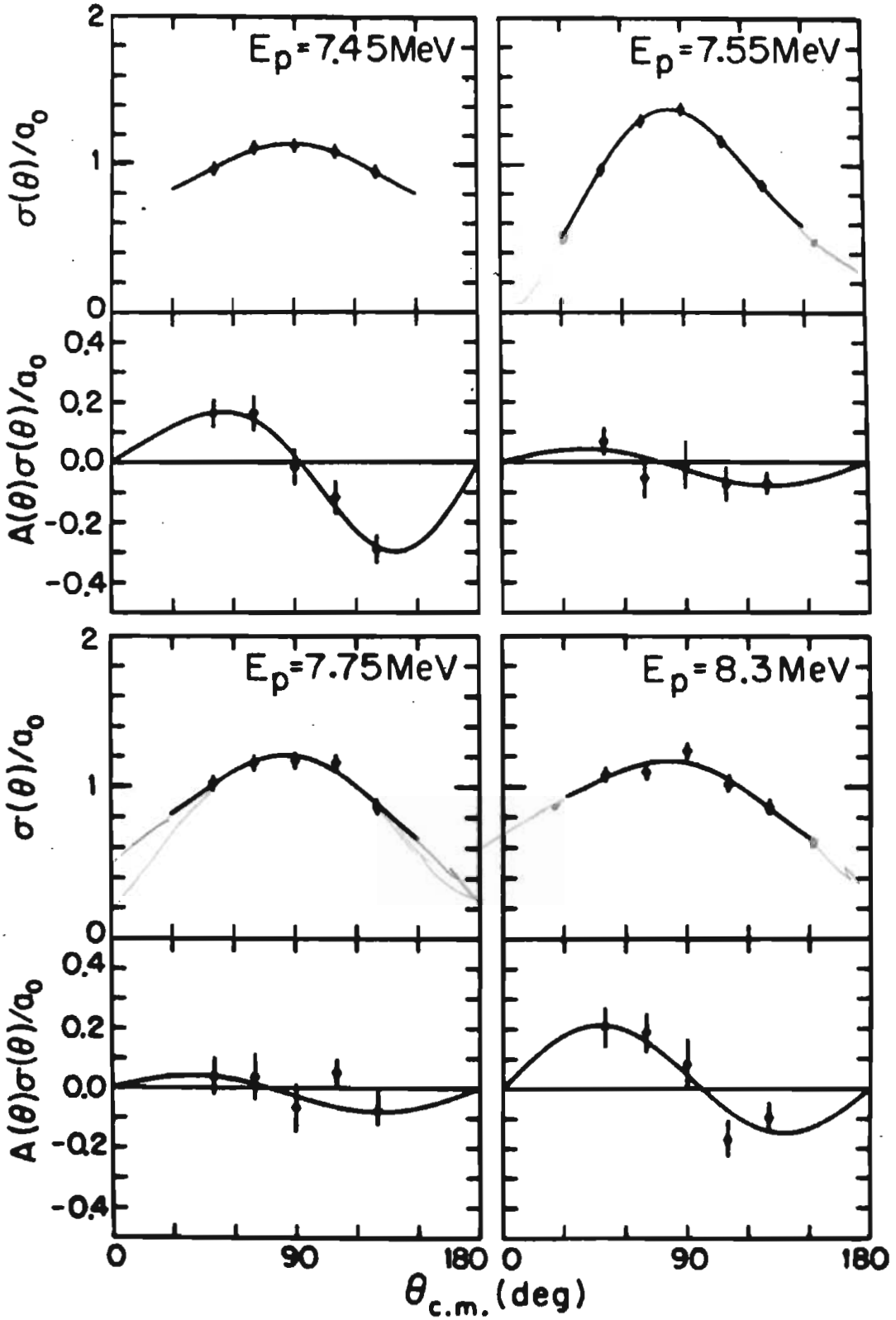
E_p=7.45MeV
E_p=7.55MeV
E_p=7.75MeV
E_p=8.3MeV
$\sigma(\theta)/a_0$
$A(\theta)\sigma(\theta)/a_0$
2
1
0
0.4
0.2
0.0
-0.2
-0.4
0
90
180
$\theta_{c.m.}$ (deg)

Figure 10. Angular distributions from the $^{88}Sr(\vec{p},\gamma_0)^{89}Y$ reaction for the quantities $\sigma(\theta)/a_0$ and $\sigma(\theta)A(\theta)/a_0$ for E_p=9.85, 10.50, 12.00, and 14.30 MeV. The error bars represent the statistical errors associated with the data points. The solid curves are the result of fitting the data as described in the text.

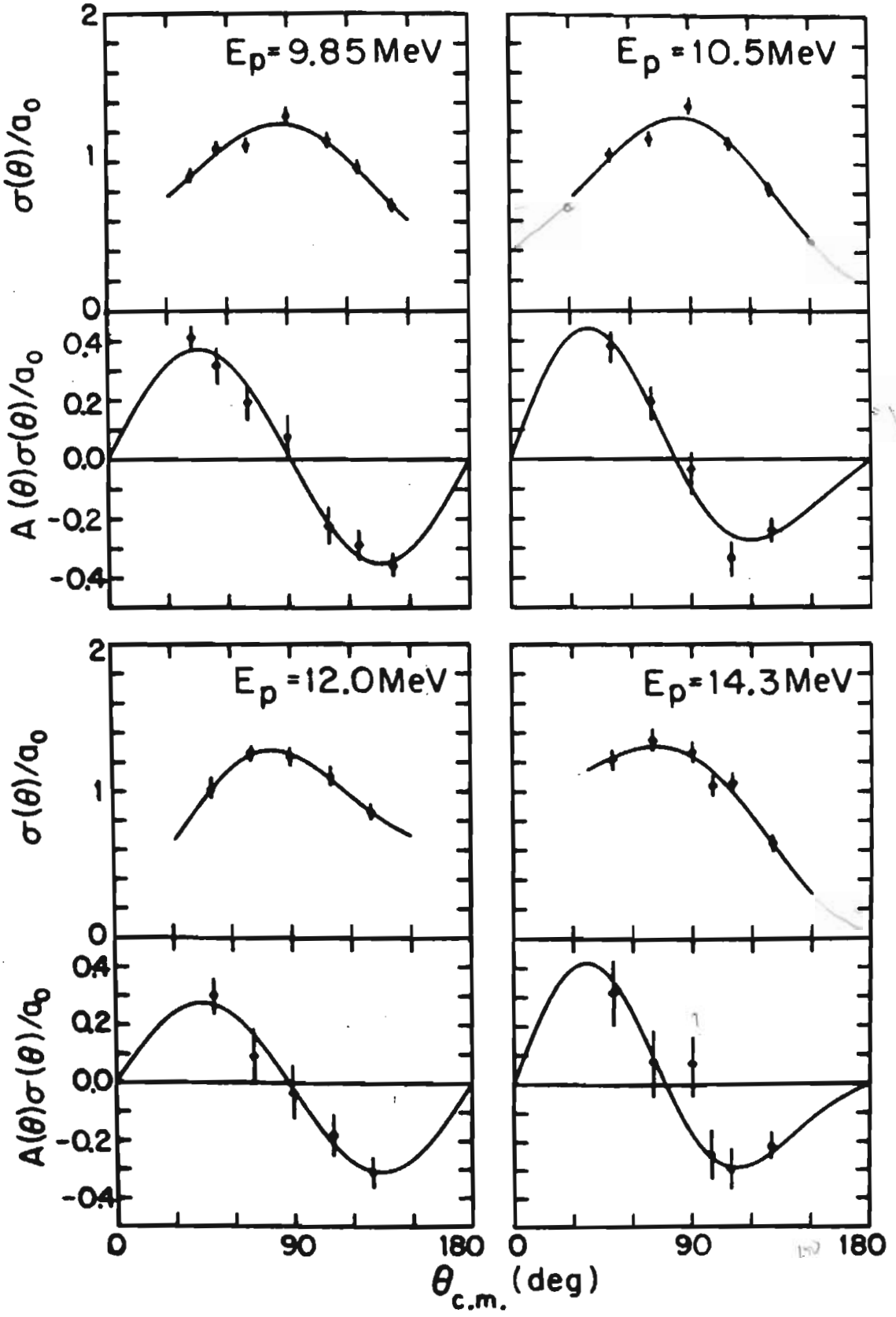
E_p= 9.85 MeV
E_p = 10.5MeV
E_p = 12.0MeV
E_p = 14.3MeV
$\sigma(\theta)/a_0$
$A(\theta)\sigma(\theta)/a_0$
2
1
0
0.4
0.2
0.0
-0.2
-0.4
0
90
180
$\theta_{c.m.}$ (deg)

Figure 11. Angular distributions from the $^{88}Sr(\vec{p},\gamma_0)^{89}Y$ reaction for the quantities $\sigma(\theta)/a_0$ and $\sigma(\theta)A(\theta)/a_0$ for E_p=8.90, 13.00, 10.90, and 15.00 MeV. The error bars represent the statistical errors associated with the data points. The solid curves are the result of fitting the data as described in the text. Note the scale for $\sigma(\theta)A(\theta)/a_0$ extends to ±1.0 for E_p=10.90 and 15.00 MeV.

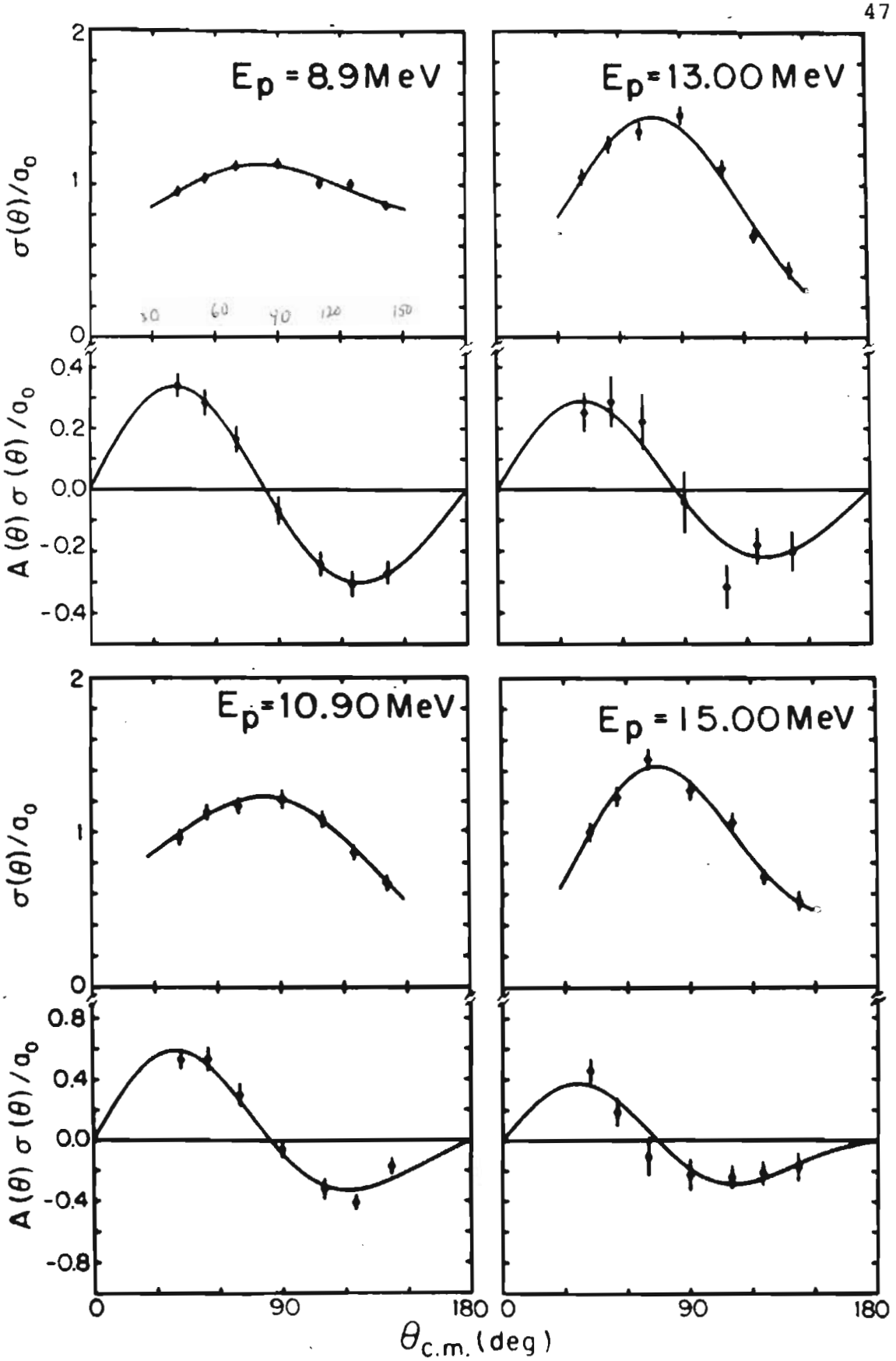
E_p = 8.9 MeV
E_p = 13.00 MeV
E_p = 10.90 MeV
E_p = 15.00 MeV
$\sigma(\theta)/a_0$
$A(\theta)\,\sigma(\theta)/a_0$
2
1
0
0.4
0.2
0.0
-0.2
-0.4
0.8
-0.8
0
90
180
$\theta_{c.m.}$ (deg)

The a_k and b_k coefficients obtained in this manner at the fourteen energies studied throughout the region of the giant dipole resonance are presented in Table I. The normalized χ^2 values obtained indicated that in all the cases studied terms having order equal four or greater were not statistically justified. In some cases, order less than three was statistically adequate to represent the data. The a_k and b_k coefficients are plotted versus proton energy in fig. 12.

The experimentally determined a_k and b_k coefficients may be related to the amplitudes of transition matrix amplitudes via eqs. (5) and (6). As will be seen below, these equations are, of course, non-linear and rather complex. The approach taken in this work is to first solve the equations assuming only E1 radiation. This allowed an understanding of the major amplitudes which are involved in the decay of GDR. The second step was then to include the smaller amplitudes which would be necessary for E2 (or M1) decay.

In ^{89}Y, the ground state is $1/2^-$ which means electric dipole (E1) radiation must come from excited states with spin and parity of $1/2^+$ or $3/2^+$. Since the ^{88}Sr target has 0^+ spin and parity, angular momentum and parity conservation require the captured proton to have ℓ equal zero or two. Furthermore, the intrinsic spin of the proton must couple to the orbital angular momentum such that the incident proton possesses total angular

Table I. The a_k and b_k Coefficients for the $^{88}Sr(\vec{p},\gamma_o)^{89}Y$ Reaction

E_p(MeV)	a_1	a_2	a_3	b_1	b_2	b_3
6.05	0.059±0.032	-0.043±0.060	0.0 ±0.109	0.006±0.020	0.070±0.016	-0.022±0.017
6.20	-0.035±0.047	-0.291±0.092	0.0 ±0.166	-0.009±0.032	0.040±0.024	-0.025±0.026
7.45	0.019±0.042	-0.297±0.083	0.0 ±0.147	-0.025±0.026	0.154±0.019	-0.032±0.021
7.55	0.003±0.081	-0.750±0.075	-0.165±0.128	-0.024±0.026	0.041±0.017	0.0 ±0.022
7.75	0.097±0.048	-0.422±0.098	0.0 ±0.173	-0.027±0.038	0.041±0.025	0.0 ±0.030
8.3	0.154±0.045	-0.327±0.090	0.0 ±0.156	0.046±0.031	0.122±0.023	0.0 ±0.026
8.9	0.029±0.029	-0.246±0.038	-0.061±0.054	-0.029±0.018	0.212±0.011	0.025±0.011
9.85	0.087±0.027	-0.510±0.049	0.0 ±0.068	0.017±0.027	0.245±0.015	-0.001±0.015
10.50	0.149±0.040	-0.613±0.089	0.0 ±0.145	-0.007±0.031	0.210±0.024	0.060±0.031
10.90	0.178±0.033	-0.436±0.058	0.0 ±0.083	0.019±0.032	0.319±0.018	0.057±0.017

Table I. (continued)

E_p (MeV)	a_1	a_2	a_3	b_1	b_2	b_3
12.00	0.034±0.120	-0.533±0.106	-0.181±0.185	-0.022±0.037	0.199±0.025	0.0 ±0.029
13.00	0.341±0.039	-0.744±0.062	-0.174±0.082	-0.001±0.033	0.169±0.017	0.023±0.015
14.30	0.458±0.057	-0.488±0.112	0.0 ±0.208	-0.052±0.046	0.206±0.035	0.082±0.031
15.00	0.237±0.046	-0.660±0.069	-0.318±0.093	-0.069±0.038	0.182±0.020	0.079±0.019

The higher order coefficients are given only when the normalized χ^2 justified their use.

Figure 12. The a_k and b_k coefficients obtained by fitting the data of figs. 8, 9, 10, and 11 as described in the text. The error bars represent statistical errors. All coefficients have been normalized such that a_o equals 1.0. The numerical values of the coefficients and errors are given in Table I.

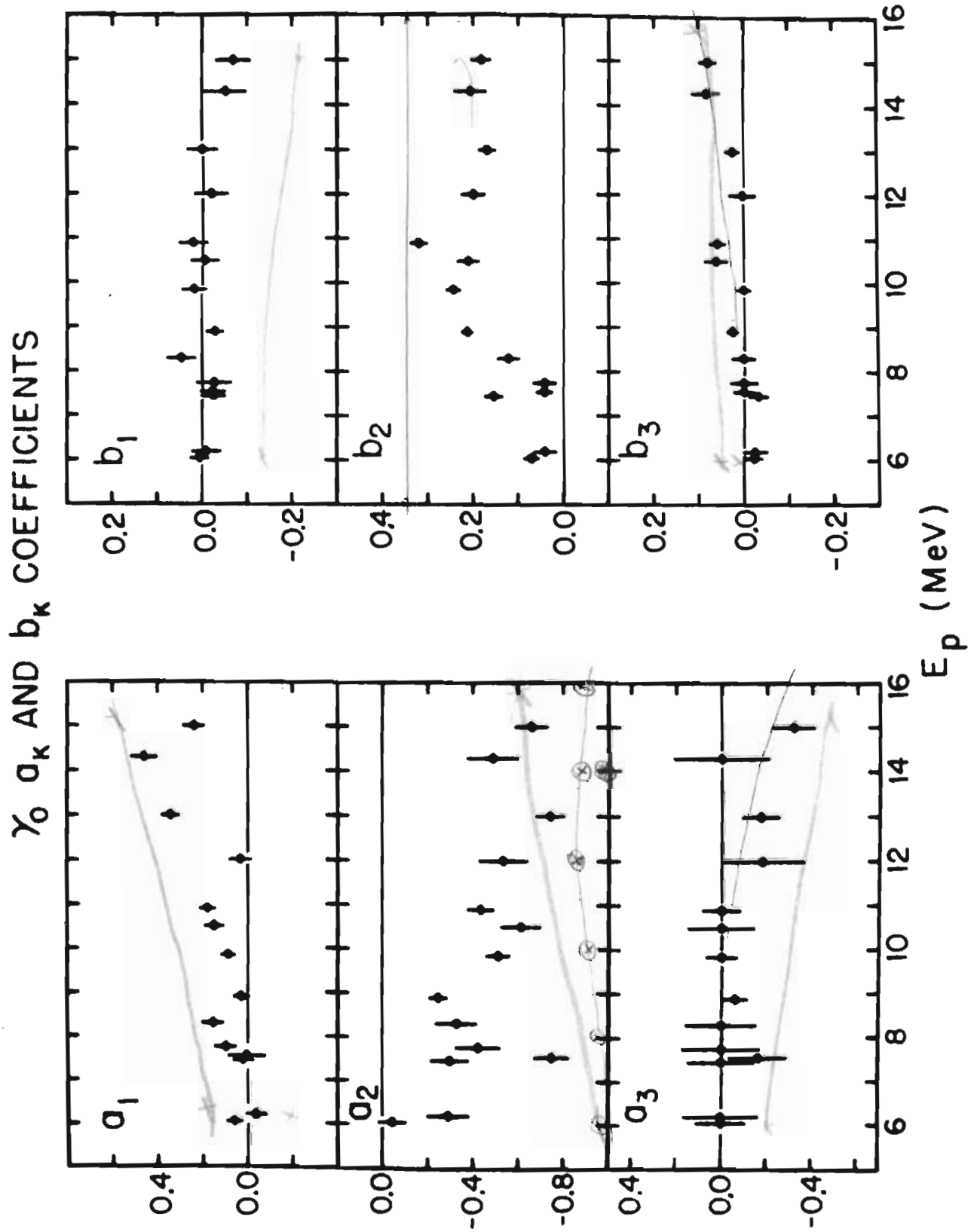
γ_0 a_k AND b_k COEFFICIENTS
a_1
a_2
a_3
b_1
b_2
b_3
E_p (MeV)

momentum of either 1/2 or 3/2 in order to populate the necessary excited states in ^{89}Y for E1 decay. These two proton configurations will be labeled as $s_{1/2}$ and $d_{3/2}$. The corresponding transition matrix elements will be designated as $s_{1/2}(E1)$ and $d_{3/2}(E1)$. Evaluating eqs. (5) and (6) with the assumption of pure E1 radiation yields only three non-zero coefficients

$$a_0 = S_{\frac{1}{2}}(E1)^2 + 2d_{\frac{3}{2}}(E1)^2$$

$$a_2 = -2S_{\frac{1}{2}}(E1)d_{\frac{3}{2}}(E1)\cos(\phi_s - \phi_d) - d_{\frac{3}{2}}(E1)^2 \qquad (9)$$

$$b_2 = S_{\frac{1}{2}}(E1)d_{\frac{3}{2}}(E1)\sin(\phi_s - \phi_d)$$

where ϕ_s-ϕ_d represents the overall phase difference between the two transition matrix elements. With the experimentally determined a_2 and b_2 coefficients, eqs. (9) may be solved explicitly for the two matrix elements and their relative phase. Two solutions are found from these equations. The first solution indicates that the E1 decay primarily results from the $s_{1/2}(E1)$ transition matrix element while the second solutions indicates that $d_{3/2}(E1)$ is the major constituent. The results

for $s_{1/2}(El)$, $d_{3/2}(El)$, and $\phi_s-\phi_d$ are presented in Table II for the fourteen energies which were measured. The two solutions are plotted as a function of proton energy in fig. 13. It is impossible with this pure El analysis to determine which of the two solutions is the correct one. The possibility of distinguishing the true composition will be investigated in a later section by utilizing the interference of isobaric analogue states (IAS) with the giant dipole resonance.

Both of the two solutions exhibit, in general, a relatively smooth trend. A notable exception to this is in the relative phase in the vicinity of the IAS at E_p=7.50 MeV. This behavior can be attributed to the single level interference of the IAS with the giant dipole background. This behavior is noticable to a lesser extent around the IAS at E_p=6.06 MeV.

Using previously determined optical model parameters (Genz, et al., 1975), optical phase shifts were calculated and plotted as the dashed curve in fig. 13. They follow the same trend versus energy as the ones calculated from the angular distributions. The difference in the two phases may be attributed to the resonant phase of the GDR.

A simple El analysis such as this is not acceptable since it does not account for the odd order a_k and b_k coefficients which are experimentally observed. These coefficients can only be explained by gamma radiation of a different type or

Table II. El Solutions to γ_o Angular Distributions

E_p (MeV)	Solution I $s_{1/2}$ (%)	Solution I $2d_{3/2}$ (%)	Solution I $\phi_d-\phi_s$ (deg)	Solution II $s_{1/2}$ (%)	Solution II $2d_{3/2}$ (%)	Solution II $\phi_d-\phi_s$ (deg)
6.25	98.9	1.1	-74.9	10.3	89.7	-161.0
6.20	95.9	4.1	-16.5	2.3	97.7	-157.9
7.45	91.3	8.7	-50.6	6.6	93.4	-118.9
7.55	73.6	26.4	-7.6	4.2	95.8	-16.8
7.75	91.7	8.3	-12.2	0.6	99.4	-132.4
8.30	92.3	7.7	-40.2	4.3	95.7	-121.8
8.90	87.8	12.2	-66.4	12.4	87.6	-114.4
9.85	74.3	25.7	-51.9	14.1	85.9	-80.6
11.50	72.2	27.8	-41.5	11.6	88.4	-67.8
12.90	62.5	37.5	-68.7	29.2	70.8	-82.7
12.00	78.4	21.6	-43.1	9.0	91.0	-78.9
13.00	66.4	33.6	-30.4	11.6	88.4	-48.2
14.30	80.0	20.0	-46.7	9.4	90.6	-85.1
15.00	72.0	28.0	-35.0	9.8	90.2	-60.2

Figure 13. The two solutions obtained from a pure E1 analysis of the coefficients a_o, a_2, and b_2 of Table II for $^{88}Sr(\vec{p},\gamma_o)^{89}Y$. The amplitudes are expressed as a percentage of a_o. The solid lines serve only to connect the points. The dashed line is an optical model calculation of the phase difference.

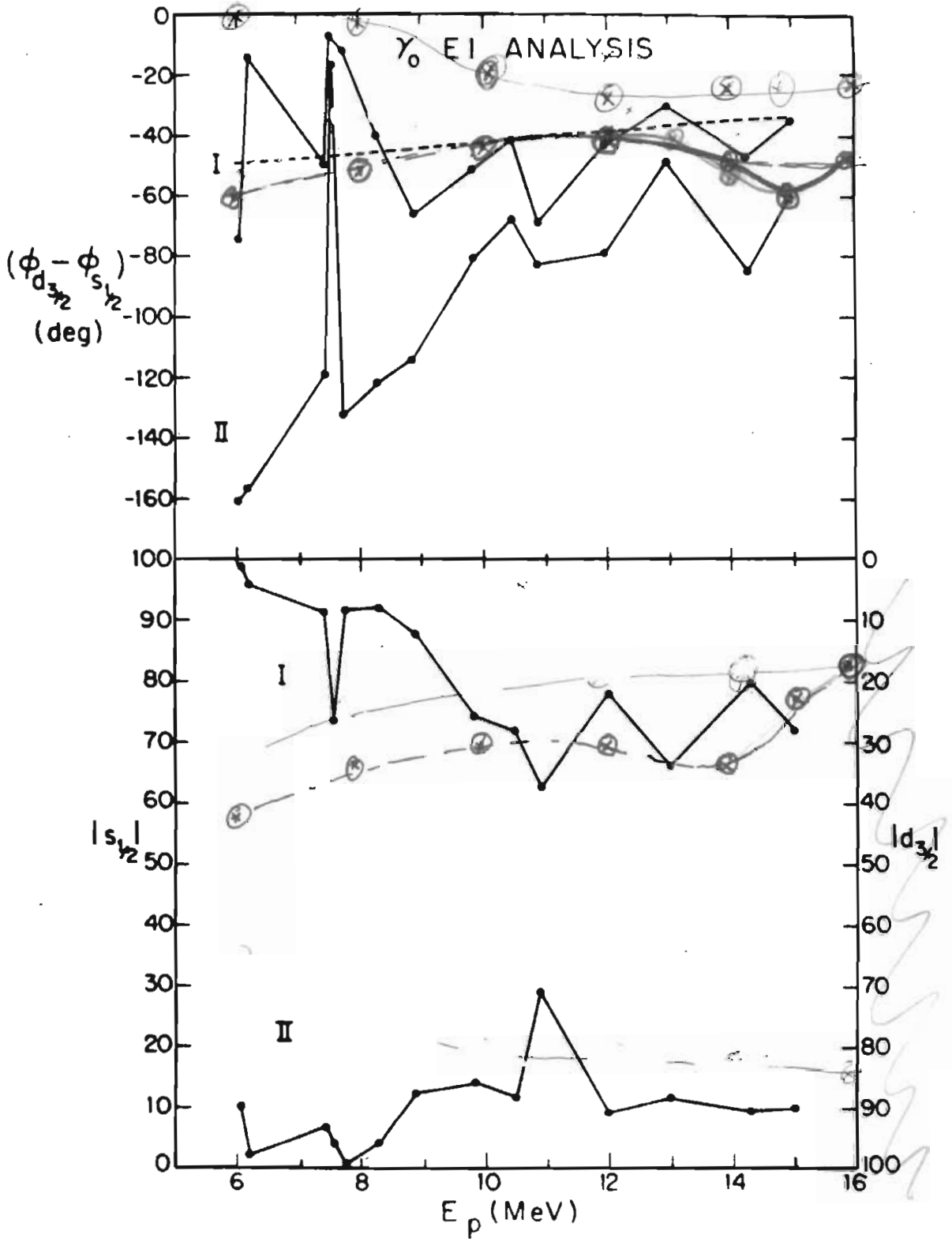
γ_0 E1 ANALYSIS
$(\phi_{d_{3/2}} - \phi_{s_{1/2}})$ (deg)
I
II
$|s_{1/2}|$
$|d_{3/2}|$
E_p (MeV)

multipolarity, such as magnetic dipole (M1) or electric quadrupole (E2). Higher electric or magnetic multipoles in this excitation region (about 17 MeV) should be more inhibited than these two types, and therefore will not be considered. Furthermore, the compilation of gamma-ray strength by Endt and van der Leun (1974) indicates that a histogram of Γ_γ/Γ_W strength for isospin allowed M1 radiation peaks at about 7×10^{-2}, where Γ_γ is the experimentally measured gamma-ray strength and Γ_W is the Weisskopf single particle estimate. Evaluation of Γ_W for M1 and E2 for ^{89}Y in the excitation region of the GDR (17 MeV) gives 103 eV and 27 eV, respectively. Using the previous hindrance factor for M1, results in a ratio of $\Gamma(E2)/\Gamma(M1)$ of approximately 4. This result would imply that, in an approximation, only E2 strength needs to be considered to explain the odd a_k and b_k coefficients. It should be noted that the Endt and van der Leun tabulation is only for bound states in the A=21-44 mass region. However, work by Wimpey (1974) indicates that in general the same ratio of strengths may be expected for higher atomic masses and unbound states ($E_{ex} \approx 10\text{-}12$ MeV) which seems to justify excluding M1 radiation from the analysis.

Perhaps a stronger argument for excluding M1 amplitudes can be made by calculating the expected location of collective M1 strength. A calculation by Bohr and Mottelson (1975) indicates that the location of this strength may be estimated as

$$E(M1) = \hbar\omega - \hbar\omega_o\sqrt{1 + \frac{\kappa}{C}} \qquad (10)$$

where C is the restoring force parameter associated with collective oscillations and κ is the interaction strength. The unperturbed energy $h\omega_o$ is equal to the spin-orbit energy splitting $\{h\omega_o=\varepsilon(j=\ell-1/2)-\varepsilon(j=\ell+1/2)\}$, taken as a mean value for neutrons and protons. It can be shown that κ and C may be related to the effective magnetic g_s factor in single-particle M1-matrix elements by the equation

$$\frac{\delta g_s}{g_s} = \frac{-\kappa}{\kappa + C} \qquad (10A)$$

Comparison of the experimental magnetic moment of ^{89}Y $\{\mu_{exp}=-0.1373$ (Brun, et al., 1954)$\}$ with the single particle value gives $\delta g_s/g_s \simeq -0.136$ which yields $\kappa/C \simeq 1/6.38$. Using the value of 6 MeV for $h\omega_o$ (Bohr and Mottelson, 1969) predicts the collective M1 strength near $E_{ex} \simeq 7$ MeV. Recent inelastic electron scattering data in ^{89}Y (Buskirk, 1976) tentatively assigns two peaks at an excitation energy of 6.7 and 8.05 MeV as M1 resonances. Since

this is below the region investigated in this work, it seems justified to exclude M1 radiation from the analysis.

The analysis of the angular distributions of cross section and analyzing power was repeated with the assumption that both E1 and E2 radiation contributed. E2 radiation to the ground state of ^{89}Y can only originate from excited states possessing $J^{\pi}=3/2^{-}$ and $5/2^{-}$. Following the discussion previously used for E1 radiation, these two excited states are formed by the capture of $p_{3/2}$ and $f_{5/2}$ protons with corresponding T-matrix elements $p_{3/2}(E2)$ and $f_{5/2}(E2)$. With the additional possibility of E2 radiation the a_k and b_k coefficients given in eqs. (9) are rewritten as

$$
\begin{aligned}
a_0 &= s_{\frac{1}{2}}(E1)^2 + 2d_{3/2}(E1)^2 + 2p_{3/2}(E2)^2 + 3f_{5/2}(E2)^2 \\
a_1 &= 3.464\, s_{\frac{1}{2}}(E1)\, p_{3/2}(E2)\cos(\phi_s-\phi_p) + 0.6928\, d_{3/2}(E1)\, p_{3/2}(E2)\cos(\phi_d-\phi_p) \\
&\quad + 6.235\, d_{\frac{3}{2}}(E1)\, f_{\frac{5}{2}}(E2)\cos(\phi_d-\phi_f) \\
a_2 &= -2\, s_{\frac{1}{2}}(E1)\, d_{\frac{3}{2}}(E1)\cos(\phi_s-\phi_d) - d_{\frac{3}{2}}(E1)^2 + p_{\frac{3}{2}}(E2)^2 + 1.714\, f_{\frac{5}{2}}(E2)^2 \\
&\quad + 0.8571\, p_{\frac{3}{2}}(E2)\, f_{\frac{5}{2}}(E2)\cos(\phi_p-\phi_f) \\
a_3 &= -4.157\, d_{\frac{3}{2}}(E1)\, p_{\frac{3}{2}}(E2)\cos(\phi_d-\phi_p) - 3.464\, s_{\frac{1}{2}}(E1)\, f_{\frac{5}{2}}(E2)\cos(\phi_s-\phi_f) \\
&\quad - 2.771\, d_{3/2}(E1)\, f_{\frac{5}{2}}(E2)\cos(\phi_d-\phi_f) \\
a_4 &= -6.857\, p_{\frac{3}{2}}(E2)\, f_{\frac{5}{2}}(E2)\cos(\phi_p-\phi_f) - 1.714\, f_{\frac{5}{2}}(E2)^2 \\
b_1 &= 1.732\, s_{\frac{1}{2}}(E1)\, p_{3/2}(E2)\sin(\phi_s-\phi_p) + 1.386\, d_{3/2}(E1)\, p_{3/2}(E2)\sin(\phi_d-\phi_p) \\
&\quad - 3.118\, d_{3/2}(E1)\, f_{5/2}(E2)\sin(\phi_d-\phi_f) \\
b_2 &= s_{\frac{1}{2}}(E1)\, d_{3/2}(E1)\sin(\phi_s-\phi_d) - 0.7143\, p_{3/2}(E2)\, f_{5/2}(E2)\sin(\phi_p-\phi_f) \\
b_3 &= -1.386\, d_{3/2}(E1)\, p_{3/2}(E2)\sin(\phi_d-\phi_p) + 1.1559\, s_{\frac{1}{2}}(E1)\, f_{5/2}(E2)\sin(\phi_s-\phi_f) \\
&\quad + 0.2309\, d_{3/2}(E1)\, f_{5/2}(E2)\sin(\phi_d-\phi_f) \\
b_4 &= 1.714\, p_{3/2}(E2)\, f_{5/2}(E2)\sin(\phi_p-\phi_f)
\end{aligned}
\tag{9A}
$$

where ϕ_p and ϕ_f are the phases corresponding to $p_{3/2}(E2)$ and $f_{5/2}(E2)$, respectively. The experimental values of a_k and b_k coefficients were used to solve these equations using a least squares criterion for the four T-matrix elements and three relative phases between them (one of the four relative phases is redundant in eq. (10) since it may be expressed in terms of the others). When a_4 and b_4 were used to fit the angular distributions, they had typical errors of 0.100 and 0.025. However, they were not necessary to fit these data; therefore, they were set to zero with these errors when solving eqs. (9A). The χ^2 was defined as

$$\chi^2 = \sum_k \left(\frac{a_k^{exp} - a_k^{calc}}{\Delta a_k^{exp}} \right)^2 + \left(\frac{b_k^{exp} - b_k^{calc}}{\Delta b_k^{exp}} \right)^2 \qquad (11)$$

In order to insure all solutions were found, a computer grid search was performed by incrementing $s_{1/2}(E1)^2$, $2d_{3/2}(E1)^2$, and $2p_{3/2}(E2)^2$ in 50 steps from 0 to 1.0. The phases were simultaneously stepped in 5^o increments. The best results of the grid search were then used as the starting points in a computer gradient search code which used the method of Rosenbrock (1960) in the following way. First, the E1 amplitudes were started at the values found by the grid search but with all the E2 strength

assigned to the $2p_{3/2}(E2)^2$ amplitude. Second, the initialization assigned all the E2 strength to the $3f_{5/2}(E2)^2$ amplitude. Finally, random strengths were assigned to the two E2 amplitudes to check whether the correct solutions had been found. The results of this search are tabulated in Table III and are plotted versus proton energy in fig. 14. The errors were determined by calculating the curvature matrix, inverting it to obtain the error matrix, and assigning the square root of the diagonal elements as the errors (Bevington, 1969). As in the earlier analysis, there are double solutions for the E1 strengths. Also in some cases, there are double solutions for the E2 strengths which are either predominantly $p_{3/2}(E2)$ or $f_{5/2}(E2)$. Since $p_{3/2}(E2)$ and $f_{5/2}(E2)$ are in general quite small, determining the relative phase between them is difficult. This is reflected in the large errors on these phases. The multiple $p_{3/2}(E2)$ and $f_{5/2}(E2)$ solutions at each energy were averaged to determine the combined E2 strength. This strength was converted to a total E2 cross section and is presented in fig. 15 as a function of proton energy. This cross section has been converted to a $^{89}Y(\gamma,p_o)^{88}Sr$ cross section by the method of detailed balancing (Fuller and Hayward, 1962). The E2 strength appears to increase with energy which would be consistent with a direct E2 reaction (I. Halpern, 1973). The integrated strength of this cross section is approximately 0.5 μb/MeV. This represents only 0.3%

Figure 14. The solutions of the a_k and b_k coefficients assuming two E1 and two E2 amplitudes and the relative phases between them. The amplitudes are given in percent of a_o and the relative phases in degrees. The energy is the proton laboratory energy.

The left diagram represents $s_{1/2}(E1)$ as the major E1 amplitude. The dashed curve represents the E2 strength as primarily $f_{5/2}(E2)$ and the solid curve represents the $p_{3/2}(E2)$ as dominant. The E1 solutions are approximately the same for both E2 solutions and are connected by a single solid line.

In the right diagram, $d_{3/2}(E1)$ is the major E1 amplitude. The dashed curve represents $p_{3/2}(E2)$ as the larger E2 amplitude and the solid curve represents $f_{5/2}(E2)$ as the larger. The E1 solutions are approximately identical for both E2 solutions and are connected by a solid line.

The numerical values of these solutions are given in Table III.

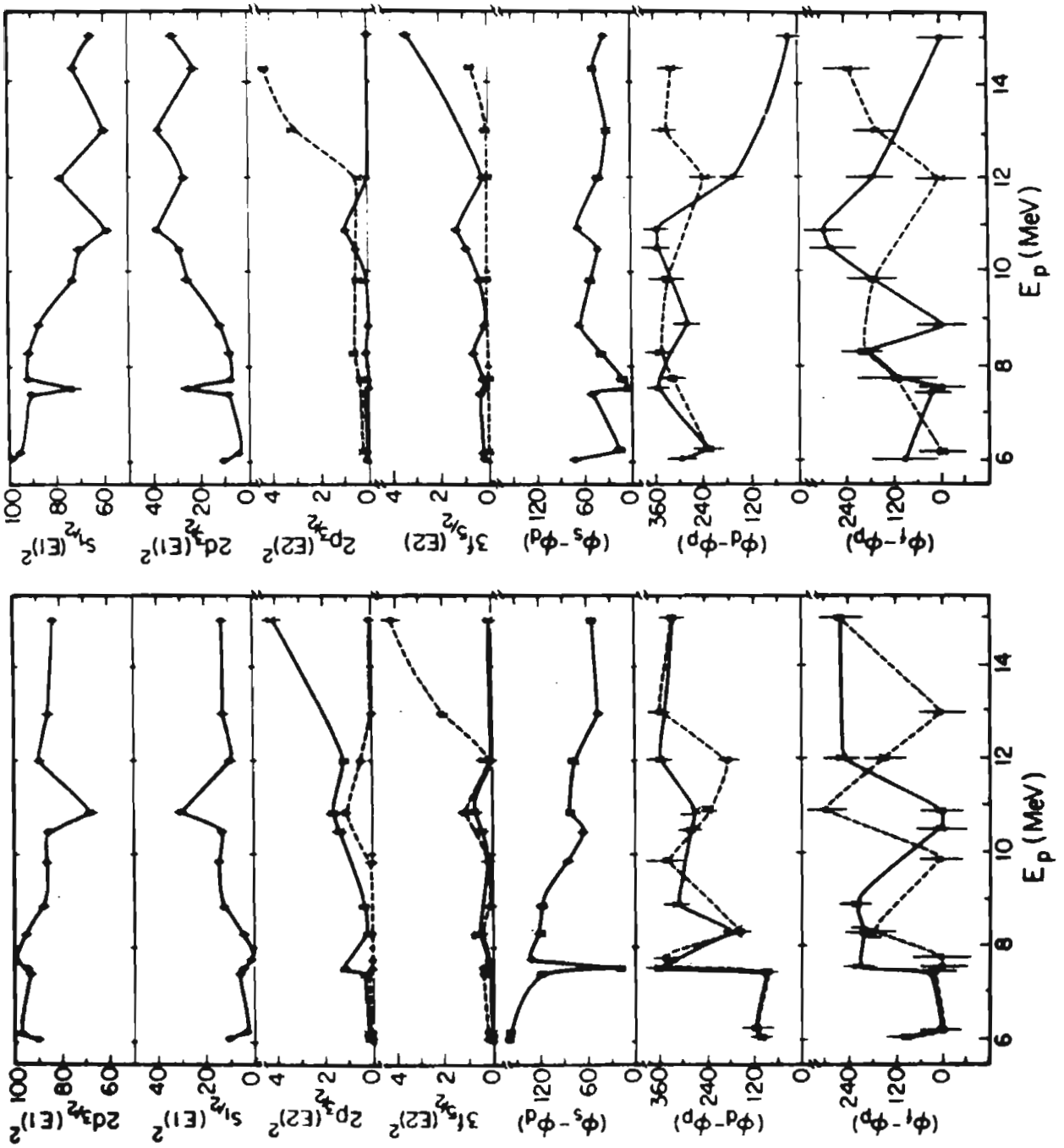
$(\phi_f - \phi_p)$
$(\phi_d - \phi_p)$
$(\phi_s - \phi_d)$
$3f_{5/2}(E2)^2$
$2p_{3/2}(E2)^2$
$s_{1/2}(E1)^2$
$2d_{3/2}(E1)^2$
E_p (MeV)

Table III. The E1 and E2 Solutions to γ_0 Angular Distributions

E_p (MeV)	$s_{1/2}(E1)^2$ (%)	$2d_{3/2}(E1)^2$ (%)	$2p_{3/2}(E2)^2$ (%)	$3f_{5/2}(E2)^2$ (%)	$\phi_d-\phi_p$ (deg)	$\phi_s-\phi_d$ (deg)	$\phi_f-\phi_d$ (deg)	χ^2
6.05	10.2+-1.8	89.6+-1.7	0.132+-0.190	0.078+-0.012	100.0+-30.0	161.0+- 3.0	98.0+-60.0	0.0009
			0.075+-0.120	0.136+-0.190	100.0+-30.0	161.0+- 3.0	98.0+-60.0	0.0026
	98.7+-2.5	1.1+-2.8	0.080+-0.130	0.128+-0.160	296.0+-37.0	74.0+- 3.0	99.0+-79.0	0.0009
6.20	2.3+-2.3	97.5+-2.2	0.189+-0.100	0.058+-0.120	113.0+-43.0	158.0+- 5.0	0.0+-68.0	0.0310
			0.060+-0.120	0.151+-0.120	113.0+-43.0	158.0+- 5.0	0.0+-62.0	0.0842
	95.6+-1.2	4.1+-1.2	0.023+-0.110	0.185+-0.120	227.0+-39.0	17.0+- 4.0	0.0+-56.0	0.9407
			0.188+-0.120	0.026+-0.110	231.0+-38.0	16.0+- 4.0	0.0+-55.0	0.0842
7.45	6.5+-1.3	93.0+-0.3	0.278+-0.110	0.223+-0.120	88.0+-32.0	118.0+- 3.0	23.0+-43.0	0.0067
			0.223+-0.110	0.278+-0.120	89.0+-31.0	118.0+- 3.0	23.0+-43.0	0.0067
	90.7+-0.5	8.8+-0.5	0.135+-0.110	0.366+-0.120	255.0+-36.0	50.0+- 3.0	26.0+-48.0	0.0067
7.55	4.7+-1.3	98.0+-1.3	0.160+-0.120	0.186+-0.120	360.0+-34.0	17.0+- 3.0	215.0+-46.0	0.0568
			0.0 +-0.120	0.315+-0.120	343.0+-36.0	17.0+- 3.0	0.0+-60.0	0.9893
	73.8+-8.3	25.3+-8.3	0.0 +-0.120	0.163+-0.120	360.0+-35.0	7.0+- 2.0	0.0+-60.0	1.5739
7.75	0.6+-2.2	99.2+-2.2	0.0 +-0.120	0.142+-0.120	345.0+-33.0	132.0+- 5.0	0.0+-80.0	0.0527
	91.8+-1.9	8.3+-2.8	0.229+-0.090	0.017+-0.110	323.0+-36.0	12.0+- 3.0	113.0+-98.0	0.0003
			0.017+-0.110	0.229+-0.190	323.0+-36.0	12.0+- 3.0	113.0+-98.0	0.0003
8.30	4.2+-2.5	95.2+-2.6	0.0 +-0.200	0.503+-0.300	187.0+-38.0	121.0+- 4.0	178.0+-61.0	0.2508
			0.131+-0.300	0.571+-0.200	164.0+-36.0	121.0+- 4.0	195.0+-68.0	0.0022
	91.8+-3.0	7.9+-2.0	0.658+-0.200	0.045+-0.050	353.0+-36.0	40.0+- 4.0	203.0+-56.0	0.0022
			0.086+-0.300	0.660+-0.210	353.0+-37.0	40.0+- 4.0	203.0+-57.0	0.0023

Table III. (continued)

E_p (MeV)	$s_{1/2}(E1)^2$ (%)	$2d_{3/2}(E1)^2$ (%)	$2p_{3/2}(E2)^2$ (%)	$3f_{5/2}(E2)^2$ (%)	$\phi_d-\phi_p$ (deg)	$\phi_s-\phi_d$ (deg)	$\phi_f-\phi_d$ (deg)	χ^2
8.90	12.4+-2.5	87.3+-1.0	0.308+-0.200	0.048+-0.200	315.0+-39.0	118.0+- 5.0	224.0+-60.0	0.0311
	87.5+-2.6	12.3+-3.1	0.0 +-0.100	0.183+-0.100	280.0+-40.0	66.0+- 5.0	0.0+-66.0	2.1873
9.85	14.1+-2.3	85.7+-2.0	0.0 +-0.100	0.132+-0.050	342.0+-41.0	81.0+- 6.0	2.0+-60.0	0.8633
	73.5+-2.0	26.0+-2.0	0.097+-0.050	0.393+-0.100	337.0+-42.0	52.0+- 6.0	174.0+-58.0	0.0024
			0.390+-0.100	0.096+-0.050	337.0+-42.0	52.0+- 5.0	174.0+-58.0	0.0024
10.50	12.8+-2.1	85.3+-1.0	1.374+-0.300	0.453+-0.300	281.0+-36.0	65.0+- 3.0	0.0+-66.0	0.6782
	70.2+-1.1	28.3+-1.0	0.525+-0.200	0.902+-0.200	360.0+-36.0	42.0+- 3.0	282.0+-60.0	0.2003
10.90	10.5+-3.4	67.1+-3.5	1.151+-0.300	1.226+-0.300	233.0+-32.0	81.0+- 4.0	299.0+-56.0	0.9918
			1.626+-0.300	0.788+-0.200	268.0+-34.0	81.0+- 4.0	0.0+-60.0	1.7474
	58.8+-1.1	38.9+-3.0	0.985+-0.300	1.362+-0.200	360.0+-35.0	69.0+- 5.0	298.0+-49.0	0.9923
12.00	9.5+-2.7	89.1+-2.6	1.174+-0.400	0.260+-0.400	360.0+-36.0	77.0+- 3.0	259.0+-40.0	0.0573
			0.424+-0.400	0.0 +-0.050	182.0+-37.0	79.0+- 2.0	144.0+-43.0	0.3677
	78.1+-2.0	21.8+-2.0	0.0 +-0.010	0.117+-0.100	168.0+-41.0	43.0+- 4.0	175.0+-48.0	0.9827
			0.032+-0.020	0.0 +-0.070	233.0+-30.0	43.0+- 4.0	0.0+-60.0	0.9473
13.00	12.6+-2.4	85.4+-2.0	0.0 +-0.040	2.007+-0.300	360.0+-30.0	46.0+- 6.0	0.0+-60.0	0.3646
	59.7+-3.6	37.1+-3.7	3.152+-0.700	0.028+-0.010	339.0+-30.0	30.0+- 4.0	160.0+-49.0	0.0371
14.30	72.5+-2.4	22.5+-3.8	4.290+-0.800	0.680+-0.200	322.0+-40.0	47.0+- 5.0	234.0+-53.0	0.3289
15.00	12.2+-1.9	83.6+-1.8	4.132+-0.500	0.047+-0.070	325.0+-40.0	54.0+- 3.0	258.0+-57.0	0.0175
			0.046+-0.010	4.130+-0.500	325.0+-35.0	54.0+- 4.0	260.0+-51.0	0.0175
	65.2+-2.1	31.5+-2.4	0.0 +-0.050	3.347+-0.400	21.0+-30.0	34.0+- 4.0	0.0+-62.0	0.6925

Figure 15. The E1 and E2 cross sections obtained as described in the text. The E1 and E2 cross sections were determined by respectively summing the two E1 and two E2 amplitudes together. The cross sections have been converted to $^{89}Y(\gamma,p_o)^{88}Sr$ via detailed balancing. The dashed curve represents the isoscalar E2 resonance using parameters obtained from inelastic electron scattering and converted to a (γ,p_o) cross section as described in the text.

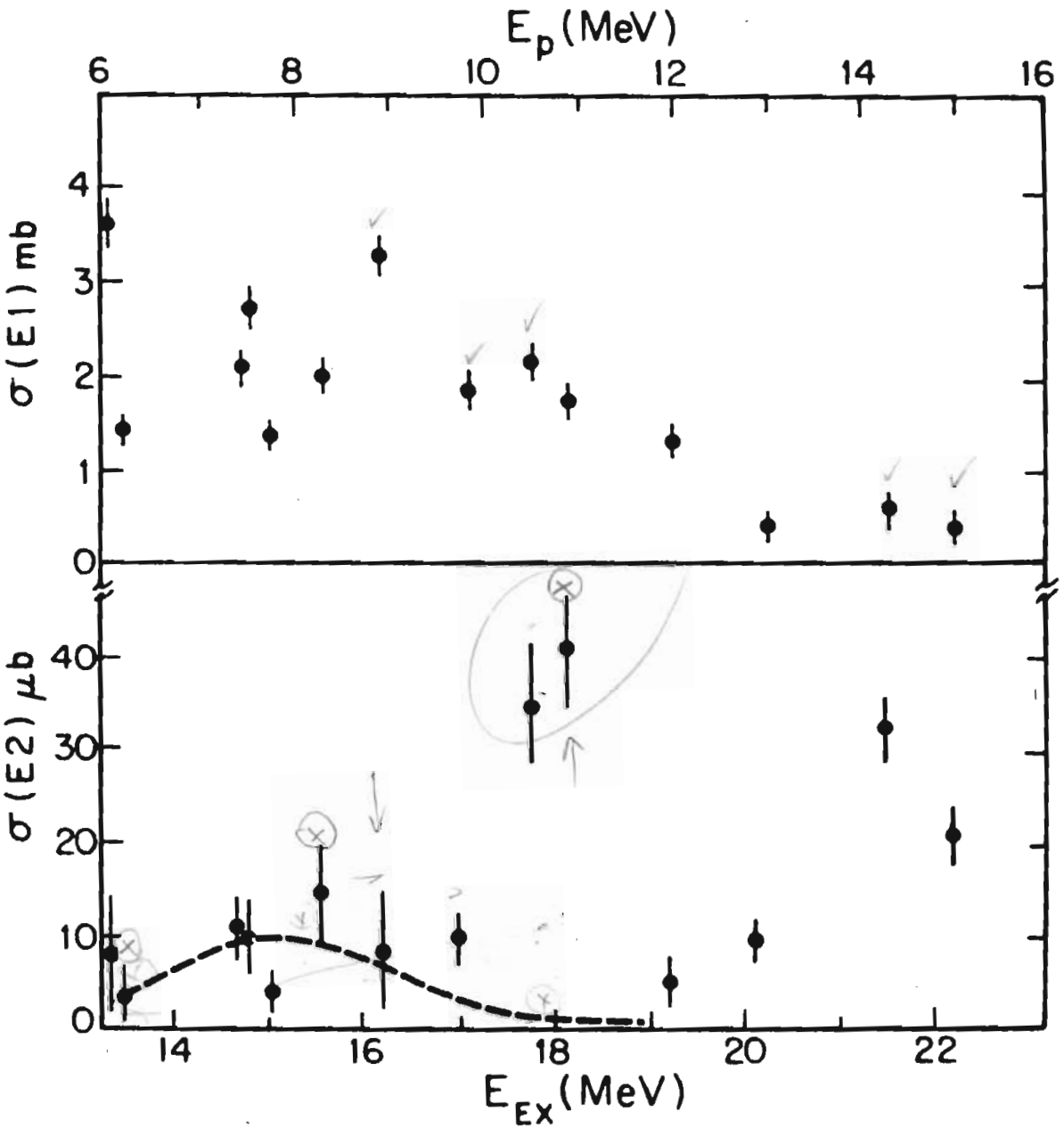
E_p (MeV)
6
8
10
12
14
16
σ(E1) mb
0
1
2
3
4
σ(E2) μb
0
10
20
30
40
14
16
18
20
22
E_Ex (MeV)

of the total E2 energy weighted sum rule (see Appendix C). Presumably, as is the case with the dipole strength, most of the strength is in the neutron channel.

Recently, inelastic electorn scattering (Buskirk, private communication, 1976) data have indicated an isoscalar E2 resonance at 14.9 MeV excitation which exhausted 25% of the $\Delta T=0$ E2 energy weighted sum rule (see Appendix C). The reported width was 3 MeV. The isoscalar E2 resonance is predicted to be near $58/A^{1/3} \simeq 13$ MeV (Bohr and Mottelson, 1975). By taking the strength in the proton channel as $(\gamma,p)/(\gamma,n)$, a resonance with these parameters is shown in the E2 cross section of fig. 15 as the dashed curve. The E2 cross section obtained from the angular distributions in this work is consistent with this resonance but cannot conclusively substantiate its existence.

D. The Analysis of the Giant Dipole Resonance Excited via the $^{88}Sr(\vec{p},\gamma_1)^{89}Y$ Reaction

After stripping the peak shape of γ_0 from the gamma-ray spectrum as described in Chapter III A, the gamma-ray transition to the first excited state of ^{89}Y, γ_1, was summed using the same fitting technique as for γ_0. The 90° cross section versus proton energy was shown in fig. 4 for this reaction. It is interesting that the cross section diminishes rapidly below the

classical angular momentum barrier of $\ell(\ell+1)h^2/2MR^2=8.7$ MeV. In this equation M=mass of the proton; $R=1.2A^{1/3}F$, the radius of the target; and ℓ=the orbital angular momentum quantum number of the incident proton. (For reasons to be explained shortly, ℓ is taken as 3).

The first excited state of ^{89}Y has $J^{\pi}=9/2^{+}$ and lies at an excitation of 909.1 keV (Hinrichsen, 1969) and (Robinson, et al., 1969). This means that El radiation may come from excited states having $J^{\pi}=7/2^{-}$, $9/2^{-}$, $11/2^{-}$. Following the notation of the previous section, the T-matrix amplitudes of each of these excited states will be designated as $f_{7/2}(El)$, $h_{9/2}(El)$, and $h_{11/2}(El)$. Since the incident proton f-wave associated with the formation of the $7/2^{-}$ state has the lowest orbital momentum, the value of $\ell=3$ was used in the previous paragraph to determine a lower limit in the expression for the classical orbital momentum barrier.

At eight energies through the region of the giant resonance, angular distributions of cross section and analyzing power were measured. These distributions were fitted in the manner described for γ_o. The a_k and b_k coefficients obtained from these fits are given in Table IV. These data and fits are shown in figs. 16 and 17. Apparent in these data is the fact that the angular distribution of cross section reverses its inflection with increasing energy. This effect is clearly seen

Table IV. The a_k and b_k Coefficients for $^{88}Sr(\vec{p},\gamma_1)^{89}Y$

E_p(MeV)	a_1	a_2	b_1	b_2	b_3
8.90	0.050±0.034	0.080±0.058	0.026±0.026	-0.136±0.019	-0.020±0.018
9.85	0.136±0.034	0.216±0.059	0.050±0.020	-0.165±0.017	0.0 ±0.018
10.50	0.043±0.032	0.105±0.057	0.030±0.019	-0.118±0.016	-0.028±0.016
10.90	0.019±0.025	0.154±0.042	0.102±0.019	-0.152±0.014	0.0 ±0.013
12.00	0.056±0.048	0.262±0.084	-0.004±0.026	-0.121±0.024	0.050±0.025
13.00	0.022±0.025	-0.044±0.043	-0.006±0.021	-0.082±0.013	0.0 ±0.015
14.30	0.212±0.029	-0.014±0.049	0.048±0.016	-0.196±0.015	0.0 ±0.014
15.00	0.162±0.024	-0.150±0.041	0.112±0.020	-0.163±0.013	-0.026±0.013

The higher order coefficients are given only when the normalized χ^2 justified their use.

Figure 16. Angular distributions from the $^{88}Sr(\vec{p},\gamma_1)^{89}Y$ reaction for the quantities $\sigma(\theta)/a_o$ and $\sigma(\theta)A(\theta)/a_o$ and for E_p=8.90, 9.85, 10.50, and 10.90 MeV. The error bars represent the statistical errors associated with the data points. The solid curves are the result of fitting the data as described in the text.

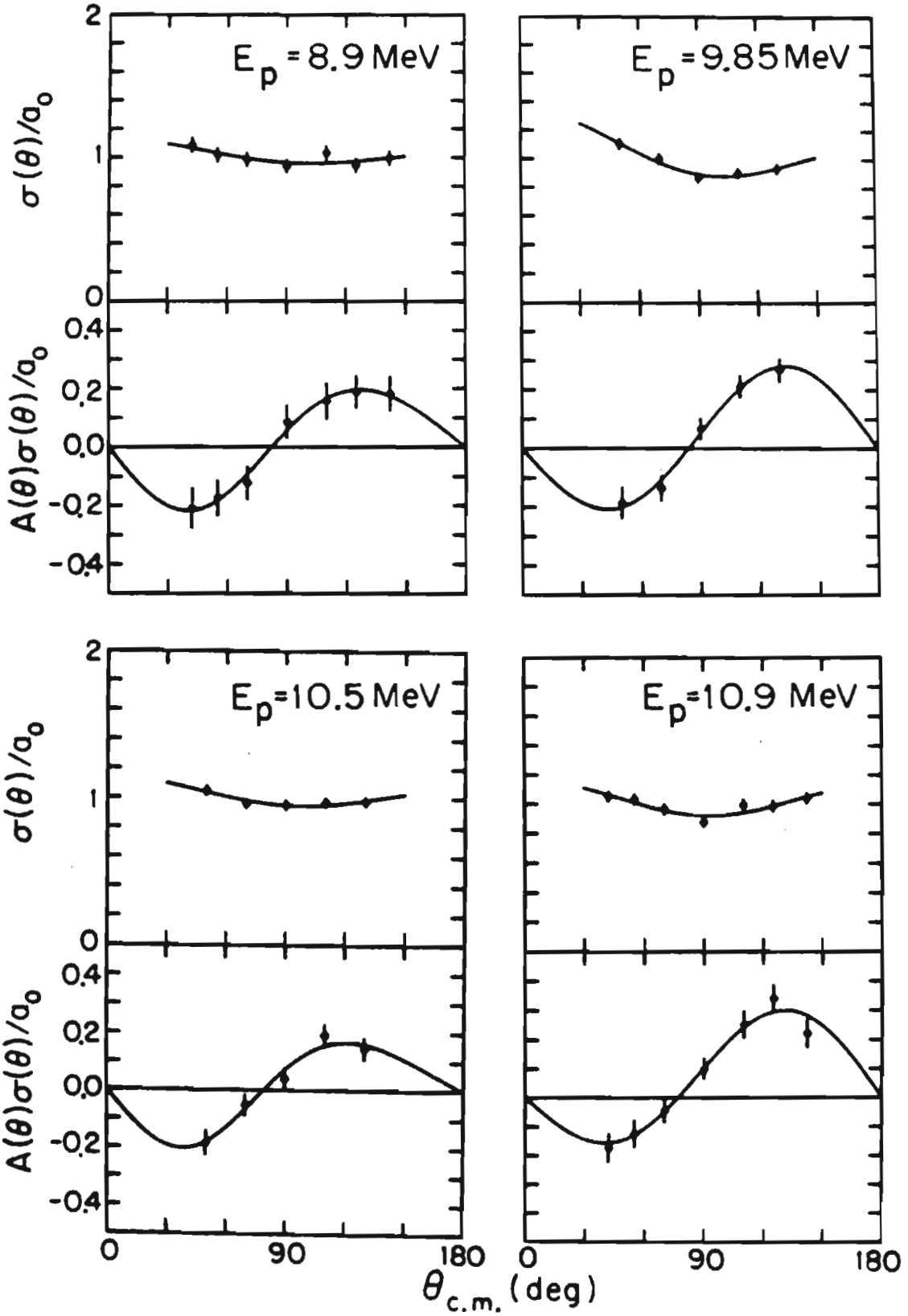
E_p = 8.9 MeV
E_p = 9.85 MeV
E_p = 10.5 MeV
E_p = 10.9 MeV
$\sigma(\theta)/a_o$
$A(\theta)\sigma(\theta)/a_o$
2
1
0
0.4
0.2
0.0
-0.2
-0.4
0
90
180
$\theta_{c.m.}$ (deg)

Figure 17. Angular distributions from the $^{88}Sr(\vec{p},\gamma_1)^{89}Y$ reaction for the quantities $\sigma(\theta)/a_o$ and $\sigma(\theta)A(\theta)/a_o$ and for E_p=12.0, 13.0, 14.3, and 15.0 MeV. The error bars represent the statistical errors associated with the data points. The solid curves are the result of fitting the data as described in the text.

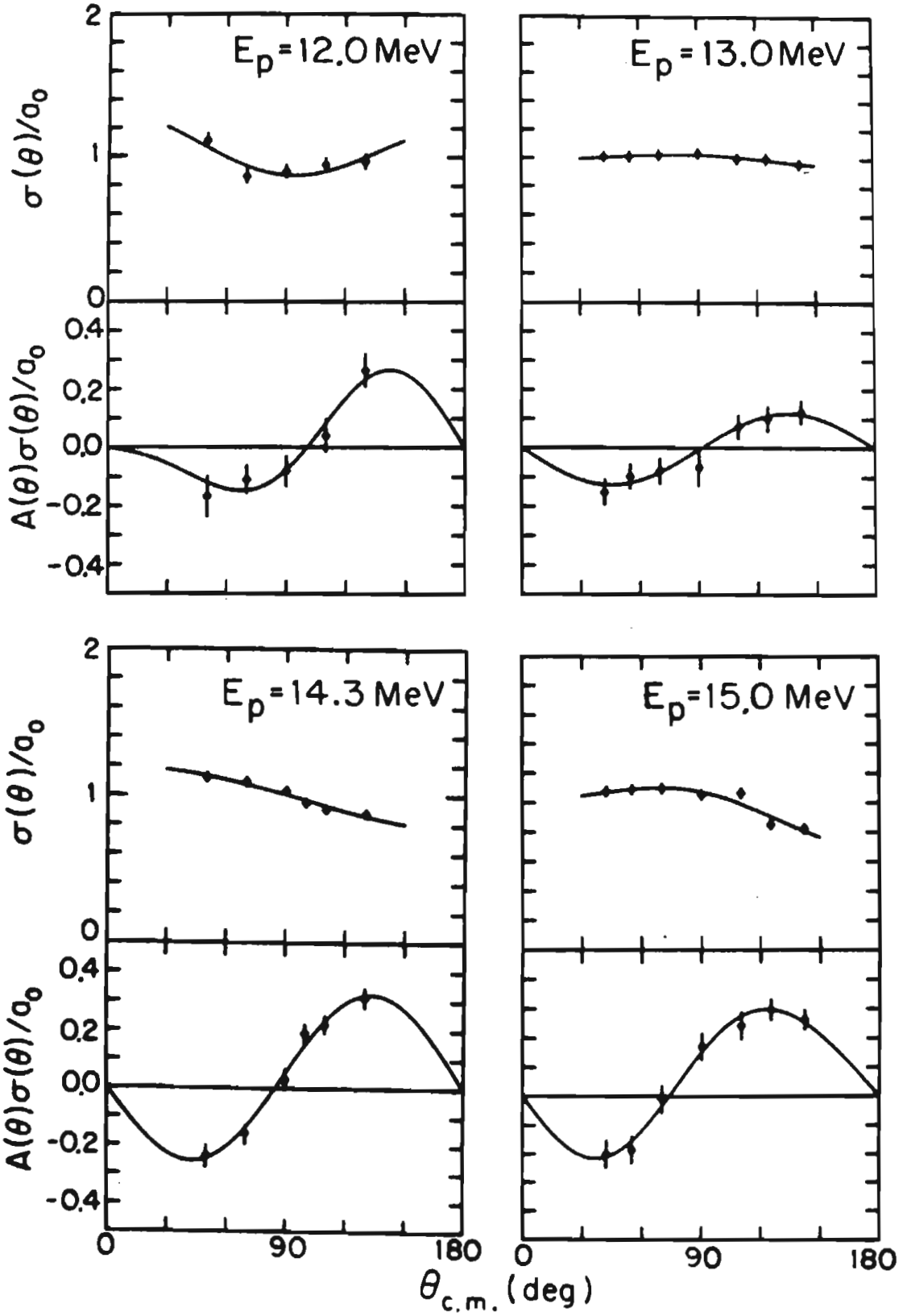
E_p=12.0 MeV
E_p=13.0 MeV
E_p=14.3 MeV
E_p=15.0 MeV
$\sigma(\theta)/a_0$
$A(\theta)\sigma(\theta)/a_0$
2
1
0
0.4
0.2
0.0
-0.2
-0.4
0
90
180
$\theta_{c.m.}$ (deg)

as a change of sign in a_2 in fig. 18. In this figure, the a_k and b_k obtained from fitting are shown as a function of proton energy. It is interesting to note that, unlike the γ_0 distributions, no a_3 was necessary to fit the data. The a_k and b_k coefficients may be related to the El radiation T-matrix elements by evaluating eqs. (5) and (6).

$$a_0 = 4 f_{\frac{7}{2}}(E1)^2 + 5 h_{\frac{9}{2}}(E1)^2 + 6 h_{\frac{11}{2}}(E1)^2$$

$$\begin{aligned} a_2 = & -0.667 f_{\frac{7}{2}}(E1)^2 + 0.8989 f_{\frac{7}{2}}(E1) h_{\frac{9}{2}}(E1) \cos(\phi_{f_{7/2}} - \phi_{h_{9/2}}) \\ & + 7.236 f_{7/2}(E1) h_{\frac{11}{2}}(E1) \cos(\phi_{f_{7/2}} - \phi_{h_{\frac{11}{2}}}) + 2.424 h_{\frac{9}{2}}(E1)^2 \\ & - 1.220 h_{\frac{9}{2}}(E1) h_{\frac{11}{2}}(E1) \cos(\phi_{h_{9/2}} - \phi_{h_{\frac{11}{2}}}) - 1.909 h_{\frac{11}{2}}(E1)^2 \end{aligned} \qquad (12)$$

$$\begin{aligned} b_2 = & -1.348 f_{7/2}(E1) h_{\frac{9}{2}}(E1) \sin(\phi_{f_{7/2}} - \phi_{h_{9/2}}) \\ & + 2.412 f_{9/2}(E1) h_{\frac{11}{2}}(E1) \sin(\phi_{f_{7/2}} - \phi_{h_{\frac{11}{2}}}) \\ & - 2.236 h_{\frac{9}{2}}(E1) h_{\frac{11}{2}}(E1) \sin(\phi_{h_{9/2}} - \phi_{h_{\frac{11}{2}}}) \end{aligned}$$

Unfortunately, one cannot solve these three equations for the three reaction amplitudes and two relative phases (one of the phase differences in eqs. (11) is redundant). Arguments can be made for assuming the $9/2^- \rightarrow 9/2^+$ (i.e., $h_{9/2}$(El)) is

Figure 18. The a_k and b_k coefficients obtained by fitting the data of figs. 16 and 17 as described in the text. The error bars represent statistical errors. All coefficients have been normalized such that a_o equals 1.0. The numerical values of the coefficients and errors are given in Table IV.

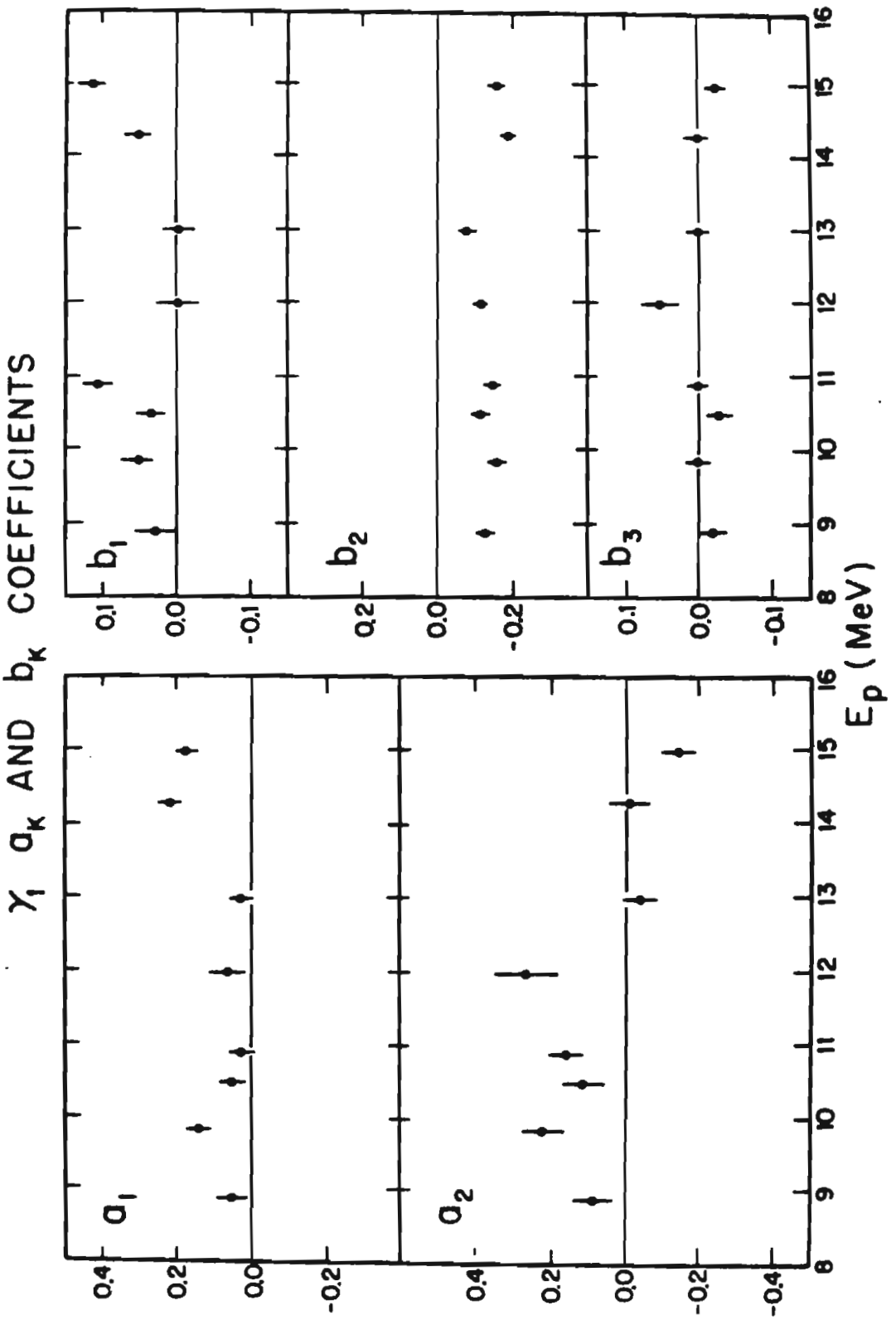
γ_1 a_k AND b_k COEFFICIENTS
a_1
a_2
b_1
b_2
b_3
E_p (MeV)

negligible. This decay corresponds to the so-called E1 "spin-flip" transition. Hayward (1970) has shown in other nuclei that "spin-flip" E1 transitions may be hindered by a factor of 5-10. By assuming $h_{9/2}(E1)$ to be zero, eqs. (12) simplify to

$$a_0 = 4 F_{\frac{7}{2}}(E1)^2 + 6 h_{\frac{11}{2}}(E1)^2$$

$$a_2 = -0.667 F_{\frac{7}{2}}(E1)^2 - 1.909 h_{\frac{11}{2}}(E1)^2 + 7.236 F_{\frac{7}{2}}(E1) h_{\frac{11}{2}}(E1) \cos(\phi_f - \phi_h) \quad (12A)$$

$$b_2 = 2.412 F_{\frac{7}{2}}(E1) h_{\frac{11}{2}}(E1) \sin(\phi_F - \phi_h)$$

As with the case of γ_0, these equations may be solved exactly for the two amplitudes and the phase difference. Also as before, two solutions for each amplitude and their relative phase are found. These solutions are shown as a function of proton energy in fig. 19. The numerical results are given in Table V.

Optical model phase shifts were calculated as described in the last section and are shown as the dotted curve in fig. 19. These phase shifts in general follow the same trend as those

Figure 19. The two solutions of a pure E1 analysis of the a_o, a_2, and b_2 coefficients of Table IV assuming no "spin-flip" E1 contribution for $^{88}Sr(\vec{p},\gamma_1)^{89}Y$. The amplitudes are expressed as a percentage of a_o. The solid lines serve only to connect the points. The dashed line is an optical model calculation of the phase difference.

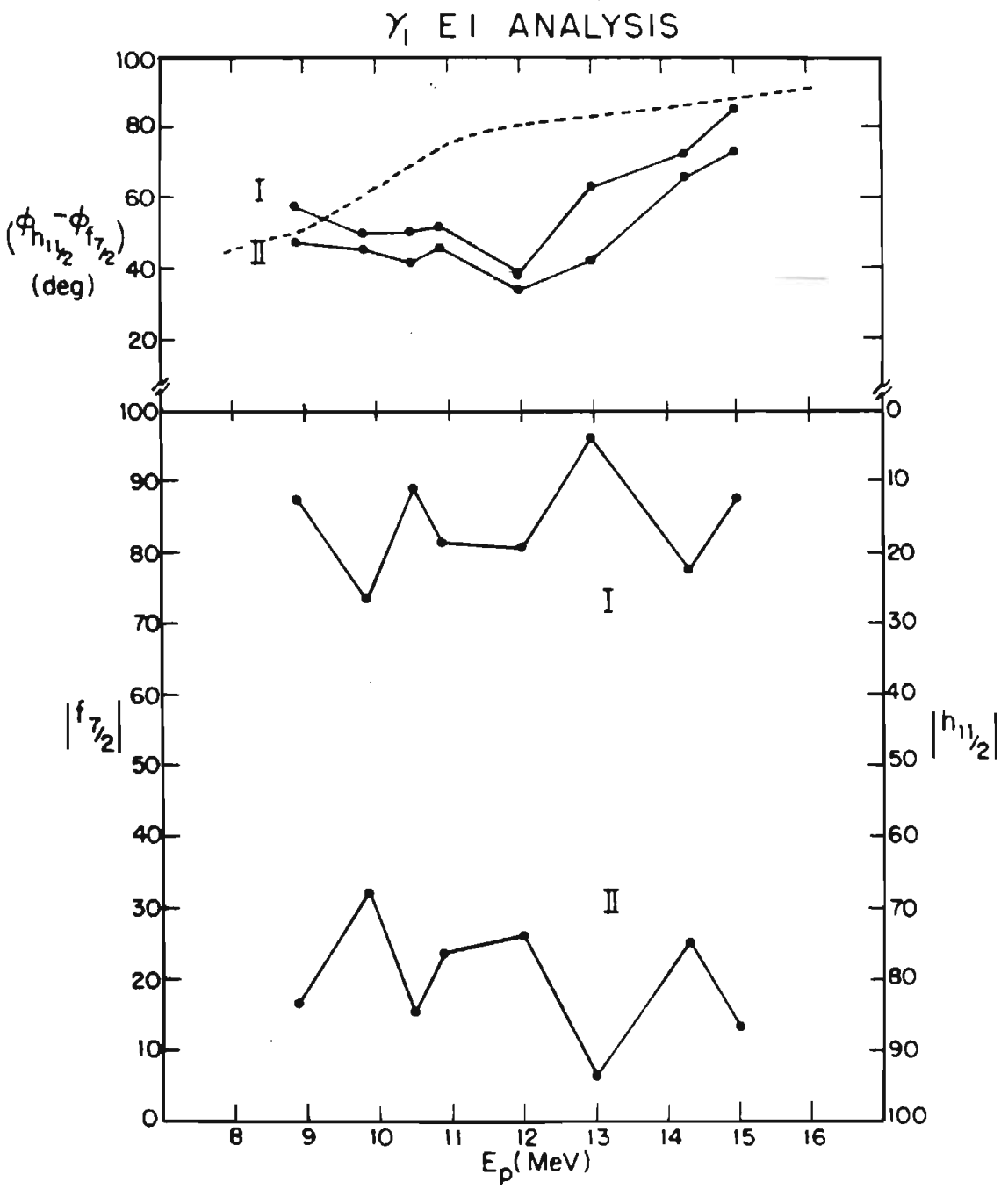
γ_1 E1 ANALYSIS
$(\phi_{h_{11/2}} - \phi_{f_{7/2}})$ (deg)
I
II
$|f_{7/2}|$
$|h_{11/2}|$
E_p (MeV)

Table V. El Solutions to γ_1 Angular Distributions

E_p (MeV)	Solution I $4f^2_{7/2}$ (%)	Solution I $6h^2_{11/2}$ (%)	Solution I $\phi_f-\phi_h$ (deg)	Solution II $4f^2_{7/2}$ (%)	Solution II $6h^2_{11/2}$ (%)	Solution II $\phi_f-\phi_h$ (deg)
8.90	87.6	12.4	-57.0	16.8	83.2	-47.6
9.85	79.4	20.6	-56.0	25.8	74.2	-50.0
10.50	89.3	10.7	-50.9	15.5	84.5	-41.5
11.90	81.5	18.5	-52.6	24.0	76.0	-46.3
12.00	90.6	19.4	-38.4	26.4	73.6	-33.9
13.00	96.3	3.7	-62.5	6.4	93.6	-42.9
14.30	85.0	15.0	-70.6	18.2	81.8	-60.9
15.00	87.4	12.6	-85.8	13.9	86.1	-73.3

calculated from the γ_1 angular distributions. The difference in the curves may be attributable to the resonant phase associated with the GDR.

The existence of finite a_1, b_1, and b_3 indicate the presence of gamma radiation of different multipolarity. However, E2 radiation could result from decays with excited states with $J^{\pi}=5/2^+$, $7/2^+$, $9/2^+$, $11/2^+$, and $13/2^+$. Any further analysis which includes the five additional amplitudes and their relative phases is impossible at this stage.

E. Analysis of Isobaric Analogue States in the Giant Dipole Resonance of ^{89}Y as Excited by the $^{88}Sr(p,\gamma_o)^{89}Y$ and $^{88}Sr(p,p_o)^{88}Sr$ Reactions

Four isobaric analogue states (IAS) have been identified in ^{89}Y in earlier work using the $^{88}Sr(p,\gamma_o)^{89}Y$ reaction (Richard, et al., 1969) (Shafroth and Legge, 1968). Of these, only the three corresponding to the first three excited states of the parent state, ^{89}Sr, are found in the region of the giant dipole of ^{89}Y. Two of these IAS, the $1/2^+$ and $3/2^+$ states at E_p=6.06 MeV and 7.50 MeV, respectively, were investigated in this study.

Previous work with an unpolarized proton beam investigated the IAS-GDR interference in ^{209}Bi but found ambig-

uous results (Snover, et al., 1971). Including the interference between these two amplitudes resulted in two solutions in which the IAS-GDR relative phase is different: 1) $\phi_{IAS}-\phi_{GDR} = 0^{o}\pm30^{o}$, or 2) $\phi_{IAS}-\phi_{GDR} = -90^{o}\pm15^{o}$. One hope of the present study was that by using polarized proton capture and by fitting the analyzing power and cross section simultaneously, this ambiguity in the relative phase could be removed. A second hope was that this same analysis would also remove the uncertainty of which one of the two GDR El amplitudes was dominant--the $s_{1/2}$(El) or the $d_{3/2}$(El).

Since both the $1/2^{+}$ and $3/2^{+}$ IAS and the GDR decay by El radiation, only a_o, a_2, and b_2 contribute to the cross section and analyzing power. The expressions for these coefficients are given in Appendix B assuming either a $1/2^{+}$ or a $3/2^{+}$ IAS. Since $\sigma(\theta)=a_o+a_2P_2(\cos\theta)$ and $A(\theta)\sigma(\theta)=b_2P_2^1(\cos\theta)$, a laboratory angle of 70^{o} was chosen for the NaI detector in order that $P_2(\cos\theta)$ and $P_2^1(\cos\theta)$ would simultaneously be significantly non-zero. Cross section and analyzing power measurements were taken in 25 keV steps for both IAS studied.

1. The $1/2^{+}$ IAS at E_p=6.06 MeV. Cross sections and analyzing powers were measured from E_p=5.5 - 6.3 MeV. The experimental value for $A(70^{o})\sigma(70^{o})$ was divided by $P_2^1(\cos70^{o})$ to obtain b_2. The values obtained from this single angle measurement of b_2 are in good agreement with the values of b_2 obtained

from fitting five-angle angular distributions at E_p=6.05 and 6.20 as discussed in Chapter III C. The experimental values of $\sigma(70^o)$ and b_2 are presented in fig. 20. The a_o, a_2, and b_2 equations for a $1/2^+$ IAS interfering with a GDR were used to fit these data using a least squares criterion. The expressions for these coefficients are derived in Appendix B. The parameters used in the search were $s_{1/2}(El)$, $d_{3/2}(El)$, $s_{1/2}^{I}(El)$, $\phi_I-\phi_d$, $\phi_I-\phi_s$, Γ, and E_R. The appropriate quantities were corrected for target thickness effects. The GDR background composed of $s_{1/2}(El)$ and $d_{3/2}(El)$ was assumed to constant across the 800 keV region studied. As in the aforementioned case of ^{209}Bi, two solutions were found in fitting the cross section data. The solution B curve represents the solution in which $\phi_I-\phi_s\simeq 0$ and the dashed curve (solution A) is the solution corresponding to $\phi_I-\phi_s\simeq 90$. The simultaneous solution to the cross section and the b_2-values indicate that while both yield satisfactory fits to the cross section, solution B had the lower χ^2 when fitting both b_2 and $\sigma(70^o)$. Furthermore, the total width obtained from solution B is in better agreement with the total width obtained in elastic proton scattering (see next section). Both solutions A and B indicate that the GDR is primarily $s_{1/2}(El)$. The effects of having $d_{3/2}(El)$ as the major GDR amplitude is shown in fig. 20 as solution C. In this solution, the $2d_{3/2}(El)^2/s_{1/2}(El)^2$ ratio is forced to have approximately the same value as in fig. 12.

Figure 20. The cross section and b_2 coefficients for the isobaric analogue state at E_p=6.06 MeV. Each curve represents a simultaneous fit to the cross section and b_2 coefficients. Curves A and B represent fits in which the phase $\phi_{IAS}-\phi_{GDR}$ is approximately 90^o and 0^o, respectively. Curve C represents a fit in which the GDR background is forced to be primarily $d_{3/2}$(El) instead of $s_{1/2}$(El). The fitting parameters of each curve are given in Table VI. The energy is center of target proton energy.

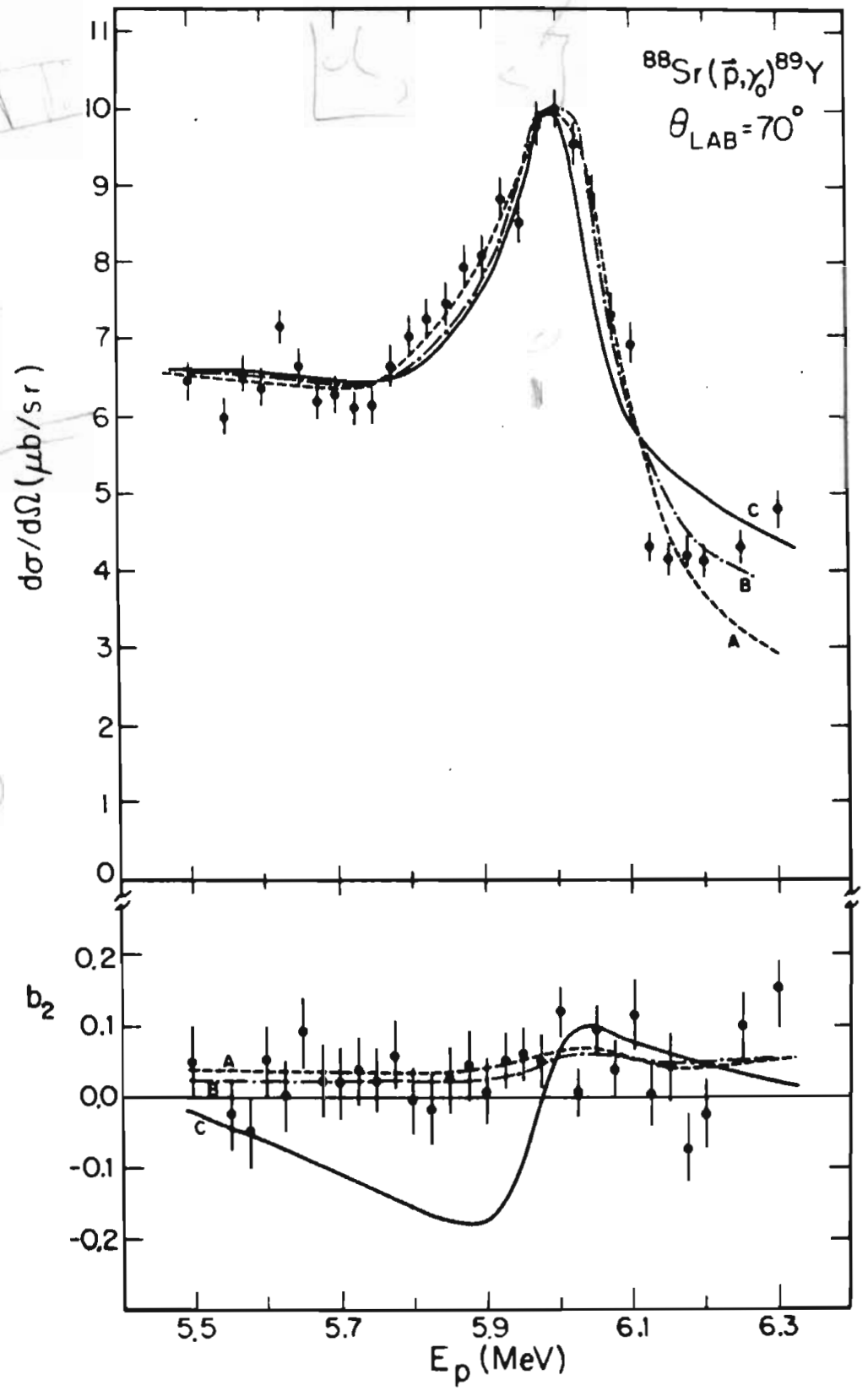
$^{88}Sr(\vec{p},\gamma_0)^{89}Y$
$\theta_{LAB}=70°$
$d\sigma/d\Omega\,(\mu b/sr)$
A
B
C
b_2
E_p (MeV)

The other parameters were searched on to obtain the fit. This solution clearly exaggerates the b_2-value because of the $d_{3/2}(E1)$-$s_{1/2}^{I}(E1)$ interference. The seven fitting parameters for all three solutions are given in Table VI. As was initially hoped, the simultaneous analysis of the analyzing powers and cross sections has removed the ambiguities from both the IAS-GDR relative phase and the dominant GDR E1 amplitude. It should be noted that the selection of $s_{1/2}(E1)$ as the major E1 amplitude in the decay of the GDR is unexpected and will be discussed below (see Chapter III E).

The analysis of the IAS as discussed above also allows for an improved evaluation of the gamma radiation with Γ_γ. Previous determination of this quantity neglected the background altogether (Shafroth and Legge, 1968). This gamma width is related to the determined T-matrix element by

$$\left\{S_{\frac{1}{2}}^{I}(E1)\right\}^2 = \lambda^2 \frac{\Gamma_p \Gamma_\gamma}{\Gamma^2} \qquad (13)$$

where Γ_p and Γ are the proton width and total width, respectively. The quantity λ is the proton wavelength divided by 2π.

The measurements of elastically scattered protons using the $^{88}Sr(\vec{p},p_o)^{88}Sr$ reaction were made simultaneously with the gamma-ray measurements. Both the cross section and the analyzing power of the elastically scattered protons were measured. These

Table VI. The Fitting Parameters for the $1/2^+$ Isobaric Analogue State at a Proton Energy of 6.06 MeV

Solution	E_R(MeV)	$s^2_{1/2}$(%)	$2d^2_{3/2}$(%)	$s^{I\ 2}_{1/2}$(%)	$\phi_I-\phi_d$(deg)	$\phi_I-\phi_s$(deg)	Γ^b(keV)
A	6.11	36	1	26	128	73	187
B	6.06	41	1	14	2	24	124
C[a]	6.02	0.7	61	41	0	209	76

[a]The C solution is forced to give the $d_{3/2}$(E1) to $s_{1/2}$(E1) ratio of strength the same value as solution II of fig. 12. The remainder of the strength in A_o is in the $s_{1/2}$(E1)-$s^{IAR}_{1/2}$(E1) interference term.

[b]Corrected for target thickness.

results can be used with a phase shift analysis to obtain Γ_p and Γ which can then be substituted into eq. (13) to determine Γ_γ. The background phase shifts above and below the resonance at each of the four laboratory angles were obtained by using the standard optical model method. Initial optical parameters were obtained from a previous work (Genz, et al., 1975). The real potential U_r, the imaginary potential derivative W_D, and the spin-orbit potential W_{sp} were varied in a computer search to simultaneously optimize the fit to both the background cross sections and analyzing powers. The background points were chosen at E_p=5.6 and at 6.3 MeV which are significantly away from the resonance. The values for the three parameters which were allowed to vary were slightly different at the two background points and were therefore averaged in order to obtain a single value for the entire background. These final optical model parameters are given in Table VII.

The resonance shape was determined by using the scattering matrix as

$$S_\ell^{\pm} = \exp\left(2i\left[\omega_\ell + \lambda_\ell\right]^{\pm}\right)\left\{\exp\left(-2\mu_\ell^{\pm}\right) + \exp\left(2i\phi_p\right)\left[\frac{i\Gamma_p}{E_R - E - i\Gamma/2}\right]\right\} \quad (14)$$

Table VII. The Optical Model Parameters[a] Used for the $1/2^+$ Isobaric Analogue Resonance at Ep=6.06 MeV

U_r[b] (MeV)	r_r (fm)	a_r (fm)	W (MeV)	W_D (MeV)	r_i (fm)	a_i (fm)	r_{coul} (fm)	U_{sp}[b] (MeV)	W_{sp} (MeV)	r_{sp} (fm)	a_{sp} (fm)
51.7	1.29	0.67	0.0	7.71	1.30	0.51	1.25	4.72	0.0	1.05	0.53

[a]These values taken from Genz, et al., (1975) except U_r, W_D, and U_{sp} which were recalculated using the data of this work.

[b]Woods-Saxon and Thomas radial shapes are used for the real well term and the spin-orbit term, respectively.

as defined by (Vesser, et al., 1967) where $\lambda_\ell^\pm + i\mu_\ell^\pm$ is the background phase shifts for the elastic scattering of the ℓth partial wave with $j=\ell\pm 1/2$, ω_ℓ is the Coulomb phase shift, and ϕ_p is a parameter which shifts the phase of the resonance with respect to the background (taken to be zero). The shape of the resonance was determined by varying E_R, Γ, and Γ_p which are the resonant energy, the total width, and the proton particle elastic width of the IAS, respectively. Figure 21 shows the proton scattering data along with the fits, while the resonance parameters are given in Table VIII. The value of Γ_γ=9.7 eV represents, as pointed out by (Shafroth and Legge, 1968), a very hindered transition (Γ_γ=0.07{single particle}) for this state even though the spectroscopic factor is 0.96 (Cosman, et al., 1966). This hindrance, as they suggest, perhaps may be understood as a collective depletion of the IAS by the higher energy $T_>$ portion of the GDR.

2. The $3/2^+$ IAS at E_p=7.50 MeV. The cross section and analyzing power for the $3/2^+$ IAS were measured from E_p=7.15 to 7.8 MeV in steps of 50 keV except from the interval 7.4 to 7.7 MeV (over the resonance) where the steps were 25 keV. As before the analyzing powers were converted to b_2-values. These results and the cross sections are shown as functions of energy in fig. 22. The values of b_2 obtained from the $\theta_{lab}=70^o$ measurements can be seen to be in good agreement with b_2-values given in Table I

Figure 21. The cross section and polarization for $^{88}Sr(\vec{p},p_o)^{88}Sr$ at the isobaric analogue resonance at E_p=6.06 MeV. The statistical errors are smaller than the data points. The angles are laboratory angles and the energy is the center of target proton energy. The optical model parameters for the background fits are given in Table VII and the resonant parameters in Table VIII. The resultant fit is shown as the solid line.

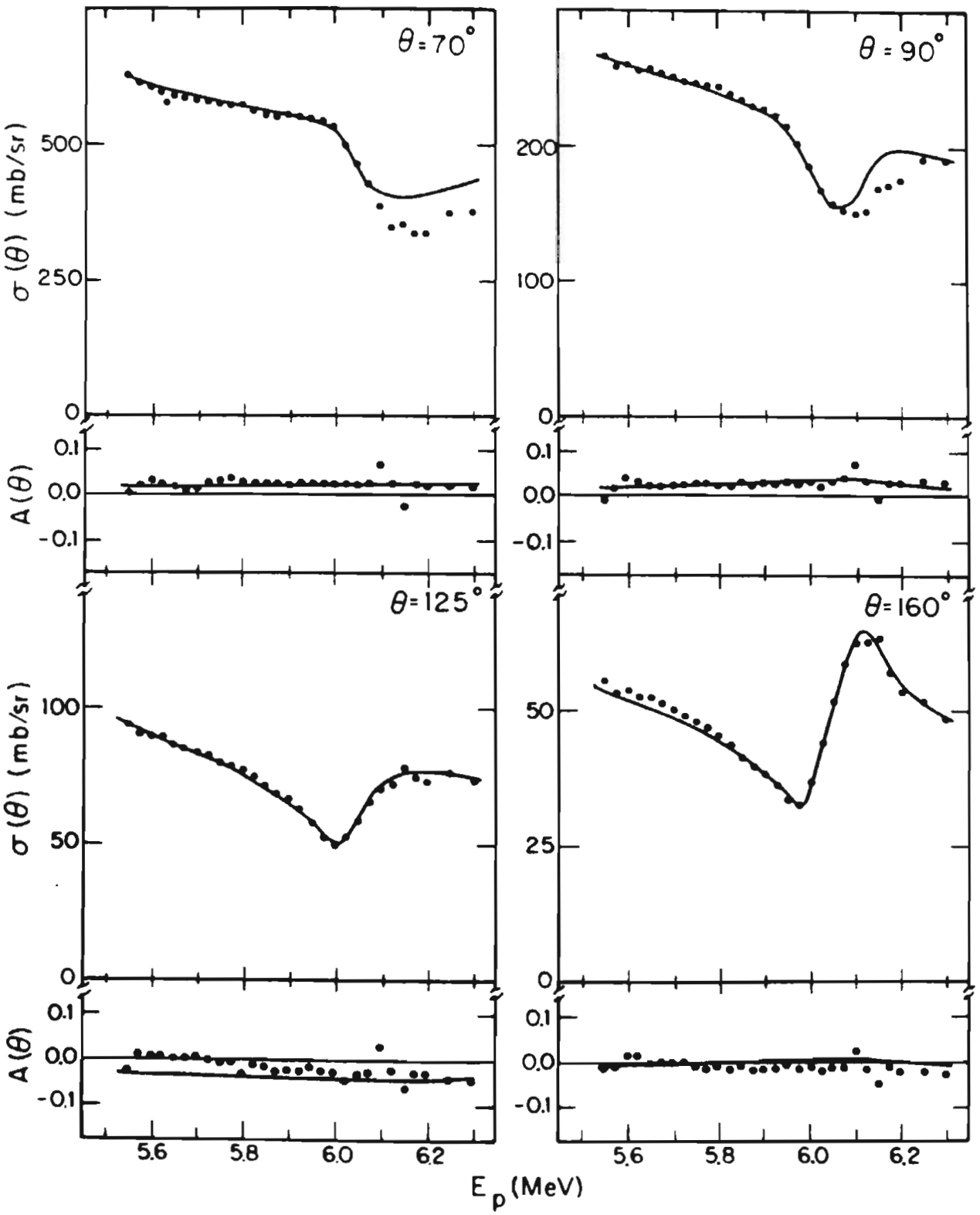
θ = 70°
θ = 90°
θ = 125°
θ = 160°
σ (θ) (mb/sr)
A (θ)
E p (MeV)
500
250
0
200
100
50
25
0.1
0.0
-0.1
5.6
5.8
6.0
6.2

Table VIII. Resonance Parameters of the $1/2^+$ Isobaric Analogue State in ^{89}Y at Proton Energy 6.06 MeV

Experiment	E_{res} (MeV)	Γ_{tot} (keV)	Γ_p (keV)	$\Gamma_{p/\Gamma}$	Γ_γ (eV)
(p,p_o)[a]	6.06	70	46	0.66	
(p,p_o)[b]	6.07	90	59	0.66	
(p,γ_o)[c]	6.10				11±4
$(\vec{p},p_o)$[d]	6.06	120	77	0.64	
$(\vec{p},\gamma_o)$[d]	6.06	124			9.7±3

[a] Cosman, et. al., 1968

[b] Genz, et. al., 1975

[c] Shafroth and Legge, 1968

[d] This work

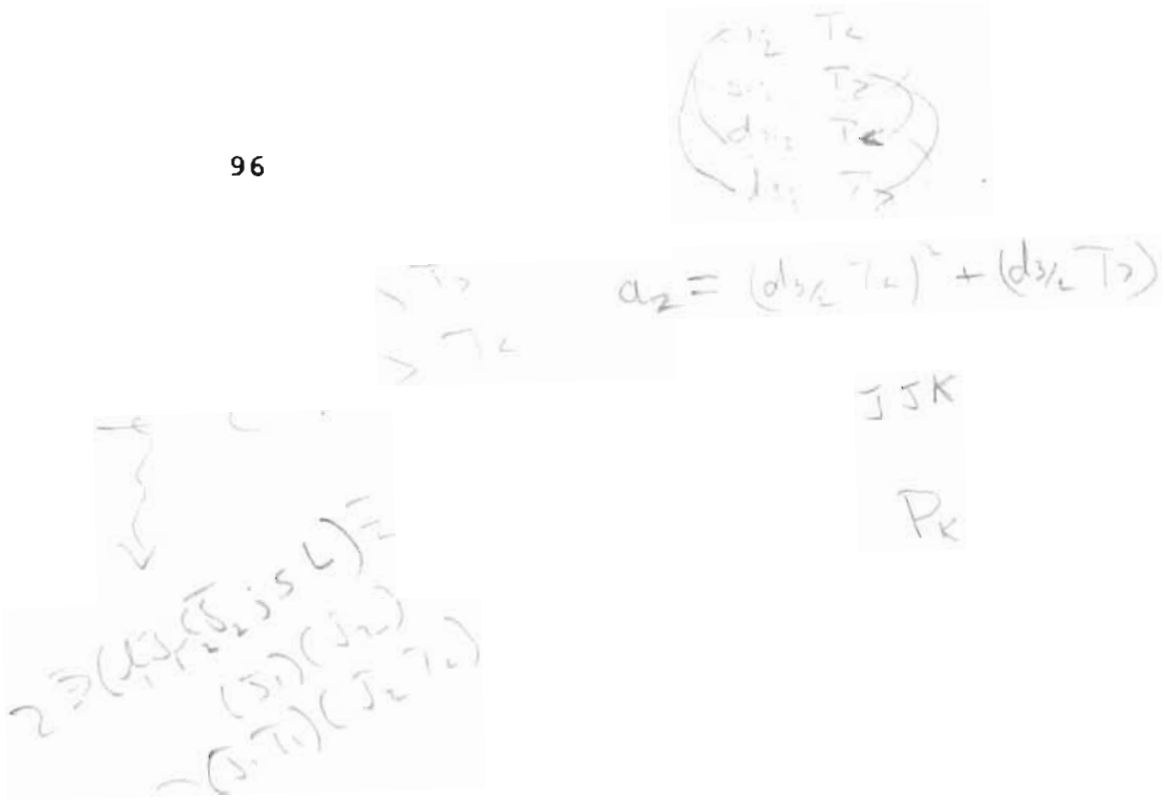

Figure 22. The cross sections and b_2 coefficients for the isobaric analogue state at E_p=7.50 MeV. Each curve represents a simultaneous fit to the cross section and b_2. Curves A and B represent fits in which the phase $\phi_{IAS}-\phi_{GDR}$ is approximately 0^o and 90^o, respectively. Curve C represents a fit in which the GDR background is forced to be primarily $s_{1/2}$(El) instead of $d_{3/2}$(El). The fitting parameters of each curve are given in Table IX. The energy is center of target proton energy.

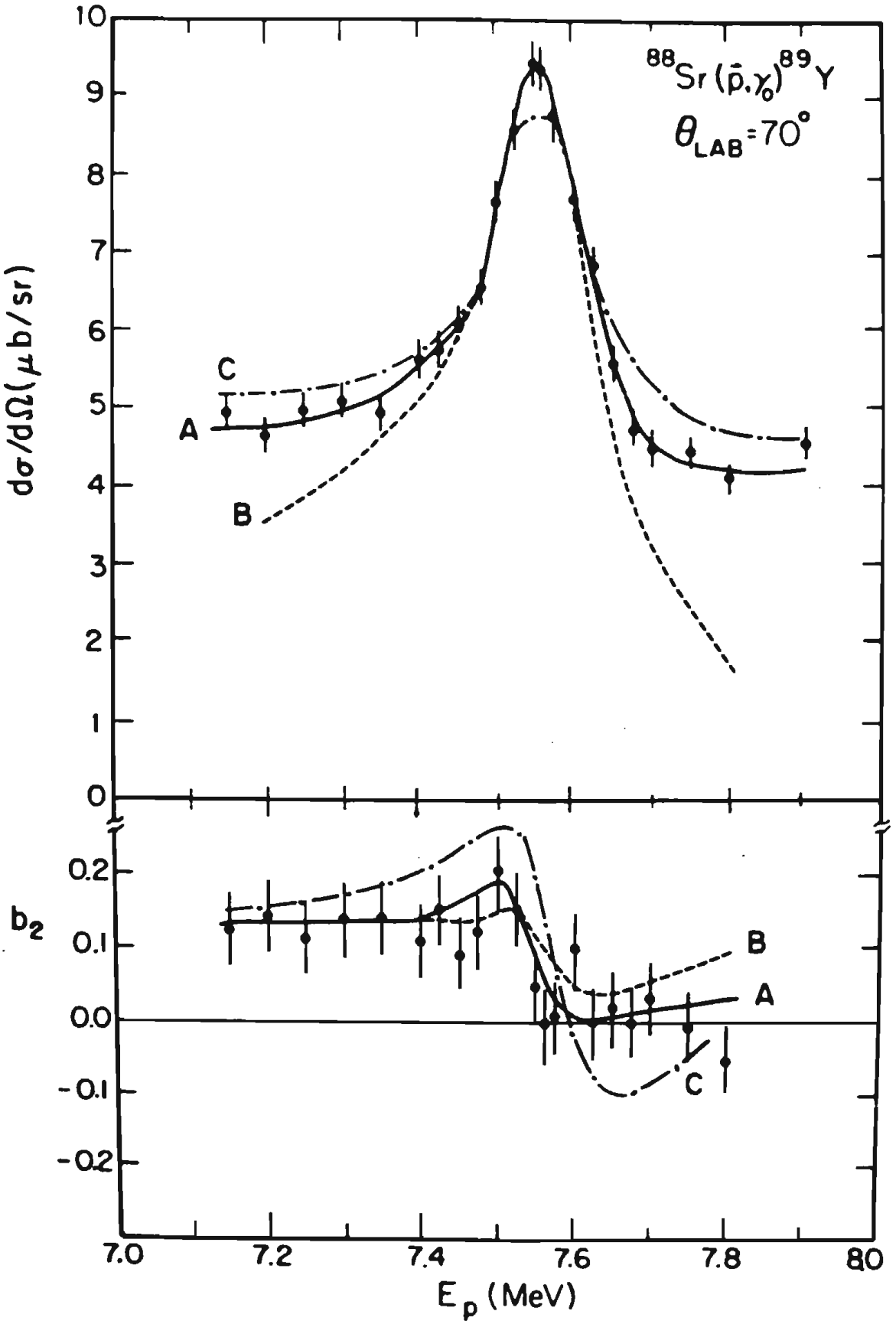
$^{88}Sr(\vec{p},\gamma_0)^{89}Y$
$\theta_{LAB}=70°$
$d\sigma/d\Omega(\mu b/sr)$
A
B
C
b_2
E_p (MeV)

obtained from five-angle distributions at E_p=7.45, 7.55, and 7.75 MeV.

These data were fitted using the equations for a_o, a_2, and b_2 for a $3/2^+$ IAS interfering with the GDR background as given in Appendix B. The fit utilizes a least squares criterion by varying the parameters $s_{1/2}(El)$, $d_{3/2}(El)$, $d_{3/2}^{I}(El)$, $\phi_I-\phi_d$, $\phi_I-\phi_s$, Γ, and E_R. Inspection of the background in fig. 22 and the excitation curve in fig. 5 indicates that it is relatively "flat" around the IAS implying that the assumption of a constant GDR in the neighborhood of the IAS may be better for this resonance than for the $1/2^+$ IAS at 6.06 MeV. The solid line in fig. 22 represents the solution where $\phi_I-\phi_d\simeq 0^o$ (solution A) and the dashed curve the one in which $\phi_I-\phi_d\simeq 90^o$ (solution B). The χ^2 obtained from fitting the b_2-values simultaneously with the cross section was a factor of two lower for the former case. Therefore, the simultaneous measurement of cross section and analyzing power removes the ambiguity of a double solution for the relative phases. For comparison, solution C forces $s_{1/2}(El)$ to be the major amplitude of the GDR in approximately the same ratio as in fig. 13. As in the case of the $1/2^+$ IAS, this results in an asymmetry too large around the IAS resonance. Solution A is clearly the best solution. The fitting parameters for the three cases are presented in Table IX and indicates that the GDR background is about 80% $d_{3/2}(El)$ which is in close agreement with solution I of fig. 13.

Table IX. The Fitting Parameters for the $3/2^+$ Isobaric Analogue State at a Proton Energy of 7.50 MeV

Solution	E_R(MeV)	$s^2_{1/2}$(%)	$2d^2_{3/2}$(%)	$2d^{IAR\ 2}_{3/2}$(%)	$\phi_I-\phi_d$(deg)	$\phi_I-\phi_s$(deg)	Γ^b(keV)
A	7.55	11	36	14	31	9	62
B	7.57	3	42	55	96	21	93
C[a]	7.57	72	2	33	116	0	93

[a]The C solution is forced to give the $s_{1/2}$(E1) to $d_{3/2}$(E1) ratio of strength the same value as solution I in fig. 12. The remainder of the strength in A_o is in the $d_{3/2}$(E1) - $d^{IAR}_{3/2}$(E1) interference term.

[b]Corrected for target thickness

As with the previous IAS, we can relate these results for the magnitude of $d_{3/2}^{I}(E1)$ to the radiative widths by the relation

$$\left\{ d_{\frac{3}{2}}^{I}(E1) \right\}^2 = \lambda^2 \frac{\Gamma_p \Gamma_\gamma}{\Gamma^2} \tag{15}$$

where the quantities are the same as previously defined. Measurements of the cross section and analyzing powers of elastically scattered protons were taken in 50 keV steps across this resonance for E_p=7.1 - 7.7. These measurements and fits are shown in fig. 23. Optical model parameters were determined as before for the background and are given in Table X. The IAS resonance shape was fit using the method previously described, and the results obtained are given in Table XI. As in the case of the $1/2^+$ IAS, the value of Γ_γ=5 eV (Γ_γ=0.02{single particle}) indicates a very hindered transition. Since the spectroscopic factor is only 0.3 (Cosman, et al., 1967), this IAS must contain significant non-single-particle components which would explain part of the hindrance. The remainder of the hindrance may be attributed to $T_>$ collective depletion as in the case of the $1/2^+$ IAS. Also similar to the $1/2^+$ case is the fact that including the GDR-IAS interference in the analysis results in a value of

Figure 23. The cross section and polarization for $^{88}Sr(\vec{p},p_o)^{88}Sr$ at the isobaric analogue resonance at E_p=7.50 MeV. The statistical errors are smaller than the data points. The angles are laboratory angles and the energy is the center of target proton energy. The optical model parameters for the background fits are given in Table X and the resonant parameters in Table XI. The resultant fit is shown as the solid line.

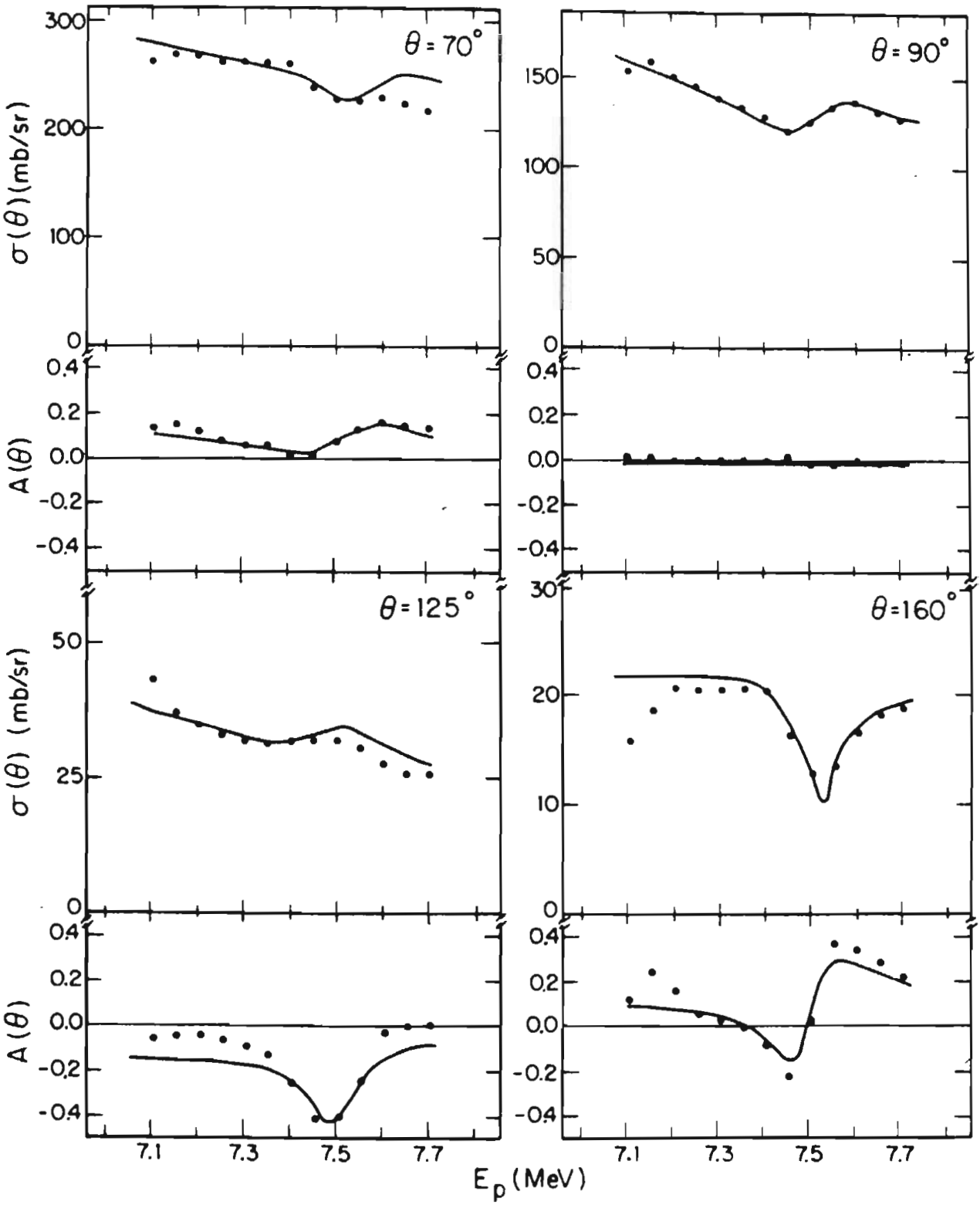
θ = 70°
θ = 90°
θ = 125°
θ = 160°
σ(θ)(mb/sr)
σ(θ) (mb/sr)
A(θ)
E_p (MeV)
7.1
7.3
7.5
7.7

Table X. The Optical Model Parameters[a] Used for the $3/2^+$ Isobaric Analogue Resonance at Ep=7.50 MeV

U_r[b] (MeV)	r_r (fm)	a_r (fm)	W (MeV)	W_D (MeV)	r_i (fm)	a_i (fm)	r_{coul} (fm)	U_{sp}[b] (MeV)	W_{sp} (MeV)	r_{sp} (fm)	a_{sp} (fm)
52.25	1.29	0.67	0.0	9.73	1.30	0.51	1.25	6.12	0.0	1.05	0.53

[a]These values taken from Genz, et. al., (1975) except U_r, W_D, and U_{sp} which were recalculated using the data of this work.

[b]Woods-Saxon and Thomas radial shapes are used for the real well term and the spin-orbit term respectively.

Table XI. Resonance Parameters of the $3/2^+$ Isobaric Analogue State in ^{89}Y at Proton Energy 7.50 MeV

Experiment	E_{res} (MeV)	Γ_{tot} (keV)	Γ_p (keV)	$\Gamma_{p/\Gamma}$	Γ_γ (eV)
(p,p_o) [a]	7.49	60	18	0.30	
(p,γ_o) [b]	7.51				14±5
$(\vec{p},p_o)$ [c]	7.50	61	24	0.39	5±3
$(\vec{p},\gamma_o)$ [c]	7.55	62			

[a] Cosman, et. al., 1968

[b] Shafroth and Legge, 1968

[c] This work

Γ_γ less than that where it is neglected.

F. Summary of the Study of Isobaric Analogue States

The analysis of the two IAS investigated was inconclusive relative to determining the E1 composition of the GDR. Each IAS analysis showed the major GDR amplitude had the same J^π value as that of the IAS. A particle-hole model for ^{16}O indicates that the most important transition is the one involving the largest angular momentum (Hayward, 1970). If this can be generalized to ^{89}Y, $d_{3/2}(E1)$ should be the dominant amplitude of the GDR.

There could be possible problems associated with the $1/2^+$ IAS which indicates that the GDR is primarily $s_{1/2}(E1)$. Both solutions for this IAS indicate that $s_{1/2}(E1)^2$ is 30-40 times larger than $2d_{3/2}(E1)^2$ which is in approximate agreement with the dominant $s_{1/2}(E1)$ solution previously obtained (Chapter III A) by a pure E1 analysis of the angular distributions at E_p=6.05 and 6.20 MeV. However, the assignment of $s_{1/2}(E1)$ as the major constituent of the GDR must be made with reservation for two reasons. First, this particular IAS is located on the low energy tail of the GDR, which can be seen from inspection of the excitation curve of fig. 5. The possibility of different

centroids for the $s_{1/2}(E1)$ and $d_{3/2}(E1)$ strength would mean that the tail of the GDR could possibly be one amplitude while the main part of the GDR was actually composed of the other.

Secondly, this IAS is located on the high energy side of a large peak of gamma-ray strength centered at $E_p \simeq 4$ MeV (not shown). Since the a_2 coefficient is very small in this energy region, the major contribution to the cross section is from a_o. Inspection of the terms of a_o indicates that the only way an appreciable asymmetry in cross section can occur is to have a significant $s_{1/2}(E1)$ - $s_{1/2}^{I}(E1)$ interference contribution. This requires a large $s_{1/2}(E1)$ amplitude because $s_{1/2}^{I}(E1)$ is necessarily large in order to produce the IAS shape itself. Experimentally, there exists an asymmetry in the cross section which has a minimum on the GDR side of the IAS. It is difficult to ascertain if this arises because the IAS is on the tail of the low energy peak or is a true GDR-IAS interference. Therefore, the result that the GDR is dominantly $s_{1/2}(E1)$ is dependent on the asymmetry which may not be a real interference, but rather, be an accidental effect.

These two problems do not apply in the case of the $3/2^+$ IAS. This resonance lies nearer the center of GDR strength, and it appears to be well isolated from contaminating effects of neighboring resonances. On this basis, the assignment of $d_{3/2}(E1)$ as the dominant component of the GDR appears the more

probable choice which agrees with the generalized predication of Hayward (1970).

In summary, the final results of these analyses of the IAS are inconclusive in rigorously determining the El composition of the GDR. In order to produce the experimental asymmetry, the GDR must dominantly be composed of an El amplitude of the same J^{π} as the IAS. There is no clear explanation available for this puzzling result. However, the possibility that the composition of the GDR is different in the two regions around these IAS cannot be ruled out.

This method, however, was able to remove the double IAS-GDR phase ambiguity of unpolarized proton capture experiments. Measurements of cross section and analyzing powers via the polarized proton capture reaction indicated that both IAS preferred $\phi_{IAS}-\phi_{GDR}\simeq 0^{o}$. It was also possible to obtain values of Γ_{γ} for the two IAS by considering the interference with the GDR. These values indicate that both transitions are more hindered than was previously reported.

G. Existence of an Isovector Giant Quadrupole Resonance in ^{89}Y

Recent experiments using inelastic electron scattering on ^{89}Y have exhibited a large resonance around 28 MeV excitation (Buskirk, 1976). The location of this resonance is in reasonable agreement with theoretical calculations which predict a collective isovector electric quadrupole resonance at $135/A^{1/3} \simeq$ 30 MeV (A. Bohr and B. R. Mottelson, 1975). It would be interesting to determine whether evidence for this resonance could be observed in the proton radiative capture reaction. Unfortunately, the cross section for the (p,γ_0) reaction is prohibitively small in this excitation region (see fig. 5). Therefore, the present work investigates the $^{88}Sr(p,\gamma_1)^{89}Y$ reaction because of its larger cross section (see fig. 6). For this reaction, the expected centroid of the resonance is expected to be shifted upward by the excitation of the first excited state in ^{89}Y (see Chapter III B) which locates it near $E_{ex} \simeq 29$ MeV (i.e., $E_{\gamma_1} \simeq 28$ MeV).

Polarized protons, which proved to be of great utility in determining the E2 strength in the GDR, were not available at the high energies necessary to excite this resonance. However, the presence of E2 or M1 radiation will interfere with a E1 background to require finite a_1 and a_3 coefficients

(for example, see eqs. (9A) for γ_0) in the Legendre expansion of the cross section measured with the unpolarized proton capture reaction. However, no significant M1 strength is expected in this region for the reasons discussed in the analysis of the GDR region (see Chapter III C). By measuring the cross section at the zeros of $P_2(\cos\theta)$ (i.e., 55^o and 125^o), one may define a quantity which is sensitive to behavior of these coefficients which can indicate the presence of quadrupole strength. This quantity, the fore-aft asymmetry, is defined by

$$A = \frac{\sigma(55^\circ) - \sigma(125^\circ)}{2 P_1(\cos 55^\circ)} = A_1 - 0.67 A_3 \qquad (16)$$

This asymmetry may be normalized to A_0 as

$$a = \frac{A}{A_0} = a_1 - 0.67 a_3 \qquad (17)$$

The results for the angular distributions of cross section for γ_1 (see Chapter III D) indicated that a_3 coefficients were not necessary to fit the data. Assuming that a_3 is zero implies that a measurement of the normalized asymmetry should approximately be equal to the a_1 coefficient. Figure 18

indicates that $a_1 \simeq 0.2$ at $E_p = 15.0$ MeV This is in agreement with the experimental asymmetry measured at $E_p \simeq 17.0$ MeV which is shown in fig. 24.

By assuming that the E2-E2 interference is small enough such that the a_4 coefficient is negligible (Chapter III D indicates a_4 is zero), one may define the total cross section from the same measurements

$$\sigma = 4\pi A_0 = 2\pi \left(\sigma(55^\circ) + \sigma(125^\circ) \right) \qquad (18)$$

The experimental values of cross section are given in fig. 25.

A means to extract the relative E2 strength in this region from the asymmetry and cross section is outlined in the following method. There are three E1 amplitudes corresponding to different ℓ and j values which could contribute to the γ_1 E1 decay, $J^\pi = 7/2^-$, $9/2^-$, and $11/2^-$. These E1 matrix elements may be expressed as

$$S_{\ell j}(E1)\, e^{i\phi_{\ell j}(E1)} \qquad (19)$$

Similarly there are five amplitudes which may produce E2 radiation; they are associated with $J^\pi = 5/2^+$, $7/2^+$, $9/2^+$,

Figure 24. The normalized asymmetry for $^{88}Sr(p,\gamma_1)^{89}Y$ for E_p=17.0 - 27.0 MeV. The two solid lines represent fits as described in the text. The fitting parameters are given in Table XII and are the same as those for fig. 25.

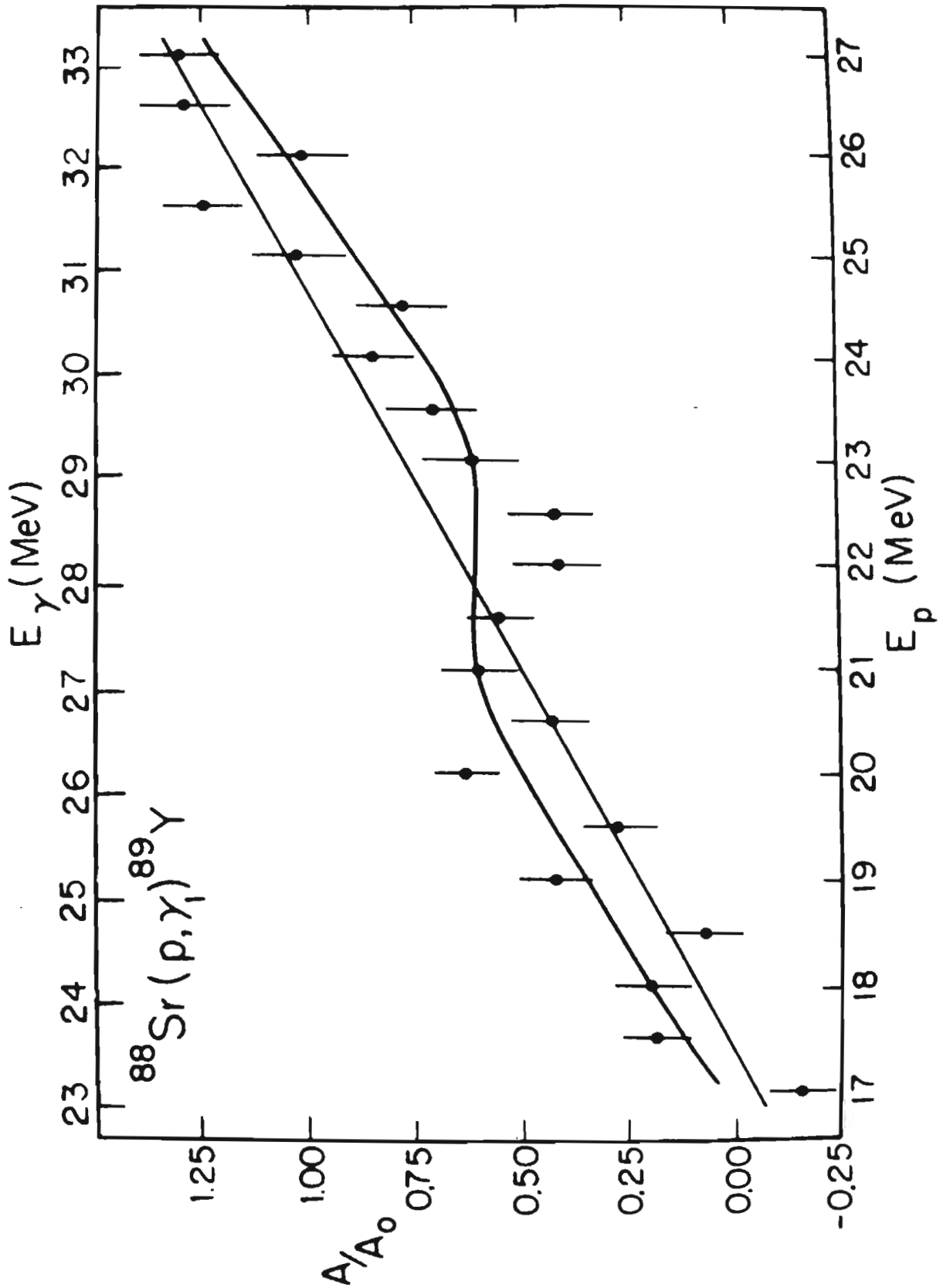
$^{88}Sr(p,\gamma_1)^{89}Y$
E_γ (MeV)
E_p (MeV)
A/A_o
23
24
25
26
27
28
29
30
31
32
33
17
18
19
20
21
22
23
24
25
26
27
1.25
1.00
0.75
0.50
0.25
0.00
-0.25

Figure 25. The $^{88}Sr(p,\gamma_1)^{89}Y$ cross section for E_p=17.0 - 27.0 MeV. The dashed curve is a Breit -Wigner shaped resonance whose parameters are given in Table XII and are the same as those for fig. 24. The solid curve is the sum of this resonance with an exponentially decaying background as described in the text. The energy to proton lab energy.

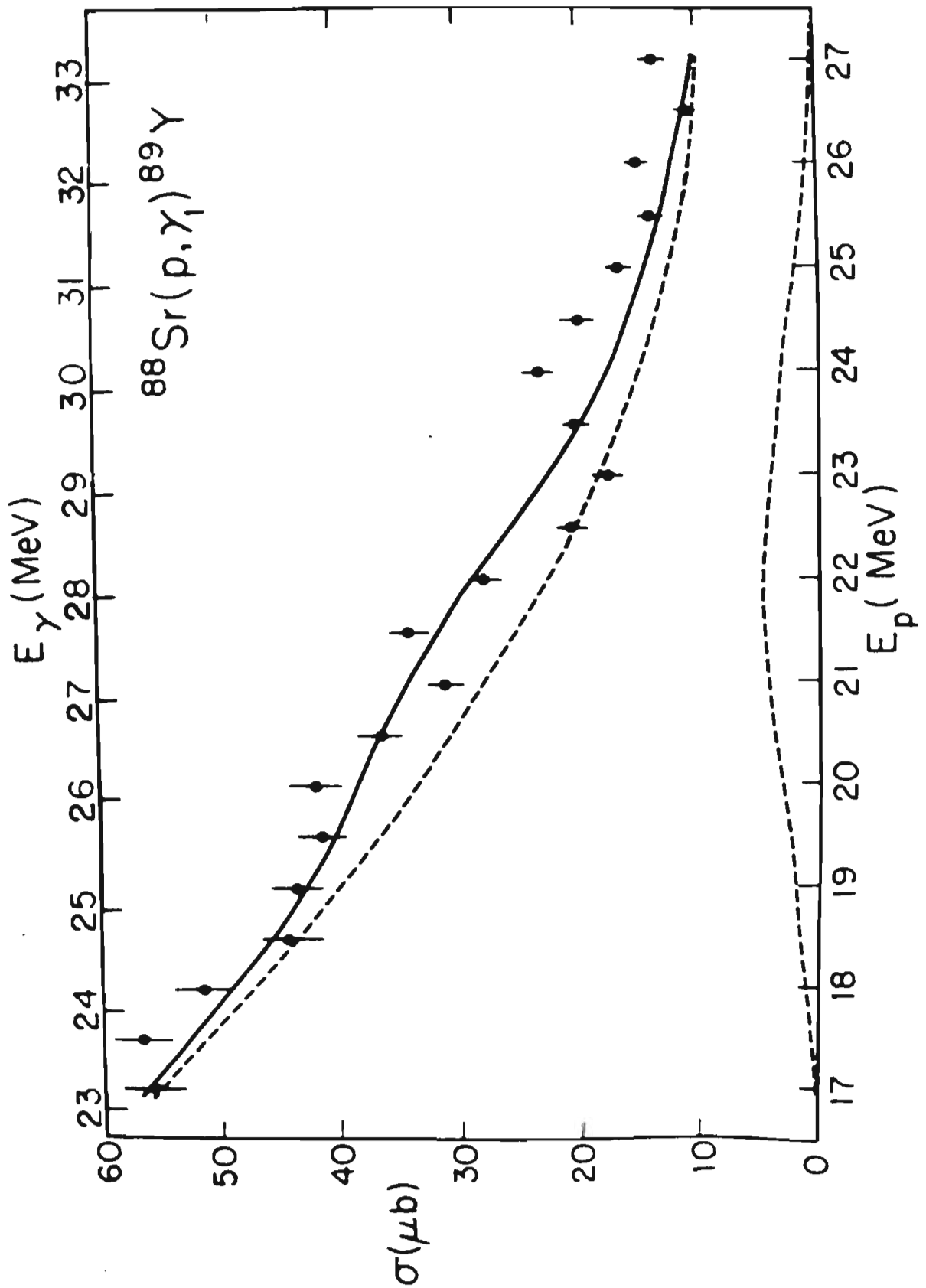
$^{88}Sr(p,\gamma_1)^{89}Y$
E_γ (MeV)
E_p (MeV)
$\sigma(\mu b)$
23
24
25
26
27
28
29
30
31
32
33
17
18
19
20
21
22
23
24
25
26
27
0
10
20
30
40
50
60

$11/2^+$, and $13/2^+$. The corresponding amplitudes may be expressed as terms contributing to a collective resonant part (which is assumed to be represented by a Breit-Wigner shape) and non-resonanting (direct) part. These matrix elements are taken as

$$S_{\ell j}(E2)\, e^{i\phi_{\ell j}(E2)} + \frac{i\frac{\Gamma}{2}\, S^{coll}_{\ell j}(E2)\, e^{i\phi^{coll}_{\ell j}(E2)}}{E - E_R + i\,\Gamma/2} \qquad (20)$$

where E_R and Γ are the resonant energy and width, respectively. The phases $\phi_{\ell j}(E\lambda)$ are considered to vary slowly with energy in the region investigated. In fig. 14, it can be seen that this is true in general for the phases of the γ_0 data. These E1 and E2 amplitudes may be used to express the cross section as

$$\sigma = \sum_{\substack{\ell j \\ \ell' j' \\ \ell'' j''}} C(\ell j)\, S_{\ell j}(E1)^2 + C(\ell' j')\, S_{\ell' j'}(E2)^2 + \frac{C(\ell'' j'')\, S_{\ell'' j''}(E2)^2\, \frac{\Gamma^2}{4}}{(E-E_R)^2 + \frac{\Gamma^2}{4}} \qquad (21)$$

where $C(\ell j)$ are the appropriate products of angular momentum coupling coefficients. The asymmetry arising from E1-E2 interference may be expressed as

$$a = \sum_{\ell_j \ell'_{j'}} C(\ell_j \ell'_{j'}) S_{\ell_j}(E1) S_{\ell'_{j'}}(E2) \cos\left(\phi_{\ell_j}(E1) - \phi_{\ell'_{j'}}(E2)\right)$$

$$+ \sum_{\ell_j \ell''_{j''}} \frac{C(\ell_j \ell''_{j''}) S_{\ell_j}(E1) S_{\ell''_{j''}}(E2) \frac{\Gamma}{2} \cos\left(\phi_{\ell_j}(E1) - \phi_{\ell''_{j''}}(E2) - \theta\right)}{\sqrt{(E-E_R)^2 + \Gamma^2/4}} \qquad (22)$$

$$= a_{nres} + a_{res}$$

where θ is the resonance phase atan $(\frac{E-E_R}{\Gamma/2})$ and a_{nres} and a_{res} represent the non-resonant and resonant parts, respectively, of the asymmetry.

As previously stated, there are several E1 and E2 amplitudes which contribute to σ and a. However, to determine each of these and their relative phase would be prohibitively difficult. The problem may be simplified by assuming that all E1 amplitudes and phases may be represented as a single E1 amplitude and phase. The same assumption is made for the E2 amplitudes and phases. Although these assumptions do not allow specific reaction amplitudes to be evaluated, they do permit an estimation of relative E1 and E2 strength.

It was found that the background in fig. 25 was well described by a term which exponentially decayed with energy.

This is consistent with the fact that as energy increases, more reaction channels are available which can reduce the strength available to the proton channel. Several theories predict that the density of states (i.e., more reaction channels) increase as exp($\sqrt{E}$) (R. R. Roy and B. P. Nigam, 1967) which supports this conjecture. Since the direct $S_{\ell j}(E2)$ amplitudes should be smaller than the $S_{\ell j}(E1)$ amplitudes, this background is taken to be representative of the E1 strength present in this region. The solid line in fig. 25 is a fit to the expression

$$\sigma = 4\pi A_0 = 4\pi \left(D_1 e^{-bE_p} + D_2 \frac{\frac{\Gamma^2}{4}}{(E-E_R)^2 + \Gamma^2/4} \right) \qquad (23)$$

In this expression D_1 represents the normalization for the background. The second term of this equation represents the total (if any) resonant strength present in the cross section in which D_2 is the magnitude of the resonance.

Inspection of the asymmetry in fig. 24 indicates an almost linear increase with energy. This smoothly increasing asymmetry has been previously observed in other nuclei (Snover, et al., 1974), and it is suggestive of an E1 background interfering with direct E2 capture. Halpern (1973) has used a semiclassical model to demonstrate that such E1-E2 interference

could produce an asymmetry which smoothly increases with energy. For the asymmetry to be non-zero requires the cosine term of a_{nres} to be non-zero. The greatest effects would be observed when $\phi_{\ell j}(E1)-\phi_{\ell j}(E2)$ was approximately 0^{o} or 180^{o}. For γ_o, fig. 14 shows $\phi_d-\phi_p$ approaches 360^{o} (i.e., 0^{o}) at higher energies which supports the agreement of this theory with experiment. Therefore, the asymmetry was fitted with the expression

$$a = \left(D_3 E_p + D_4\right) + \frac{D_5 \sqrt{\dfrac{D_1 e^{-bE_p} D_2 \Gamma^2/4}{(E-E_R)^2 + \Gamma^2/4}}\ \cos\left(\phi(E1)-\phi^{coll}(E2)-\theta\right)}{A_o} \qquad (24)$$

where $(D_3E_p+D_4)$ is taken to describe a_{nres} in eq. (22) and should be an indication of the amount of direct E1-E2 interference present. The last term assumes that the background is dominantly E1 such that $S_{\ell j}(E1)$ of a_{res} in eq. (22) is approximately $\sqrt{D_1 e^{-bE}}$. The normalization D_5 accounts for the different angular momentum coefficients in eqs. (21) and (22). Experimentally, the resonant portion of the asymmetry appears to cross the linear background at the resonant energy reported in inelastic electron scattering (Buskirk, 1976) if the upward shift in energy associated with γ_1 is considered. Since θ is zero at resonance, this feature of the data requires $\phi(E1)-\phi^{coll}(E2)$ in eq. (24) to be approximately -90^{o}. Using this value for the relative phase,

D_1, D_2, D_3, D_4, D_5, b, E_R, and Γ were varied to simultaneously fit the cross section and asymmetry according to a least squares criterion. Values of 96.8 μb and 0.8 μb were obtained for D_1 and D_2, respectively. D_3, D_4, D_5, and b were respectively given by $\frac{0.146}{\text{MeV}}$, -2.59, 0.422, and $\frac{0.176}{\text{MeV}}$. The resonance parameters are compared with the inelastic electron scattering data in Table XII.

The value of E_R=28.8 MeV (gamma-ray energy) is in good agreement with the inelastic electron scattering data and the theoretical prediction of $\frac{135 \text{ MeV}}{A^{1/3}} \simeq 30$ MeV. The total width Γ is somewhat smaller than was reported. The values from this work correspond to approximately 0.4% of the $|\Delta T|=1$ energy weighted sum rule (EWSR) (see Appendix C). By comparing the $^{89}Y(\gamma,p_0)^{88}Sr$ cross section of fig. 7 with the $^{89}Y(\gamma,n)$ cross section (which accounts for ≃100% of the dipole sum rule) of Lepretre, et al. (1971), the proton channel appears to represent about 1% of the total absorption cross section. The inelastic scattering data of Buskirk (1976) claims this resonance contains (46 ± 14)% of the isovector EWSR. Assuming the same branching ratio, this would imply that the proton channel should have about 0.4% of the strength which is in reasonable agreement with this work.

While these results alone do not conclusively estab-

Table XII. Resonance Parameters of the Proposed Isovector Quadrupole Resonance

Experiment	E_{res} (MeV)	Γ_{tot} (MeV)	Amount $\Delta T = 1$ EWSR (%)
(e,e')[a]	28±1	6	46±14
(p,γ_1)[b]	28.8±1[d]	5.6	0.4[c]

[a] F. R. Buskirk, Private Communication, 1976

[b] This work

[c] To compare with the (e,e') data, this should be multiplied by the ratio of total strength in all reaction channels to the proton channel. This is approximately $(\gamma,n)/(\gamma,p)=100$

[d] The resonance energy is higher by approximately the excitation energy, 909.1 keV, of the first excited state

lish an E2 resonance, when combined with the results of the (e,e') experiment, the existence of an E2 isovector resonance is strongly suggested.

Chapter IV

CONCLUSIONS

The giant dipole resonance of ^{89}Y has been analyzed with the $^{88}Sr(\vec{p},\gamma_0)^{89}Y$ reaction to determine transition matrix elements and the relative phases between them. From these matrix elements, an E2 cross section in the GDR is obtained which indicates a direct E2 reaction process may be occurring in this region.

A similar analysis was applied to the $^{88}Sr(\vec{p},\gamma_1)^{89}Y$ reaction to obtain only the E1 T-matrix elements and relative phases. The extended cross section data of this reaction complicates a previous discussion of isospin splitting of the giant resonance.

The analysis of isobaric analogue states in the giant dipole resonance of ^{89}Y yielded ambiguous results relative to the E1 composition of the GDR; however, this analysis did indicate that the radiative widths of the IAS are more hindered than previously reported. In addition, the use of polarized

proton capture removed the double phase solution of the GDR-IAS which exists in unpolarized proton capture.

The isoscalar and isovector quadrupole resonances studied in this work were compared to those reported in inelastic electron scattering. While the E2 strength obtained in the region of the GDR is consistent with an isoscalar E2 resonance, the results appear to be obscured by a relatively large direct E2 component. On the other hand, the high energy fore-aft measurements of cross section strongly support the existence of a resonance at the reported energy of the isovector giant quadrupole resonance.

APPENDIXES

APPENDIX A

HANDLING OF ^{88}Sr TARGETS

The targets used in this experiment were 99.84% ^{88}Sr foils obtained from Oak Ridge National Laboratory Isotope Division. These foils oxidized readily and required special handling. The Al target rings used in mounting these foils were supplied to Oak Ridge by TUNL. The targets were sealed in evacuated glass ampules for shipping. The ampules were stored in vacuum upon their receipt. The following method was devised to remove the targets from the ampules and place them in the experimental target chamber.

An interlock system equipped with a sliding piston which held the target ring was used to transfer the target to the target chamber. The interlock was designed to fit both the top of a vacuum storage chamber as well as the target chamber. A vacuum pump-out on the cylindrical housing of the piston enabled a vacuum to be applied to the target after the transfer from the glass ampule was accomplished.

Before the actual transfer of the target, cyclohexane was distilled over sodium and stored in a glass bottle over sodium to eliminate water. The sodium was necessary to "dry" the cyclohexane because Sr reacts violently with water by forming the hydroxide. The cyclohexane is dropped on a vertically positioned target allowing it to run down over the surface of the Sr foil forming a protective film. Since cyclohexane is extremely volatile, it quickly evaporates when in the vacuum and leaves a clean strontium surface.

An inert atmosphere of 99.99% He was used which was obtained from the Duke University liquid helium recovery system. This inert gas was filtered through a liquid nitrogen-trapped activated charcoal filter into a glove bag where the glass ampules could be opened. Prior to use, the charcoal was degassed by heating under vacuum. Simultaneously the gas line to the He supply and the glove bag was evacuated so as only helium would flow through the system.

Approximately 24 hours before the target transfer, the following items were placed inside of the glove bag: (1) the bottle of distilled cyclohexane with a dropper, (2) a bottle of sodium in mineral oil, (3) a bottle of pentane, (4) a Petri dish filled with the dessicant phosphorous pentoxide (P_2O_5), (5) an empty Petri dish, (6) a metal spatula, (7) pliers, (8) tweezers, (9) a screwdriver, and (10) the piston interlock system (still

connected to its vacuum line). This was done in order that the P_2O_5 dessicant could dry the bag and these items. Upon completion of this drying, an ampule containing a target was removed from its storage vacuum and placed inside the bag. The helium was used to flush the bag several times. All bottles and the interlock were opened and carefully flushed as well. To test the inertness of the atmosphere, the spatula was used to cut a piece of sodium while under the mineral oil. The mineral oil was rinsed off with the pentane and the sodium placed in the empty Petri dish. When the cut sodium would keep its metallic shine for over five minutes, the atmosphere was considered acceptably inert. The pliers were then used to crack the glass ampule. Tweezers were used to remove the target from the ampule, and the cyclohexane was applied immediately. The target was placed in the target holder in the interlock's piston and tightened in place with the screwdriver. The piston was pulled immediately into the interlock and vacuum pumping was begun while still in the glove bag. The time from the actual breaking of the ampule to the beginning of pumping (that is, the time the target was not under vacuum) was estimated to be 20-30 seconds. The interlock was then removed from the bag and positioned in the bottom of the target chamber. After the beam leg was evacuated, the piston was pushed up such that the target would be in the line of the incident proton beam. A centering point in the chamber top assured correct alignment.

After the completion of the experiment, the piston could be pulled back into the evacuated cyclinder of the interlock and stored in a specially prepared vacuum chamber until further use.

APPENDIX B

INTERFERENCE OF AN ISOBARIC ANALOGUE STATE
WITH A GIANT DIPOLE BACKGROUND

The interference of an observed isobaric analog resonance has been analyzed by expressing the S-matrix as a sum of single level amplitudes for the giant dipole (GD) and isobaric analog resonance (IA) (Ejiri and Bondorf, 1968):

$$S^J = \frac{i A^J_{GD} \frac{\Gamma^J_{GD}}{2} e^{i\phi^J_{GD}}}{E - E^J_{GD} + i\frac{\Gamma^J_{GD}}{2}} + \frac{i A^J_{IA} \frac{\Gamma^J_{IA}}{2} e^{i\phi^J_{IA}}}{E - E^J_{IA} + i\frac{\Gamma^J_{IA}}{2}} \qquad \text{(B1)}$$

where A^J, ϕ^J, Γ^J, and E^J are the amplitude, phase, total width, and energy of each resonance.

In the present case, the IAS's were studied in an energy interval (approximately 700 keV) small compared with the total width of the GDR (about 7-8 MeV). The amplitudes of GDR

were therefore assumed to be constant over the energy interval surrounding the IAS. As discussed in Chapter III, the GDR can only consist of $s_{1/2}(E1)$ and $d_{3/2}(E1)$ amplitudes. Under these assumptions eq. (B1) can be used to write

$$S^{\dagger}S = \left(S_{\frac{1}{2}}(E1)\, e^{-i\phi_s} + d_{3/2}(E1)\, e^{-i\phi_d} - \frac{i\frac{\Gamma}{2} A^{J}_{IA} e^{-i\phi^{J}_{IA}}}{E - E_R - i\Gamma/2} \right) \times \left(S_{\frac{1}{2}}(E1)\, e^{i\phi_s} + d_{\frac{3}{2}}(E1)\, e^{i\phi_d} + \frac{i\frac{\Gamma}{2} A^{J}_{IA} e^{i\phi^{J}_{IA}}}{E - E_R + i\Gamma/2} \right) \tag{B2}$$

where $\Gamma = \Gamma^{J}_{IA}$ and $E_R = E^{J}_{IA}$.

Straightforward evaluation gives the result

$$\begin{aligned} S^{\dagger}S = {} & S_{\frac{1}{2}}(E1)^2 + d_{3/2}(E1)^2 + \frac{(A^{J}_{IA})^2 \frac{\Gamma^2}{4}}{(E-E_R)^2 + \Gamma^2/4} \\ & + S_{\frac{1}{2}}(E1) d_{3/2}(E1)\, e^{-i(\phi_s - \phi_d)} + d_{3/2}(E1) S_{\frac{1}{2}}(E1)\, e^{-i(\phi_d - \phi_s)} \\ & + \sqrt{\frac{1}{(E-E_R)^2 + \Gamma^2/4}} \left\{ S_{\frac{1}{2}}(E1) A^{J}_{IA} \frac{\Gamma}{2} e^{-i(\phi_s - \phi_I - \beta)} \right. \\ & + A^{J}_{IA} \frac{\Gamma}{2} S_{\frac{1}{2}}(E1)\, e^{-i(\phi_I - \phi_s + \beta)} + d_{3/2}(E1) A^{J}_{IA} \frac{\Gamma}{2} e^{-i(\phi_d - \phi_I - \beta)} \\ & \left. + A^{J}_{IA} \frac{\Gamma}{2} d_{3/2}(E1)\, e^{-i(\phi_I - \phi_d + \beta)} \right\} \end{aligned} \tag{B3}$$

where $\beta=\text{atan}(2(E-E_R)/\Gamma)$ is the resonant phase associated with a Breit-Wigner resonance. Evaluation of the angular momentum coupling coefficients in eqs. (3.5) and (3.6) for E1 radiation gives the result that the only non-zero coefficients are a_0, a_2, and b_2. Substitution of eq. (B3) into these equations give expressions for these coefficients dependent on the spin of the IAS.

The two IAS studied in this case have $J^\pi=1/2^+$ and $3/2^+$. The coefficients for $J^\pi=1/2^+$ are given below:

$$a_0 = S_{\frac{1}{2}}'(E1)^2 + 2d_{3/2}'(E1)^2 + \frac{S_{\frac{1}{2}}^I(E1)^2\frac{\Gamma^2}{4}}{(E-E_R)^2+\Gamma^2/4} + \frac{2\,S_{\frac{1}{2}}'(E1)\,S_{\frac{1}{2}}^I(E1)\,\frac{\Gamma}{2}\cos(\phi_I-\phi_S+\beta)}{\left[(E-E_R)^2+\Gamma^2/4\right]^{1/2}} \tag{B4}$$

$$a_0\cdot a_2 = -2S_{\frac{1}{2}}'(E1)\,d_{3/2}'(E1)\cos(\phi_S-\phi_d) - d_{3/2}'(E1)^2 - \frac{2S_{\frac{1}{2}}^I(E1)\,d_{3/2}'(E1)\,\Gamma/2\cos(\phi_I-\phi_d+\beta)}{\left[(E-E_R)^2+\Gamma^2/4\right]^{1/2}}$$

$$a_0\cdot b_2 = S_{\frac{1}{2}}'(E1)\,d_{\frac{3}{2}}'(E1)\sin(\phi_S-\phi_d) + \frac{S_{\frac{1}{2}}^I(E1)\frac{\Gamma}{2}\,d_{3/2}'(E1)\,(\phi_I-\phi_d+\beta)}{\left[(E-E_R)^2+\Gamma^2/4\right]^{1/2}}$$

where $s^{I}_{1/2}(E1)$ replaces A^{J}_{IA} as the amplitude of the IAS. Similar evaluation for an IAS with $J^{\pi}=3/2^{+}$ gives the equations:

$$a_0 = S_{\frac{1}{2}}(E1)^2 + 2d_{3/2}(E1)^2 + \frac{2d^{I}_{3/2}(E1)^2\frac{\Gamma^2}{4}}{(E-E_R)^2+\Gamma^2/4}$$

$$+ \frac{4d^{I}_{3/2}(E1)\frac{\Gamma}{2}d_{3/2}(E1)\cos(\phi_I-\phi_d+\beta)}{\left[(E-E_R)^2+\Gamma^2/4\right]^{\frac{1}{2}}}$$

$$a_2 = -2S_{\frac{1}{2}}(E1)d_{3/2}(E1)\cos(\phi_s-\phi_d) - d_{3/2}(E1)^2 \qquad \text{(B5)}$$

$$- \frac{d^{I}_{3/2}(E1)^2\Gamma^2/4}{(E-E_R)^2+\Gamma^2/4} - \frac{2S_{\frac{1}{2}}(E1)d^{I}_{3/2}(E1)\frac{\Gamma}{2}\cos(\phi_I-\phi_s+\beta)}{\left[(E-E_R)^2+\Gamma^2/4\right]^{1/2}}$$

$$- \frac{2d_{3/2}(E1)d^{I}_{3/2}(E1)\Gamma/2\cos(\phi_I-\phi_d+\beta)}{\left[(E-E_R)^2+\Gamma^2/4\right]^{1/2}}$$

$$b_2 = S_{\frac{1}{2}}(E1)d_{3/2}(E1)\sin(\phi_s-\phi_d) + \frac{S_{\frac{1}{2}}(E1)d^{I}_{3/2}(E1)\frac{\Gamma}{2}\sin(\phi_s-\phi_I-\beta)}{\left[(E-E_R)^2+\Gamma^2/4\right]^{1/2}}$$

where A^{J}_{IA} has been replaced by $d^{I}_{3/2}(E1)$.

APPENDIX C

SUM RULES

The two sum rules which are used in this work are for dipole and quadrupole integrated strength. The oldest of these is the dipole, or Thomas-Reiche-Kuhn (TRK), sum rule. By using effective charges for the proton ($\varepsilon_p = \frac{N}{A}e$) and neutron ($\varepsilon_n = -\frac{Z}{A}e$) and Siegert's theorem (A. J. F. Siegert, 1937), the dipole sum for nuclei can be determined to be (J. S. Levinger, 1960)

$$\sigma_{INT} = \int_0^{\mu} \sigma_{E1}(\gamma, x)\, dE_\gamma = 60\, \frac{NZ}{A}\ (mb \cdot MeV) \qquad (C1)$$

where σ_{INT} is the energy integrated cross section for photons up to the meson threshold μ. The use of effective charges can be shown to be identical to a center of mass correction for the nucleus which recoils because of gamma-ray emission (J. S. O'Connell, 1973).

A sum rule for integrated quadrupole strength for $|\Delta T|=1$ transitions in self-conjugate nuclei was derived by Telegdi and Gell-Mann (1953) to be

$$\int \frac{\sigma_{E2}(\gamma,x)}{E_\gamma^2}\, dE_\gamma = \frac{\pi^2}{137}\,\frac{A}{12}\,\frac{\langle r^2\rangle_{oo}}{Mc^2} \qquad \text{(C2)}$$

where $\langle r^2\rangle_{oo}$ is the mean squared displacement of a nucleon from the center of mass in the ground state of the nucleus, A is the nuclear mass number, and M is the nucleon mass. By taking a constant radial wave function up to the nuclear radius R_o, the quantity $\langle r^2\rangle_{oo}$ is readily evaluated as

$$\langle r^2\rangle_{oo} = \frac{3}{5}R_o^2 = \frac{3}{5}\left(1.2\,A^{1/3}\right)^2 (F)^2 \qquad \text{(C3)}$$

For nuclei with $N\neq Z$, the problem is more detailed. The operator, Q_{2m}, for E2 radiation is

$$Q_{2M} = \sum_i \left(1 - T_z^i\right) e r_i^2 \, Y_2^{M*}(\Omega_i) \qquad \text{(C4)}$$

where the sum is over A particles in the nucleus, τ_z is the isospin projection, and r is the radial coordinate of the ith nucleon. When this operator is squared in obtaining an E2 matrix element, cross terms mix the isoscalar ($\sum_i e r_i^2 Y_2^{M*}(\Omega_i)$) and isovector ($-\sum_i e r_i^2 \tau_z^i Y_2^{M*}(\Omega_i)$) parts of the operator making evaluation of separate isovector and isoscalar sum rules difficult. Warburton and Weneser (1969) have demonstrated that by modifying the E2 operator one may group the $\Delta T=0$ strength resulting from the isovector operator together with the isoscalar operator. The result allows evaluation of separate $\Delta T=0$ and $|\Delta T|=1$ sum rules. These are not, however, to be confused with isoscalar and isovector sum rules. The result for $|\Delta T|=1$ is given by

$$\int \frac{\sigma_{E2}(\gamma,x)}{E_\gamma^2}\, dE_\gamma = 2.2 \times 10^{-4} \frac{NZ}{A^{1/3}} \left(\frac{mb}{MeV}\right) \qquad \text{(C5)}$$

which reduces to the value of Gell-Mann and Telegdi for self-conjugate nuclei. The $\Delta T=0$ sum rule is given by

$$\int \frac{\sigma_{E2}(\gamma,x)}{E_\gamma^2}\, dE_\gamma = 2.2 \times 10^{-4} \frac{Z^2}{A^{1/3}} \left(\frac{mb}{MeV}\right) \qquad \text{(C6)}$$

The sum of eqs. (C5) and (C6) is

$$\int \frac{\sigma_{E2}(\gamma, x)}{E_\gamma^2}\, dE_\gamma = 2.2 \times 10^{-4}\, \mathcal{Z} A^{3/3} \left(\frac{mb}{MeV}\right) \qquad \text{(C7)}$$

which represents all integrated E2 strength independent of isospin.

Both sum rules use the total angle integrated cross section. The total cross section may be approximated by multiplying the 90° excitation curve by the ratio $4\pi A_o/\sigma(90^o)$ determined from the nearest angular distribution of cross section. The total dipole strength may then be estimated from this cross section and the E1 sum rule.

LIST OF REFERENCES

R. O. Akyuz and S. Fallieros, Phys. Rev. Lett. 27 (1971) 1016.

P. R. Bevington, Data Reduction and Error Analysis for the Physical Sciences (McGraw Hill, Inc., 1969).

J. M. Blatt and L. C. Biedenharn, Revs. Mod. Phys. 24 (1952) 258.

A. Bohr and B. R. Mottelson, Nuclear Structure, Vol. 1 (W. A. Benjamin, Inc., New York, New York, 1969).

A. Bohr and B. R. Mottelson, Nuclear Structure, Vol. 2 (W. A. Benjamin, Inc., Reading, Mass., 1975).

E. Brun, J. Oeser, H. H. Staub, and G. G. Telschow, Phys. Rev. 93 (1954) 172.

F. R. Buskirk, Private Communication (1976).

T. B. Clegg, G. A. Bissinger, W. Haeberli, P. A. Quin, Polarization Phenomena in Nuclear Reactions ed. H. H. Barschall and W. Haeberli, (Univ. of Wisconsin Press, Madison, Wis., 1970).

E. R. Cosman, H. A. Enge, and A. Sperduto, Phys. Lett. 22 (1966) 195.

E. R. Cosman, J. Joyce, and S. M. Shafroth, Bull. Am. Phys. Soc. 12 (1967) 697.

E. R. Cosman, J. M. Joyce, S. M. Shafroth, Nucl. Phys. A108 (1968) 519.

E. R. Cosman, R. Kalish, D. D. Armstrong, and H. C. Britt, Phys. Rev. C11 (1970) 945.

A. de-Shallit and I. Talmi, Nuclear Shell Theory (Academic Press, New York, 1963).

S. Devons and L. J. B. Goldfarb, Handbuch der Physik 42 (Springer-Verlag, Berlin, 1957).

F. S. Dietrich, M. Suffert, A. V. Nero, S. S. Hanna, Phys. Rev. 168 (1968) 1169.

H. Ejiri and U. P. Bondorf, Phys. Lett. 28B (1968) 304.

P. M. Endt and C. van der Leun, Atomic and Nuclear Data Tables 13 (1974) C7.

A. J. Ferguson, Angular Correlation Methods in Gamma Ray Spectroscopy (North Holland Publishing Company, Amsterdam, 1965).

E. G. Fuller and E. Hayward, Nuclear Reactions Vol. 2 ed. P. M. Endt and P. B. Smith, (North Holland Publishing Company, Amsterdam, 1962) 113.

M. Gell-Mann and V. L. Telegdi, Phys. Rev. 91 (1953) 169.

H. Genz, E. Blanke, A. Richter, and G. Schrieder, Nucl. Phys. A254 (1975) 29.

H. F. Glavish, Private Communication (1974).

H. F. Glavish, S. S. Hanna, R. Avida, R. N. Boyd, C. C. Chang, and E. Diener, Phys. Rev. Lett. 28 (1972) 766.

H. L. Gove, Nuclear Reactions Vol. 1 ed. P. M. Endt and M. DeMeur, (North Holland Publishing Company, Amsterdam, 1959).

I. Halpern, Proceedings of the International Conference on Photonuclear Reactions and Applications, Asilomar, 1973 ed. B. L. Berman, (Lawrence Livermore Laboratory, Univ. of California, 1973) 909.

S. S. Hanna, H. F. Glavish, R. Avida, J. R. Calarco, E. Kuhlman, and R. LaCanna, Phys. Rev. Lett. 32 (1974) 114.

S. S. Hanna, H. F. Glavish, E. M. Diener, J. R. Calarco, C. C. Chang, R. Avida, and R. N. Boyd, Phys. Lett. 40B (1972) 631.

E. Hayward, Nat. Bur. Stand. (U. S.) Monograph 118, 1970.

P. F. Hinrichsen, Nucl. Phys. A118 (1968) 538.

R. Huby, Proc. Phys. Soc. Lond. 67 (1954) 1103.

M. W. Johns, J. Y. Park, S. M. Shafroth, and D. M. Van Patter, Nucl. Data A8 (1970) 373.

E. Kuhlmann, E. Ventura, J. R. Calarco, D. G. Mavis, and S. S. Hanna, Phys. Rev. C11 (1975) 1521.

W. Kuhn, 2 Phys. K. 33 (1925) 408.

A. Lepretre, H. Beil, R. Bergere, P. Carlos, A. Veyssiere, and M. Sugawara, Nuc. Phys. A175 (1971) 609.

J. S. Levinger, Nuclear Photodisintegration (Oxford Press, London, 1960).

R. E. Mans, E. G. Addberger, K. A. Snover, M. D. Cooper, Phys. Rev. Lett. 35 (1975) 202.

R. C. McBroom, unpublished Ph.D. thesis, University of Florida, 1977.

W. E. Meyerhof and T. A. Tombrello, Nucl. Phys. A109 (1968) 1.

J. S. O'Connell, Proceedings of International Conference on Photonuclear Reactions and Applications, Asilomar, 1973 ed. B. L. Berman, (Lawrence Livermore Laboratory, Univ. of California, 1973) 71.

P. Paul, Proceedings of the International Conference on Photonuclear Reactions and Applications, Asilomar, 1973 ed. B. L. Berman, (Lawrence Livermore Laboratory, Univ. of California, 1973) 407.

F. O. Purser, H. W. Newson, N. R. Roberson, E. G. Bilpuch, and R. L. Walter, Fifth International Cyclotron Conference ed. R. W. Mellray, (1969) 13.

F. Reiche and W. Thomas, Z. Physik 34 (1925) 510.

P. Richard, F. Gabbard, A. C. Porter, and F. F. Hopkins, Phys. Lett. 29B (1969) 649.

E. L. Robinson, R. C. Hagenauer, E. Eichler, Nucl. Phys. A122 (1969) 471.

H. H. Rosenbrock, Comput. J. 3 (1960) 175.

R. R. Roy and B. P. Nigam, Nuclear Physics (John Wiley and Sons, Inc., New York, 1957).

S. M. Shafroth and G. J. E. Legge, Nucl. Phys. A107 (1968) 181.

A. J. F. Siegert, Phys. Rev. 52 (1937) 787.

K. A. Snover, J. F. Amann, W. Hering, and P. Paul, Phys. Lett. 37B (1971) 29.

K. A. Snover, K. Ebisawa, D. R. Brown, and P. Paul, Phys. Rev. Lett. 32 (1974) 317.

M. Suffert, W. Feldman, J. Mahieuk, and S. S. Hanna, Nucl. Inst. and Methods 63 (1968).

W. Thomas, Naturwiss 13 (1925) 627.

T. A. Trainer, T. B. Clegg, P. W. Lisowski, Nucl. Phys. A220 (1974) 533.

J. D. Vergados and T. T. S. Kuo, Nucl. Phys. A168 (1971) 225.

L. Vesser, J. Ellis, and W. Haeberli, Phys. Rev. Lett. 18 (1967) 1063.

E. K. Warburton and J. Wenrser, Isospin in Nuclear Physics ed. D. H. Wilkinson, (North Holland Publishing Company, Amsterdam, 1969) 173.

H. R. Weller, R. A. Blue, N. R. Roberson, D. G. Rickel, S. Maripuu, C. P. Cameron, R. D. Ledford, and D. R. Tilley, Phys. Rev. C13 (1976) 922.

H. R. Weller, N. R. Roberson, D. G. Rickel, C. P. Cameron, R. D. Ledford, T. B. Clegg, Phys. Lett. 32 (1974) 177.

J. F. Wimpey, unpublished Ph.D. thesis, North Carolina State University, 1974.

BIOGRAPHY

RANDALL D. LEDFORD

PERSONAL: Born January 14, 1950, Johnson City, Tennessee
Married

EDUCATION: B. S. in Physics
Wake Forest University (1972)

POSITIONS: Teaching Assistant, Duke University (1972-1973)
Research Assistant, Duke University (1973-1976)

MEMBERSHIPS: Phi Beta Kappa, Sigma Pi Sigma, American Physical Society

PUBLICATIONS:

1. Evidence for E2 and M1 Radiation in the Giant-Dipole-Resonance Region of ^{15}N (with H. R. Weller, N. R. Roberson, D. G. Rickel, C. P. Cameron, and T. B. Clegg) Phys. Rev. Lett. 32 (1974) 177.

2. Measurements of γ-ray Angular Distributions and Linear Polarizations in ^{48}V (with D. G. Rickel, N. R. Roberson, C. P. Cameron, S. G. Buccino, and D. R. Tilley) Nucl. Phys. A256 (1976) 152.

3. Mean Lifetimes in ^{55}Co (with R. O. Nelson, J. R. Williams, D. R. Tilley, D. G. Rickel, N. R. Roberson, S. Maripuu, and C. P. Cameron) Nucl. Phys. A261 (1976) 427.

4. Giant Resonance Region of ^{15}N Studied by Polarized and Unpolarized Proton Capture Measurements (with H. R. Weller, R. A. Blue, N. R. Roberson, D. G. Rickel, S. Maripuu, C. P. Cameron, and D. R. Tilley) Phys. Rev. C13 (1976) 922.

5. Comment on "El Excitations in A 15 Nuclei" (with H. R. Weller, N. R. Roberson, D. G. Rickel, C. P. Cameron, and D. R. Tilley) Phys. Rev. C13 (1976) 2062.

6. The Giant Dipole Resonance Region in ^{56}Fe Observed via (p,γ) and (α,γ) Reactions (with D. G. Rickel, C. P. Cameron, N. R. Roberson, H. R. Weller, and D. R. Tilley) Phys. Rev. C14 (1976) 338.

7. The Giant Dipole Resonance in $^{55, 57, 59}Co$ Using Polarized Proton Capture (with C. P. Cameron, N. R. Roberson, D. G. Rickel, H. R. Weller, R. A. Blue, and D. R. Tilley) Phys. Rev. C14 (1976) 553.

8. Polarized Beam Angular Correlation Measurements in ^{41}Ca (with C. R. Gould, D. R. Tilley, C. P. Cameron, N. R. Roberson, and T. B. Clegg) Proceedings of the Fourth International Symposium on Polarization Phenomena in Nuclear Reactions ed. W. Gruebler and V. Konig (Birkhauser Verlag Basel und Stuttgart, Switzerland, 1976) 807.

9. A Study of the Giant Dipole Resonance Region in Co Isotopes Using Polarized Proton Capture Measurements (with H. R. Weller, R. A. Blue, G. Rochau, R. McBroom, N. R. Roberson, D. G. Rickel, and C. P. Cameron) Proceedings of the Fourth International Symposium on Polarization Phenomena in Nuclear Reactions ed. W. Gruebler and V. Konig (Birkhauser Verlag Basel und Stuttgart, Switzerland, 1976) 757.

10. A Study of the Giant Resonance Region of ^{55}Co, ^{57}Co, and ^{59}Co Using Polarized Proton Capture and Elastic Scattering Measurements (with H. R. Weller, N. R. Roberson, D. G. Rickel, C. P. Cameron, D. R. Tilley, J. Szucs, J. A. Kuehner, G. D. Jones, and D. T. Petty) Proceedings of the Symposium on Nuclear Structure: Coexistence of Single Particle and Collective Type Excitations (Balatonfrued, Hungary, 1975) To be published.

ABSTRACTS:

1. Evidence for E2 and M1 Radiation in the Giant Dipole Resonance Region of ^{15}N (with N. R. Roberson, D. G. Rickel, C. P. Cameron, T. B. Clegg, and H. R. Weller) Bull. Am. Phys. Soc. 18 (1973) 1387.

2. Study of Giant Dipole Resonances in the Co Isotopes Using Proton Capture and Polarized Proton Capture Measurements (with H. R. Weller, R. A. Blue, D. Griggs, N. R. Roberson, D. G. Rickel, C. P. Cameron, J. D. Turner, and D. R. Tilley) Bull. Am. Phys. Soc. 19 (1974) 988.

3. The Giant Resonance Region of ^{56}Fe from (p,γ) and (α,γ) Reactions (with D. G. Rickel, N. R. Roberson, C. P. Cameron, D. R. Tilley, H. R. Weller, and R. A. Blue) Bull. Am. Phys. Soc. 20 (1975) 1156.

4. The Giant Dipole Resonance Region of ^{31}P (with C. P. Cameron, D. G. Rickel, J. D. Turner, N. R. Roberson, D. R. Tilley, R. C. McBroom, R. A. Blue, and H. R. Weller) Bull. Am. Phys. Soc. 21 (1976) 556.

5. Investigation of the 3/2 Analogue State in ^{89}Y at E_{ex} 14.62 MeV Using the $^{88}Sr(p,\gamma)^{89}Y$ Reaction (with C. P. Cameron, D. G. Rickel, J. D. Turner, N. R. Roberson, D. R. Tilley, R. McBroom, and H. R. Weller) Bull. Am. Phys. Soc. 21 (1976) 581.

6. Study of the Giant Dipole Resonance of ^{89}Y (with N. R. Roberson, C. P. Cameron, D. G. Rickel, J. D. Turner, D. R. Tilley, R. McBroom, and H. R. Weller) Bull. Am. Phys. Soc. 21 (1976) 516.

7. The $^{3}H(p,\gamma)^{4}He$ Reaction for $17 \leq E_p \leq 30$ MeV (with R. McBroom, H. R. Weller, N. R. Roberson, D. G. Rickel, J. D. Turner, C. P. Cameron, and D. R. Tilley) Bull. Am. Phys. Soc. 21 (1976) 534.

8. Evidence for $J^{\pi}=2^{+}$ States in ^{4}He (with R. McBroom, H. R. Weller, N. R. Roberson, J. D. Turner, C. P. Cameron, and D. R. Tilley) Bull. Am. Phys. Soc. 21 (1976) 997.

9. Search for Collective E2 Resonances Above the Giant Dipole Resonance (with C. P. Cameron, J. D. Turner, N. R. Roberson, H. R. Weller, R. A. Blue, R. McBroom, and D. R. Tilley) Bull. Am. Phys. Soc. 21 (1976) 996.